Nutrient sensing by the mTORC1 pathway in physiology

by

Andrew L. Cangelosi

B.S., Biology
Duke University

Submitted to the Department of Biology on March 31, 2022 in Partial Fulfillment of the Requirements for the Degree of Doctor of Philosophy at the Massachusetts Institute of Technology

June 2022

Signature of Author: _____
Department of Biology March 3, 2021

Certified by: _____
Mary Gehring
Member, Whitehead Institute
Professor of Biology
Thesis Supervisor

Accepted by: _____
Amy Keating
Professor of Biology
Co-director, Biology Graduate Committee

Nutrient sensing by the mTORC1 pathway in physiology

by

Andrew L. Cangelosi

Submitted to the Department of Biology on March 31, 2022 in Partial Fulfillment of the Requirements for the Degree of Doctor of Philosophy at the Massachusetts Institute of Technology

Abstract:

Cellular growth and metabolism must be linked to the environmental status of the cell to maintain organismal function. This coordination is achieved by mTORC1, a master growth regulator that senses and integrates a diverse array of environmental inputs, including nutrients like glucose and the amino acids leucine and arginine, whose sensing mechanisms are beginning to be identified. However, the role and implications of nutrient sensing by mTORC1 in mammalian physiology remains poorly understood.

Here, we identified a critical role of leucine sensing by mTORC1 in adapting to leucine availability *in vivo*. Mice lacking the leucine sensors Sestrin1 and Sestrin2 fail to inhibit mTORC1 in tissues when deprived of dietary leucine. These mice suffer from severe loss of white adipose tissue and skeletal muscle when deprived of leucine, but not other essential amino acids. We showed that their white adipose tissue loss results from mTORC1 dysregulation in the liver and is driven by aberrant production of the hepatokine FGF21. We also found that leucine sensing is compartmentalized within the liver, which is established by zonated expression of Sestrin1 and Sestrin2 in the liver lobule and demonstrates an unappreciated spatial organization of nutrient sensing in tissues.

Further, we identified a functionally-important temporal shift in nutrient sensitivity of the mTORC1 pathway in pancreatic β cells. We found that this shift is required for β cells to acquire glucose-responsive insulin secretion after birth. We further demonstrated that modulating nutrient-responsive mTORC1 activity can be therapeutically exploited to improve the generation of stem cell-derived β cells. Collectively, these findings demonstrate a subset of the likely many important roles of nutrient sensing by mTORC1 in physiology and begin to unravel the spatial and temporal complexity of nutrient sensing within tissues of the body.

Thesis supervisor: Mary Gehring
Title: Member, Whitehead Institute; Professor of Biology, MIT

Acknowledgements

I am immensely grateful for my experience during my PhD, thanks to the support of many inside and outside of the lab. In the lab, I have been lucky to be surrounded by incredibly talented and inspiring people. A large part of my scientific growth I credit to the mentorship of my advisor, David, who consistently struck an effective balance between providing critical guidance and giving me the freedom to carve out the direction of my work. His push to always chase big questions and impactful concepts I will carry with me. Additionally, I am thankful for the support of my thesis committee members, Matthew Vander Heiden and Harvey Lodish.

I was also fortunate to join the lab with and learn from a great cohort of students in my class: Hank Adelmann, Jose Orozco, Kendall Condon, and Xin Gu. Getting started in the lab was a steep learning curve for me, and I am especially grateful to Bill Comb, who dedicated numerous afternoons to teaching me how to work with mice and get my feet on the ground. I'm also thankful to have become friends with Andrea Armani; our many long conversations taught me a lot about science and also my Italian heritage. I also had the valuable opportunity to work on a collaborative project with Ronny Helman. Ronny, his postdoc advisor Doug Melton, and the other Melton lab members were wonderful to work with and incredibly generous in helping me to expand my scientific knowledge about their field. Finally, I am extremely thankful to have met Anna Puszynska, who has been a brilliant colleague to work with and also an amazing friend. Her rigorous yet selfless approach to science is one I hope to emulate.

I'm also grateful for having such a strong support system in my family: my mom, my dad, and my brother Philip. The past several years have brought challenging times, and they have always been there to lean on. The extraordinary experience I've had during my PhD I owe to my parents' devoted support for my brother and me; it would not be possible without their continued encouragement to pursue what we love. Particularly, experiencing as a child my mom's own journey through her PhD and academic career has been a major inspiration throughout my education. Lastly, I'm beyond lucky to have the support of my partner, Carolyn. Over the years she has kept me grounded and shown unending patience with my long days and nights in the lab. I'm also thankful for her parents and siblings for welcoming me as one of their own and supporting me along the way with many vacations, meals, and fun occasions (especially intense games of tug-of-war with their dog Meymoon).

Table of Contents

Chapter 1

Introduction

Andrew L. Cangelosi[1,2,3]

[1] Whitehead Institute for Biomedical Research, 455 Main Street, Cambridge, MA 02142.
[2] Howard Hughes Medical Institute, Department of Biology, Massachusetts Institute of Technology, Cambridge, MA 02139.
[3] Department of Biology, Massachusetts Institute of Technology, Cambridge, MA 02139.

Introduction

Cellular growth is a resource-demanding process that must be coupled to the conditions of the cell. This regulation is in large part controlled by the mechanistic target of rapamycin complex 1 (mTORC1). A diverse array of nutrient, hormonal, and stress-related inputs regulates the activity of mTORC1. In turn, mTORC1 controls cellular growth and metabolism by activating anabolic processes like protein synthesis and lipid biosynthesis, while inhibiting catabolic processes like autophagy. Dysregulated mTORC1 activity occurs in a broad range of clinical pathologies, highlighting the importance of this coordination between cellular status and growth. Understanding and targeting the mTORC1 pathway is therefore of great interest for the development of new disease therapies.

The discovery of mTOR

Elucidation of the mTORC1 pathway began in 1964 with the identification of rapamycin, a compound isolated from soil on the island of Rapa Nui which was found to have antifungal, tumor suppressive, and immunosuppressive properties (Vézina et al., 1975; Eng et al., 1984; Martel et al., 1977). For many years the mechanistic basis of rapamycin's effects remained unknown. In the early 1990s, rapamycin was determined to exert its anti-growth effects in complex with the prolyl-isomerase FKPB12 (Chung et al., 1992). Around the same time, screens in *S. cerevisiae* identified mutations in the yeast genes TOR1 and TOR2 as critical for rapamycin sensitivity (Cafferkey et al., 1993; Heitman et al., 1991; Kunz et al., 1993). Shortly thereafter, the mammalian protein target of the rapamycin-FKBP12 complex was identified as the homolog to the

yeast TOR genes (Sabatini et al., 1994; Brown et al., 1994; Sabers et al., 1995); this protein was thus named mTOR.

The mTOR complexes

mTOR is a serine/threonine kinase which acts in complex with several interacting partners. Two mTOR-containing complexes have been identified (named mTORC1 and mTORC2). The particular binding partners within each complex determine the regulation of and substrates targeted by mTOR's kinase activity, conferring distinct cellular roles on mTORC1 and mTORC2 signaling.

mTORC2

mTORC2 consists of mTOR, Rictor (rapamycin insensitive companion of mTOR) (Jacinto et al., 2004; Sarbassov et al., 2004), mLST8 (mammalian lethal with Sec13 protein 8) (Kim et al., 2003), DEPTOR (DEP domain containing mTOR interacting protein) (Peterson et al., 2009), mSin1(Frias et al., 2006; Jacinto et al., 2006; Yang et al., 2006), and Protor1/2 (Pearce et al., 2007; Thedieck et al., 2007; Woo et al., 2007). mTORC2 impacts cellular metabolism by phosphorylating AKT ((Sarbassov et al., 2005), thereby impinging on many effector functions downstream of AKT activity. Other substrates of mTORC2 kinase activity include several AGC protein kinases which regulate the cell migration, the cytoskeleton, and cell survival (Jacinto et al., 2004; Sarbassov et al., 2004; Gan et al., 2012; Li and Gao, 2014; Thomanetz et al., 2013; Garcia-Martinez and Alessi, 2008).

mTORC1

mTORC1 is comprised of mTOR, Raptor (regulatory protein associated with mTOR), mLST8, PRAS40 (proline-rich Akt substrate of 40 kDa), and DEPTOR (Kim et

al., 2003; Peterson et al., 2009; Hara et al., 2002; Kim et al., 2002; Sancak et al., 2007; Vander Haar et al., 2007; Wang et al., 2007). Structural studies have determined that rapamycin-FKBP12 binding inhibits mTORC1's activity towards its substrates by occluding the kinase active site of mTORC1 (Yang et al., 2013).

Effectors of mTORC1

When mTORC1 is active, the phosphorylation of its substrate proteins collectively induce a multifactorial shift to an anabolic cellular state, by promoting various biosynthetic processes and suppressing degradative processes (Figure 1).

mTORC1 activity drives protein synthesis via the downstream substrates p70S6 Kinase 1 (S6K1) and eIF4E Binding Protein 1 (4EBP1). S6K1, when phosphorylated and activated by mTORC1, enhances mRNA biogenesis, ribosome biogenesis, and cap-dependent translation and elongation (Holz et al., 2005; Dorrello et al., 2006; Ma et al., 2008). Phosphorylation of 4EBP1 impedes its binding to eIF4E, allowing eIF4E to drive cap-dependent translation (Brunn et al., 1997; Gingras et al., 1999). mTORC1 also controls protein catabolism by inhibitory phosphorylation of the autophagy-related substrates Unc-51 Like Autophagy Activating Kinase 1/2 (ULK1/2), ATG13, and the transcription factors TFEB, TFE3, and MITF. Phosphorylation of ULK1/2 and ATG13 inhibits early autophagosome formation (Hosokawa et al., 2009; Kim et al., 2011). TFEB, TFE3, and MITF promote the expression of many genes important for autophagy and lysosome biogenesis (Sardiello et al., 2009; Settembre et al., 2011); their phosphorylation by mTORC1 sequesters them in the cytosol to block their transcriptional activity (Martina et al., 2012; Settembre et al., 2012).

mTORC1 also regulates the biosynthesis and metabolism of lipids via regulation of the SREBP and PPARα pathways, respectively. mTORC1 promotes SREBP activity via S6K1, as well as phosphorylation and nuclear exclusion of Lipin1, an inhibitor of nuclear SREBP (Duvel et al., 2010; Peterson et al., 2011). PPARα, a master transcription factor of fatty acid oxidation genes, is regulated by mTORC1-mediated localization of its repressor NCoR1 (Sengupta et al., 2010).

Other anabolic processes controlled by mTORC1 activity include nucleotide biosynthesis, via S6K1-mediated phosphorylation of the de novo pyrimidine biosynthesis enzyme CAD (Ben-Sahra et al., 2013; Robitaille et al., 2013), and insulin signaling, via S6K1-mediated inhibitory phosphorylation of IRS1 (Um et al., 2004).

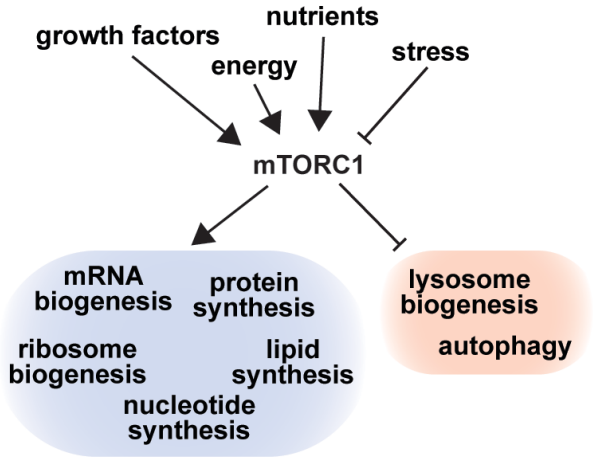

Figure 1: Inputs and outputs of mTORC1. The mTORC1 pathway senses and integrates many cellular conditions to promote anabolic processes and inhibit catabolic processes.

Regulation of mTORC1

Cellular conditions must be favorable for growth to permit mTORC1 activation. Many inputs, including stress, energy, growth factors, and nutrients are signaled to

mTORC1 via an extensive upstream network (Figure 1). These signals converge into a two-pronged coincidence detection system for mTORC1 activation: growth factors, stress, and energy status dictate the activity of the mTORC1 kinase activator Ras homolog enriched in brain (Rheb), a small GTPase located on the lysosome, and nutrient availability controls mTORC1's engagement with Rheb via recruitment to the lysosomal membrane (Figure 2).

Growth factors, stress, and energy

Activation of Rheb is directed by the Tuberous Sclerosis Complex (TSC), a negative regulator of mTORC1 via its GTPase activating protein (GAP) activity towards Rheb (Dibble et al., 2012; Li et al., 2004). Numerous signaling pathways impact TSC function, including growth factor-responsive PI3K/AKT and ERK activity (which inhibit the GAP activity of TSC) (Inoki et al., 2002; Manning et al., 2002; Ma et al., 2005; Roux et al., 2004), and 5' AMP-activated protein kinase (AMPK) activity (which activates TSC) in response to energetic stress (Inoki et al., 2003; Shaw et al., 2004). Further, hypoxia regulates TSC via AMPK activation and increased expression of regulated in development and DNA damage responses 1 (REDD1) (Brugarolas et al., 2004). AKT and AMPK also control mTORC1 signaling via the phosphorylation of the mTORC1 components PRAS40 and Raptor, respectively (Gwinn et al., 2008; Sancak et al., 2007; Vander Haar et al., 2007).

Nutrients

In order to be activated by Rheb, mTORC1 must be appropriately docked on the lysosomal surface. The heterodimeric Rag GTPases (as a dimer of RagA or RagB and RagC or RagD) are bound to the lysosomal pentameric complex Ragulator and act as

the lysosomal docking site for mTORC1 by interacting with Raptor (Sancak et al., 2008). The ability of the Rag GTPases to dock mTORC1 is dictated by their guanine nucleotide loading state. RagA/B must be GTP-bound and RagC/D GDP-bound to accommodate the docking of mTORC1 (Sancak et al., 2010). Regulation of Rag GTPase nucleotide loading state is thus the point of convergence by which nutrients control mTORC1 lysosomal recruitment and activation.

Availability of nutrients in the cytosol as well as within the lysosomal lumen are signaled to mTORC1 via the Rag GTPases (Figure 2). The lysosomal amino acid transporter SLC38A9 signals lysosomal arginine and cholesterol levels via direct regulation of the Rag GTPases. Lysosomal arginine or cholesterol bind SLC38A9 on transmembrane helix 1 and transmembrane helix 8, respectively, to enable guanine nucleotide exchange factor (GEF) activity towards RagA/B (Castellano et al., 2017; Wyant et al., 2017; Lei et al., 2018).

Cytosolic nutrients direct Rag GTPase nucleotide loading through two protein complexes. The Folliculin complex (consisting of FLCN and FNIP1 or FNIP2) displays GAP activity towards RagC/D and translocates to the lysosome in an amino acid-dependent manner through a currently unknown mechanism (Petit et al., 2013; Tsun et al., 2013). The nucleotide loading state of the Rag GTPases is also regulated by the GAP Activity Towards the Rags 1 (GATOR1) complex, a negative regulator of mTORC1 that has GAP activity towards RagA/B and consists of DEPDC5, NPRL2, and NPRL3 (Bar-Peled et al., 2013). GATOR1 is retained on the lysosomal surface via interaction with the scaffolding complex KPTN, ITFG2, C12orf66, and SZT2 containing regulator of TOR (KICSTOR) (Peng et al., 2017; Wolfson et al., 2017).

The availability of numerous cytosolic nutrients has been found to control the GAP activity of GATOR1 towards the Rag GTPases. Methionine levels are signaled indirectly by SAMTOR, which directly binds the methionine-derived metabolite S-adenosylmethionine (SAM) and interacts with GATOR1 when not bound to SAM to inhibit mTORC1 (Gu et al., 2017). Other cytosolic nutrient inputs are signaled to GATOR1 via the GATOR2 complex, a positive regulator of mTORC1 consisting of MIOS, WDR59, WDR24, Seh1L, and SEC13. GATOR2 directly interacts with GATOR1 and disrupts GAP activity of GATOR1 towards RagA/B, but its mechanistic function remains unclear (Bar-Peled et al., 2013). Glucose availability activates mTORC1 and is indirectly relayed to the GATOR2-GATOR1 axis by the glycolytic intermediate dihydroxyacetone phosphate (DHAP) through a currently unknown mechanism (Orozco et al., 2020). Cytosolic arginine is sensed by Cellular Arginine Sensor for mTORC1 1 (CASTOR1), which directly binds arginine. In the absence of arginine, CASTOR1 interacts with and inhibits GATOR2, either as a homodimer or as a heterodimer with CASTOR2, to permit mTORC1 activation (Chantranupong et al., 2016).

Leucine sensing

Leucine is widely regarded as a potent activator of mTORC1 and anabolic processes downstream of mTORC1 like protein synthesis. The nature by which mTORC1 responds to leucine availability therefore has sparked great interest and multiple proposed mechanisms of leucine sensing, including involvement of the leucine tRNA synthetase, AMPK, phospholipase D, p62, taste receptors, leucylation of proteins, and direct acetylation of mTORC1 (Han et al., 2012; Kim et al., 2017; He et al., 2018; Durán et al., 2012; Linares et al., 2013; Lawrence et al., 2018; Son et al., 2019;

Budanov et al., 2008). Clarifying this mechanism was the identification of Sestrin1 and Sestrin2 as leucine-binding proteins which interact with GATOR2 to inhibit mTORC1 in the absence of leucine (Wolfson et al., 2016). Sestrin2 binds leucine with a Kd of 20 μM through a lid-latch mechanism. Mutations in the leucine binding pocket of Sestrin2, elucidated by the crystal structure of Sestrin2, modulate its affinity for leucine and, correspondingly, mTORC1 responsiveness to leucine (Saxton et al., 2016).

The Sestrin proteins

The Sestrins are a family of proteins, comprised of Sestrin1, Sestrin2, and Sestrin3, initially recognized for their stress-responsive properties. Sestrin1 was first identified as a target gene of p53, followed by the identification of Sestrin2 in a screen for hypoxia-induced genes. Sestrin3 was later determined to be a third member of the protein family based on sequence homology (Buckbinder et al., 1994; Velasco-Miguel et al., 1999; Budanov et al., 2002; Peeters et al., 2003). Both Sestrin1 and Sestrin2 are induced by genotoxic stress via p53 activity (Budanov and Karin, 2008). Sestrin2 is also induced by various other stresses, including oxidative stress, mitochondrial stress, hypoxia, amino acid limitation, and ER stress, due to the presence of a C/EBP-ATF Response Element (CARE) sequence in its promoter which is recognized by Activating Transcription Factor 4 (ATF4) (Garaeva et al., 2016). Sestrin3 is transcriptionally regulated by FoxO transcription factors (Nogueira et al., 2008; Chen et al., 2010; Hagenbuchner et al., 2012). All 3 Sestrin proteins are ubiquitously expressed throughout the mammalian body with few exceptions, most notably very low Sestrin2 expression in skeletal muscle (Xu et al., 2019).

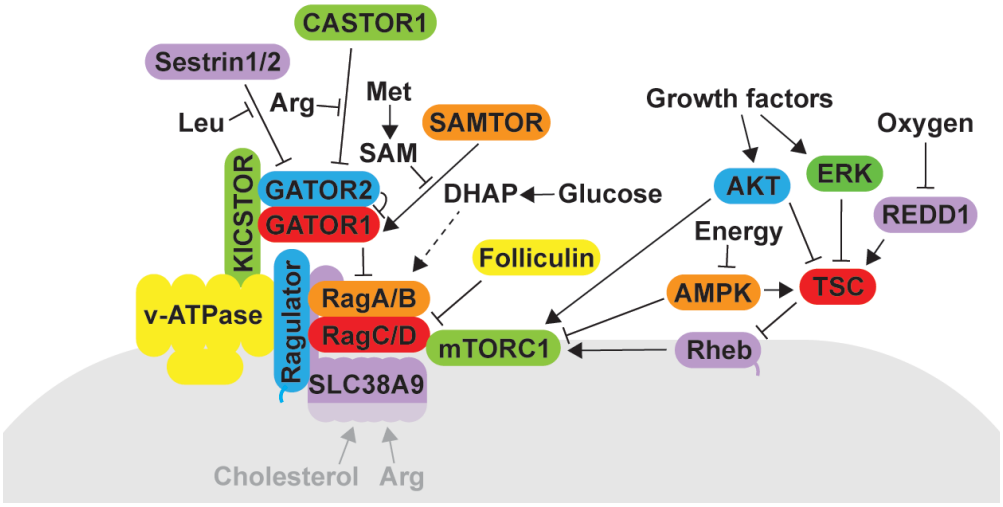

Figure 2: Current model of mTORC1 regulation on the lysosomal surface. mTORC1 is recruited to the Rag GTPases on the lysosome in a manner dependent on cytosolic and lysosomal nutrients. On the lysosome, mTORC1 is activated by Rheb in a growth factor, energy, and oxygen-sensitive manner.

mTORC1 crosstalk with other nutrient-sensitive signaling pathways

In addition to the mTORC1 pathway, a parallel nutrient-sensitive cellular signaling cascade is established by general control nonderepressible 2 (GCN2) kinase, which is activated by reduced amino acid availability and subsequent accumulation of uncharged tRNAs. When activated, GCN2 phosphorylates the α subunit of eIF2, impeding the GEF activity of eIF4 towards eIF2 and inhibiting translation initiation of most genes while promoting preferential translation of genes containing an upstream open reading frame (uORF) within their 5' untranslated region (UTR), most notably ATF4.

mTORC1 and GCN2 can regulate, and be regulated by, the other kinase's activity through multiple feedback mechanisms to maintain cellular amino acid

homeostasis. Activation of GCN2 and induction of ATF4 increases expression of Sestrin2, which may potentiate inhibition of mTORC1 when leucine is limited (Ye et al., 2015). In addition to Sestrin2, ATF4 drives the expression of many genes involved in the biosynthesis and transport of amino acids in order to increase amino acid availability, promoting cellular conditions permissive for mTORC1 activation (Kilberg et al., 2009). Conversely, mTORC1 can also impact amino acid availability to modulate GCN2 activity, through regulation of amino acid consumption during translation and the recycling of amino acids generated by proteolysis during autophagy.

mTORC1 in physiology

As a master regulator of many cellular metabolic functions, mTORC1 activity and its regulation is critical for organismal function and homeostasis. Genetic manipulation of the mTORC1 pathway components and its regulators in mouse models have elucidated numerous roles of mTORC1 signaling in mammalian physiology.

Glucose and lipid homeostasis

During periods of fasting, the liver mobilizes macronutrients via autophagy, gluconeogenesis, and ketogenesis to buffer nutrient levels. Nutrient-regulated mTORC1 activity in the liver plays a key role in these homeostatic functions. Mice with liver-specific deletion of TSC1 are unable to inhibit mTORC1 during fasting, impairing ketogenesis due to suppressed PPARα activity (Sengupta et al., 2010). Mice expressing a constitutively active form of RagA die from hypoglycemia shortly after birth, as they fail to inhibit mTORC1, mobilize amino acids through autophagy, and maintain glucose levels through gluconeogenesis (Efeyan et al., 2013). Likewise, global deletion of

Sestrin1, Sestrin2, and Sestrin3 in mice results in similar mTORC1 hyperactivity and early-life lethality, likely through similar mechanisms (Peng et al., 2014).

Glucose levels are sensed and tightly regulated by β-cells in the pancreatic islets, and appropriate mTORC1 signaling is essential for β-cell function and glucose homeostasis. Constitutive activation of mTORC1 in the β-cells of mice via β-cell-specific deletion of TSC2 produces increased β-cell mass and hyperinsulinemia initially, followed by reduced β-cell mass, hypoinsulinemia, and hyperglycemia later in life (Shigeyama et al., 2008). Disruption of mTORC1 with deletion of Raptor in β-cells results in hypoinsulinemia and hyperglycemia by impairing β-cell maturation and glucose-responsiveness (Ni et al., 2017).

White adipose tissue acts as the primary site of lipid storage in the body, and regulation of mTORC1 is critical for its lipid-storing capacity. Either constitutive activation or disruption of mTORC1, via deletion of TSC2 or raptor, respectively, diminish the lipid content and increase mitochondrial uncoupling in white adipose tissue (Magdalon et al., 2016; Polak et al., 2008).

Muscle maintenance

Skeletal muscle mass is dictated by the cumulative balance of myofibrillar hypertrophy and proteolysis. mTORC1 activity in muscle strongly impacts muscle mass through regulation of protein synthesis and autophagy. Supplementation of amino acids, particularly leucine, activates mTORC1 in muscle and is widely practiced to enhance muscle hypertrophy (Bodine et al., 2001; Anthony et al., 2000). As in white adipose tissue, an appropriate balance of mTORC1 activity is necessary for muscle homeostasis. Muscle-specific Raptor knockout mice are dystrophic with dramatically

reduced lifespan (Bentzinger et al., 2008), while chronic hyperactivation of mTORC1 in mice with muscle-specific TSC1 deletion develop late-onset myopathy as a result of impaired autophagy (Castets et al., 2013).

Neural function

The central nervous system relies on appropriate regulation of mTORC1 activity for its development, function, and maintenance. Mice with constitutive activation of either growth factor signaling, via TSC1 deletion, or nutrient signaling, via DEPDC5 deletion, in neurons suffer from epileptic seizures and early death (Miekle et al., 2007; Yuskaitis et al., 2018). Genetic inactivation of mTORC1 via Raptor deletion in neural stem cells develop microencephaly and die shortly after birth, highlighting a role of mTORC1 activity in brain development (Cloëtta et al., 2013). mTORC1 activity is also critical for myelination, as mTORC1 inhibition via deletion of either Raptor or Mios specifically in oligodendrocytes results in hypomyelination of the neurons in these mice (Lebrun-Julien et al., 2014; Yu et al., 2022).

Immune function

mTORC1 signaling is also implicated in several aspects of immune function. Before the identification of mTOR as its target protein, rapamycin was well-appreciated as a potent immunosuppressant (Martel et al., 1977). Genetic studies in mouse models have subsequently demonstrated critical roles of mTORC1 signaling in key steps of the adaptive immune response, including the development, activation, and expansion of T cells (Powell et al., 2012; Zheng et al., 2007; Araki et al., 2009; Haxhinasto et al., 2008).

mTORC1 in pathophysiology

Cancer

Given the role of mTORC1 signaling in cellular growth, it is not surprising that many negative regulators upstream of mTORC1 have been identified as tumor suppressors, including components of the MAPK/ERK, AMPK, and PI3K/AKT signaling cascades, as well as components of TSC. Correspondingly, mice with liver-specific deletion of TSC1 develop hepatocellular carcinoma at high frequency (Menon et al., 2012). Among the nutrient-sensing machinery upstream of the Rag GTPases, mutations in FLCN, GATOR1 components, and RagC are implicated in Birt-Hogge Dube syndrome, glioblastoma, and follicular lymphoma, respectively (Bar-Peled et al., 2013; Okosun et al., 2016; Nickerson et al., 2002).

Diabetes

Widespread overnutrition in modern society is coupled to an increasing prevalence of diet-induced metabolic dysfunction, including Type 2 diabetes. Consistent with its strong regulation by nutrient availability, mTORC1 signaling is hyperactivated in multiple metabolic tissues during diet-induced obesity, including in the liver and pancreas (Khamzina et al., 2005). Chronic overactivation of mTORC1 in β-cells of the pancreas contributes to β-cell dysfunction and potentiation of hyperglycemia, as indicated by genetic mouse models of β-cell-specific mTORC1 hyperactivation (Shigeyama et al., 2008). Type 2 diabetes is characterized by the development of insulin resistance in peripheral tissues, including the liver, white adipose tissue, and skeletal muscle, which are normally highly sensitive to insulin stimulation. Aberrant mTORC1 activity in these tissues blunts cellular signaling downstream of the insulin

receptor via inhibitory phosphorylation of IRS1 by S6K1 (Um et al., 2004). mTORC1 dysregulation therefore contributes to both decreased insulin secretion by β-cells and peripheral insulin resistance during diet-induced obesity and Type 2 diabetes.

Aging

mTORC1 is strongly implicated in age-associated functional decline. During aging, aberrant mTORC1 activity is observed in multiple tissues including the liver, skeletal muscle, and pancreatic β-cells (Joseph et al., 2019; Sengupta et al., 2010; Helman et al., 2016). Accordingly, several cellular functions dependent on mTORC1 inhibition, including autophagy and fasting-induced ketogenesis, become impaired. The resulting inability to maintain cellular homeostasis contributes to age-associated dysfunction like neurodegeneration, sarcopenia, and blunted stem cell self-renewal (Joseph et al., 2019; Spilman et al., 2010; Chen et al., 2009; Yilmaz et al., 2012).

mTORC1 is thus an enticing target for anti-aging efforts. Indeed, conditions which attenuate mTORC1 signaling, including rapamycin treatment, calorie restriction, and genetic reduction of insulin/IGF-1 signaling are known to increase lifespan in model organisms ranging from yeast to mice (Vellai et al., 2003; Jia et al., 2004; Kapahi et al., 2004; Kaeberlein et al., 2005; Lamming et al., 2012; Wu et al., 2013). Studies in mice have demonstrated that multiple properties of aged tissues are counteracted by rapamycin treatment, including increased autophagy and stem cell function (Schinaman et al., 2019; Chen et al., 2009; Yilmaz et al., 2012). However, unfavorable side effects of rapamycin, at least in part due to its disruption of mTORC2 assembly (Lamming et al., 2012; Sarbassov et al., 2006), warrant optimization of clinically-suitable rapalogs. Work by the field is ongoing towards this goal.

Preface

At the cellular level, mTORC1 serves as a master controller through its broad regulation of anabolic and catabolic processes. As such, ever-increasing evidence implicates mTORC1 signaling in a plethora of physiological functions critical for health and disease. However, much of the regulatory mechanisms of the mTORC1 pathway, particularly nutrient sensing upstream of the Rag GTPases, remain a black box in many contexts. To date, the vast majority of information known about nutrient sensing in the mTORC1 pathway derives from studies involving a limited set of cultured cell lines. While extensive cell culture-based work in recent years has yielded great clarity towards a mechanistic understanding, nutrient sensing upstream of mTORC1 remains largely unexplored outside of this experimental system, particularly in mammalian physiology. The field's current knowledge of the physiological roles of mTORC1 relies predominantly on mouse models with genetic manipulation of established mTORC1 regulators upstream of Rheb. Studies involving genetic perturbation specifically of nutrient-sensitive signaling upstream of the Rag GTPases have only recently begun in model organisms.

There is thus an unmet need for understanding how nutrients and their direct sensing contribute to the regulation of physiological function through mTORC1. Further, the modular nature of individual amino acid sensors communicating with and converging on the mTORC1 pathway presents a mechanistic basis for tuning sensitivity towards specific nutrient inputs. Given the diversity of metabolic needs and cellular functions across cell types in the mammalian body, how is the specificity of sensing

particular nutrients exploited to tune mTORC1 activity for these heterogeneous demands?

To this end, we interrogated the *in vivo* role of nutrient sensing upstream of mTORC1. We characterized the direct sensing of leucine as critical in directing the homeostatic adaptation to dietary leucine availability in mice, establishing direct nutrient sensing upstream of mTORC1 as a mediator of tuning physiological function in response to specific nutrients. We also identified previously-unappreciated spatial and temporal heterogeneity of mTORC1's nutrient sensitivity in two metabolically important tissues, the liver and pancreatic β-cells. Collectively, this work has demonstrated a coordination of nutrient-sensitive cellular signaling to accommodate the complexity of functional demands facing mammalian physiology.

References

Anthony, J.C., F. Yoshizawa, T.G. Anthony, T.C. Vary, L.S. Jefferson, and S.R. Kimball. 2000. Leucine stimulates translation initiation in skeletal muscle of postabsorptive rats via a rapamycin-sensitive pathway. *J. Nutr.* 30:2413-2419.

Araki, K., A.P. Turner, V.O. Shaffer, S. Gangappa, S.A. Keller, M.F. Bachmann, C.P. Larsen, and R. Ahmed. 2009. mTOR regulates memory CD8 T-cell differentiation. *Nature*. 460:108-112.

Bar-Peled, L., L. Chantranupong, A.D. Cherniack, W.W. Chen, K.A. Ottina, B.C. Grabiner, E.D. Spear, S.L. Carter, M. Meyerson, and D.M. Sabatini. 2013. A Tumor suppressor complex with GAP activity for the Rag GTPases that signal amino acid sufficiency to mTORC1. *Science*. 340:1100-1106.

Ben-Sahra, I., J.J. Howell, J.M. Asara, and B.D. Manning. 2013. Stimulation of de novo pyrimidine synthesis by growth signaling through mTOR and S6K1. *Science*. 339:1323-1328.

Bentzinger, C.F., K. Romanino, D. Cloëtta, S. Lin, J.B. Mascarenhas, F. Oliveri, J. Xia, E. Casanova, C.F. Costa, M. Brink, F. Zorzato, M.N. Hall, and M.A. Rüegg. 2008. Skeletal muscle-specific ablation of raptor, but not of rictor, causes metabolic changes and results in muscle dystrophy. *Cell Metab*. 8:411-424.

Bodine, S.C., T.N. Stitt, M. Gonzalez, W.O. Kline, G.L. Stover, R. Bauerlein, E. Zlotchenko, A. Scrimgeour, J.C. Lawrence, D.J. Glass, and G.D. Yancopoulos. 2001. Akt/mTOR pathway is a crucial regulator of skeletal muscle hypertrophy and can prevent muscle atrophy in vivo. *Nat. Cell Biol*. 3:1014-1019.

Brown, E.J., M.W. Albers, T.B. Shin, K. Ichikawa, C.T. Keith, W.S. Lane, and S.L. Schreiber. 1994. A mammalian protein targeted by G1-arresting rapamycin-receptor complex. *Nature*. 369:756-758.

Brugarolas, J., K. Lei, R.L. Hurley, B.D. Manning, J.H. Reiling, E. Hafen, L.A. Witters, L.W. Ellisen, and W.G. Kaelin, Jr. 2004. Regulation of mTOR function in response to hypoxia by REDD1 and the TSC1/TSC2 tumor suppressor complex. *Genes Dev*. 18:2893-2904.

Brunn, G.J., C.C. Hudson, A. Sekulić, J.M. Williams, H. Hosoi, P.J. Houghton, J.C. Lawrence Jr., and R.T. Abraham. 1997. Phosphorylation of the translational repressor PHAS-I by the mammalian target of rapamycin. *Science*. 277:99-101.

Buckbinder, L., R. Talbott, B.R. Seizinger, and N. Kley. 1994. Gene regulation by temperature-sensitive p53 mutants: identification of p53 response genes. *Proc. Natl. Acad. Sci. U.S.A.* 91:10640–10644.

Budanov, A.V. and M. Karin M. 2008. p53 target genes sestrin1 and sestrin2 connect genotoxic stress and mTOR signaling. *Cell*. 134:451-60.

Budanov, A. V., T. Shoshani, A. Faerman, E. Zelin, I. Kamer, H. Kalinski, S. Gorodin, A. Fishman, A. Chajut, P. Einat, R. Skaliter, A.V. Gudkov, P.M. Chumakov, and E. Feinstein. 2002. Identification of a novel stress-responsive gene Hi95 involved in regulation of cell viability. *Oncogene* 21:6017–6031.

Cafferkey, R., P.R. Young, M.M. McLaughlin, D.J. Bergsma, Y. Koltin, G.M. Sathe, L. Faucette, W.K. Eng, R.K. Johnson, and G.P. Livi. 1993. Dominant missense mutations in a novel yeast protein related to mammalian phosphatidylinositol 3-kinase and VPS34 abrogate rapamycin cytotoxicity. *Mol Cell Biol*. 13:6012-6023.

Castellano, B.M., A.M. Thelen, O. Moldavski, M. Feltes, R.E. van der Welle, L. Mydock-

McGrane, X. Jiang, R.J. van Eijkeren, O.B. Davis, S.M. Louie, R.M. Perera, D.F. Covey, D.K. Nomura, D.S. Ory, and R. Zoncu. 2017. Lysosomal cholesterol activates mTORC1 via an SLC38A9-Niemann-Pick C1 signaling complex. *Science*. 355:1306-1311.

Castets, P. S. Lin, N. Rion, S. Di Fulvio, K. Romanino, M. Guridi, S. Frank, L.A. Tintignac, M. Sinnreich, and M.A. Rüegg. 2013. Sustained activation of mTORC1 in skeletal muscle inhibits constitutive and starvation-induced autophagy and causes a severe, late-onset myopathy. *Cell Metab*. 17:731-744.

Chantranupong, L., S.M. Scaria, R.A. Saxton, M.P. Gygi, K. Shen, G.A. Wyant, T. Wang, J.W. Harper, S.P. Gygi, and D.M. Sabatini. 2016. The CASTOR Proteins Are Arginine Sensors for the mTORC1 Pathway. *Cell*. 165:153-164.

Chen, C., S. Jeon, P.T. Bhaskar, V. Nogueira, D. Sundararajan, I. Tonic, Y. Park, and N. Hay. 2010. FoxOs inhibit mTORC1 and activate Akt by inducing the expression of Sestrin3 and Rictor. *Dev. Cell.* 18:592–604.

Chen, C., Y. Liu, Y. Liu, and P. Zheng. 2009. mTOR regulation and therapeutic rejuvenation of aging hematopoietic stem cells. *Sci. Signal*. 2:ra75.

Chung, J., C.J. Kuo, G.R. Crabtree, and J. Blenis. 1992. Rapamycin-FKBP specifically blocks growth-dependent activation of and signaling by the 70 kd S6 protein kinases. *Cell*. 69:1227-1236.

Cloëtta, D., V. Thomanetz, C. Baranek, R.M. Lustenberger, S. Lin, F. Oliveri, S. Atanasoski, and M.A. Rüegg. 2013. Inactivation of mTORC1 in the Developing Brain Causes Microcephaly and Affects Gliogenesis. *J Neurosci*. 33:7799-7810.

Dibble, C.C., W. Elis, S. Menon, W. Qin, J. Klekota, J.M. Asara, P.M. Finan, D.J. Kwiatkowski, L.O. Murphy, and B.D. Manning. 2012. TBC1D7 is a third subunit of the TSC1-TSC2 complex upstream of mTORC1. *Mol Cell*. 47:535-546.

Dorrello, N.V., A. Peschiaroli, D. Guardavaccaro, N.H. Colburn, N.E. Sherman, and M. Pagano M. 2006. S6K1- and betaTRCP-mediated degradation of PDCD4 promotes protein translation and cell growth. *Science*. 2006; 314: 467-471.

Durán, R.V., W. Oppliger, A.M. Robitaille, L. Heiserich, R. Skendaj, E. Gottlieb, and M.N. Hall. 2012. Glutaminolysis activates Rag-mTORC1 signaling. *Mol Cell*. 47:349-58.

Düvel, K., J.L. Yecies, S. Menon, P. Raman, A.I. Lipovsky, A.L. Souza, E. Triantafellow, Q. Ma, R. Gorski, S. Cleaver, M.G. Vander Heiden, J.P. MacKeigan, P.M. Finan, C.B. Clish, L.O. Murphy, and B.D. Manning. Activation of a metabolic gene regulatory network downstream of mTOR complex 1. *Mol. Cell*. 2010; 39:171-183.

Efeyan, A., R. Zoncu, S. Chang, I. Gumper, H. Snitkin, R.L. Wolfson, O. Kirak, D.D. Sabatini, and D.M. Sabatini. 2013. Regulation of mTORC1 by the Rag GTPases is necessary for neonatal autophagy and survival. *Nature*. 493:679-683.

Eng, C.P., S.N. Sehgal, and C. Vézina. 1984. Activity of rapamycin (AY-22,989) against transplanted tumors. *J Antibiot (Tokyo)*. 37:1231-1237.

Frias, M.A., C.C. Thoreen, J.D. Jaffe, W. Schroder, T. Sculley, S.A. Carr, and D.M. Sabatini. 2006. mSin1 is necessary for Akt/PKB phosphorylation, and its isoforms define three distinct mTORC2s. *Curr Biol*. 16:1865-1870.

Gan, X., J. Wang, B. Su, and D. Wu. 2011. Evidence for Direct Activation of mTORC2

Kinase Activity by Phosphatidylinositol 3,4,5-Trisphosphate*. *Journal of Biological Chemistry*. 286:10998-11002.
Garaeva, A.A., I.E. Kovaleva, P.M. Chumakov, and A.G. Evstafieva. 2016. Mitochondrial dysfunction induces SESN2 gene expression through Activating Transcription Factor 4. *Cell Cycle*. 15:64–71.
García-Martínez, J.M. and D.R. Alessi. 2008. mTOR complex 2 (mTORC2) controls hydrophobic motif phosphorylation and activation of serum- and glucocorticoid-induced protein kinase 1 (SGK1). *Biochem. J*. 416:375-385.
Gingras, A.C., S.P. Gygi, B. Raught, R.D. Polakiewicz, R.T. Abraham, M.F. Hoekstra, R. Aebersold, and N. Sonenberg. 1999. Regulation of 4E-BP1 phosphorylation: A novel two-step mechanism. *Genes Dev*. 13:1422-1437.
Gu, X., J.M. Orozco, R.A. Saxton, K.J. Condon, G.Y. Liu, P.A. Krawczyk, S.M. Scaria, J.W. Harper, S.P. Gygi, and D.M. Sabatini. 2017. SAMTOR is an S-adenosylmethionine sensor for the mTORC1 pathway. *Science*. 358:813-818.
Gwinn, D.M., D.B. Shackelford, D.F. Egan, M.M. Mihaylova, A. Mery, D.S. Vasquez, B.E. Turk, and R.J. Shaw. 2008. AMPK phosphorylation of raptor mediates a metabolic checkpoint. *Mol Cell*. 30:214-226.
Hagenbuchner, J., A. Kuznetsov, M. Hermann, B. Hausott, P. Obexer, and M.J. Ausserlechner. 2012. FOXO3-induced reactive oxygen species are regulated by BCL2L11 (Bim) and SESN3. *J. Cell Sci*. 125:1191–1203.
Han, J.M., S.J. Jeong, M.C. Park, G. Kim, N.H. Kwon, H.K. Kim, S.H. Ha, S.H. Ryu, and S. Kim. 2012. Leucyl-tRNA synthetase is an intracellular leucine sensor for the mTORC1-signaling pathway. *Cell*. 149:410-24.
Hara, K., Y. Maruki, X. Long, K. Yoshino, N. Oshiro, S. Hidayat, C. Tokunaga, J. Avruch, and K. Yonezawa. 2002. Raptor, a binding partner of target of rapamycin (TOR), mediates TOR action. *Cell*. 110:177-189.
Haxhinasto, S., D. Mathis, and C. Benoist. 2008. The AKT-mTOR axis regulates de novo differentiation of CD4+Foxp3+ cells. *J. Exp. Med*. 205: 565-574.
He, X.D., W. Gong, J.N. Zhang, J. Nie, C.F. Yao, F.S. Guo, Y. Lin, X.H. Wu, F. Li, J. Li, W.C. Sun, E.D. Wang, Y.P. An, H.R. Tang, G.Q. Yan, P.Y. Yang, Y. Wei, Y.Z. Mao, P.C. Lin, J.Y. Zhao, Y. Xu, W. Xu, and S.M. Zhao. 2018. Sensing and transmitting intracellular amino acid signals through reversible lysine aminoacylations. *Cell Metab*. 27:151-166.e6.
Heitman, J., N.R. Movva, and M.N. Hall. 1991. Targets for cell cycle arrest by the immunosuppressant rapamycin in yeast. *Science*. 253:905-909.
Helman, A., A. Klochendler, N. Azazmeh, Y. Gabai, E. Horwitz, S. Anzi, A. Swisa, R. Condiotti, R.Z. Granit, Y. Nevo, Y. Fixler, D. Shreibman, A. Zamir, S. Tornovsky-Babeay, C. Dai, B. Glaser, A.C. Powers, A.M.J. Shapiro, M.A. Magnuson, Y. Dor, and I. Ben-Porath. 2016. p16Ink4a-induced senescence of pancreatic beta cells enhances insulin secretion. *Nat Med*. 22:412–420.
Holz, M.K., B.A. Ballif, S.P. Gygi, and J. Blenis. 2005. mTOR and S6K1 mediate assembly of the translation preinitiation complex through dynamic protein interchange and ordered phosphorylation events. *Cell*. 123:569-580.
Hosokawa, N., T. Hara, T. Kaizuka, C. Kishi, A. Takamura, Y. Miura, S. Iemura, T.

Natsume, K. Takehana, N. Yamada, J.L. Guan, N. Oshiro, and N. Mizushima. 2009. Nutrient dependent mTORC1 association with the ULK1-Atg13-FIP200 complex required for autophagy. *Molecular biology of the cell*. 20:1981-1991.
Inoki, K., Y. Li, T. Zhu, J. Wu, and K.L. Guan. 2002. TSC2 is phosphorylated and inhibited by Akt and suppresses mTOR signalling. *Nat Cell Biol*. 4:648-657.
Inoki, K., T. Zhu, and K.L. Guan. 2003. TSC2 mediates cellular energy response to control cell growth and survival. *Cell*. 115:577-590.
Jacinto, E., V. Facchinetti, D. Liu, N. Soto, S. Wei, S.Y. Jung, Q. Huang, J. Qin, and B. Su. 2006. SIN1/MIP1 maintains rictor-mTOR complex integrity and regulates Akt phosphorylation and substrate specificity. *Cell*. 127:125-137.
Jacinto, E., R. Loewith, A. Schmidt, S. Lin, M.A. Rüegg, A. Hall, and M.N. Hall. 2004. Mammalian TOR complex 2 controls the actin cytoskeleton and is rapamycin insensitive. *Nat. Cell Biol*. 6:1122-1128.
Jia, K., D. Chen, and D.L. Riddle. 2004. The TOR pathway interacts with the insulin signaling pathway to regulate C. elegans larval development, metabolism and life span. *Development*. 131:3897-3906.
Joseph, G.A., S.X Wang, C.E. Jacobs, W. Zhou, G.C. Kimble, H.W. Tse, J.K. Eash, T. Shavlakadze, and D.J. Glass. 2019. Partial Inhibition of mTORC1 in Aged Rats Counteracts the Decline in Muscle Mass and Reverses Molecular Signaling Associated with Sarcopenia. *Mol Cell Biol*. 39:e00141-19.
Kaeberlein, M., R.W. Powers 3rd, K.K. Steffen, E.A. Westman, D. Hu, N. Dang, E.O. Kerr, K.T. Kirkland, S. Fields, and B.K. Kennedy. 2005. Regulation of yeast replicative life span by TOR and Sch9 in response to nutrients. *Science*. 310:1193-1196.
Kapahi, P., B.M. Zid, T. Harper, D. Koslover, V. Sapin, and S. Benzer. 2004. Regulation of lifespan in Drosophila by modulation of genes in the TOR signaling pathway. *Curr. Biol.* 14:885-890.
Khamzina, L., A. Veilleux, S. Bergeron, and A. Marette. 2005. Increased activation of the mammalian target of rapamycin pathway in liver and skeletal muscle of obese rats: Possible involvement in obesity-linked insulin resistance. *Endocrinology*. 146:1473-1481.
Kilberg, M.S., J. Shan, and N. Su. 2009. ATF4-dependent transcription mediates signaling of amino acid limitation. *Trends Endocrinol Metab*. 20:436–443.
Kim, J., M. Kundu, B. Viollet, and K.L. Guan. 2011. AMPK and mTOR regulate autophagy through direct phosphorylation of Ulk1. *Nat Cell Biol*. 13:132-141.
Kim, J.H., C., Lee, M. Lee, H. Wang, K. Kim, S.J. Park, I. Yoon, J. Jang, H. Zhao, H.K. Kim, N.H. Kwon, S.J. Jeong, H.C. Yoo, J.H. Kim, J.S. Yang, M.Y. Lee, C.W. Lee, J. Yun, S.J. Oh, J.S. Kang, S.A. Martinis, K.Y. Hwang, M. Guo, G. Han, J.M. Han, and S. Kim. 2017. Control of leucine-dependent mTORC1 pathway through chemical intervention of leucyl-tRNA synthetase and RagD interaction. *Nat Commun*. 8:732.
Kim, D.H., D.D. Sarbassov, S.M. Ali, King J.E., Latek R.R., Erdjument-Bromage H., Tempst P., and D.M. Sabatini. 2002. mTOR interacts with raptor to form a nutrient-sensitive complex that signals to the cell growth machinery. *Cell*. 110:163-175.
Kim, D.H., D.D. Sarbassov, S.M. Ali, R.R. Latek, K.V. Guntur, H. Erdjument-Bromage,

P. Tempst, and D.M. Sabatini. 2003. GbetaL, a positive regulator of the rapamycin-sensitive pathway required for the nutrient-sensitive interaction between raptor and mTOR. *Mol Cell*. 11:895-904.

Kunz, J., R. Henriquez, U. Schneider, M. Deuter-Reinhard, N.R. Movva, and M.N. Hall. 1993. Target of rapamycin in yeast, TOR2, is an essential phosphatidylinositol kinase homolog required for G1 progression. *Cell*. 73:585-596.

Lamming, D.W., L. Ye, P. Katajisto, M.D. Goncalves, M. Saitoh, D.M. Stevens, J.G. Davis, A.B. Salmon, A. Richardson, R.S. Ahima, D.A. Guertin, D.M. Sabatini, and J.A. Baur. 2012. Rapamycin-induced insulin resistance is mediated by mTORC2 loss and uncoupled from longevity. *Science*. 335:1638-43.

Lawrence, R.E., K.F. Cho, R. Rappold, A. Thrun, M. Tofaute, D.J. Kim, O. Moldavski, J.H. Hurley, and R. Zoncu. 2018. A nutrient-induced affinity switch controls mTORC1 activation by its Rag GTPase-Ragulator lysosomal scaffold. *Nat Cell Biol*. 20:1052-1063.

Lebrun-Julien, F., L. Bachmann, C. Norrmén, M. Trötzmüller, H. Köfeler, M.A. Rüegg, M.N. Hall, and U. Suter. 2014. Balanced mTORC1 Activity in Oligodendrocytes Is Required for Accurate CNS Myelination. *J Neurosci*. 34:8432–8448.

Lei, H.T., J. Ma, S. Sanchez Martinez, and T. Gonen. 2018. Crystal structure of arginine-bound lysosomal transporter SLC38A9 in the cytosol-open state. *Nat Struct Mol Biol*. 25:522-527.

Li, Y., M.N. Corradetti, K. Inoki, and K.L. Guan. 2004. TSC2: filling the GAP in the mTOR signaling pathway. *Trends Biochem Sci*. 29:32-38

Li, X. and T. Gao. 2014. mTORC2 phosphorylates protein kinase Cζ to regulate its stability and activity. *EMBO Rep*. 15:191-198.

Linares, J.F., A. Duran, T. Yajima, M. Pasparakis, J. Moscat, and M.T. Diaz-Meco. 2013. K63 polyubiquitination and activation of mTOR by the p62-TRAF6 complex in nutrient-activated cells. *Mol Cell*. 51:283-96.

Ma, L., Z. Chen, H. Erdjument-Bromage, P. Tempst, and P.P. Pandolfi. 2005. Phosphorylation and functional inactivation of TSC2 by Erk implications for tuberous sclerosis and cancer pathogenesis. *Cell*. 121:179-193.

Ma, X.M., S.O. Yoon, C.J. Richardson, K. Jülich, and J. Blenis. 2008. SKAR links pre-mRNA splicing to mTOR/S6K1-mediated enhanced translation efficiency of spliced mRNAs. *Cell*. 133:303-313.

Magdalon, J., P. Chimin, T. Belchior, R.X. Neves, M.A. Vieira-Lara, M.L. Andrade, T.S. Farias, A. Bolsoni-Lopes, V.A. Paschoal, A.S.Yamashita, A.J. Kowaltowski, W.T. Festuccia. 2016. Constitutive adipocyte mTORC1 activation enhances mitochondrial activity and reduces visceral adiposity in mice. *Biochim Biophys Acta*. 1861:430-8.

Manning, B.D., A.R. Tee, M.N. Logsdon, J. Blenis, and L.C. Cantley. 2002. Identification of the Tuberous Sclerosis Complex-2 Tumor Suppressor Gene Product Tuberin as a Target of the Phosphoinositide 3-Kinase/Akt Pathway. *Molecular Cell*. 10:151-162.

Martel, R.R., J. Klicius, and S. Galet. 1977. Inhibition of the immune response by rapamycin, a new antifungal antibiotic. Can J Physiol Pharmacol. 55:48-51.

Martina, J.A., Y. Chen, M. Gucek, and R. Puertollano. 2012. MTORC1 functions as a transcriptional regulator of autophagy by preventing nuclear transport of TFEB.

Autophagy. 8:903-914.
Meikle, L., D.M. Talos, H. Onda, K. Pollizzi, A. Rotenberg, M. Sahin, F.E. Jensen, and D.J. Kwiatkowski. 2007. A Mouse Model of Tuberous Sclerosis: Neuronal Loss of Tsc1 Causes Dysplastic and Ectopic Neurons, Reduced Myelination, Seizure Activity, and Limited Survival. *J Neurosci*. 27: 5546–5558.
Menon, S., J.L. Yecies, H.H. Zhang, J.J. Howell, J. Nicholatos, E. Harputlugil, R.T. Bronson, D.J. Kwiatkowski, and B.D. Manning. 2013. Chronic Activation of mTOR Complex 1 is Sufficient to Cause Hepatocellular Carcinoma. *Sci Signal*. 5:ra24.
Ni, Q., Y. Gu, Y. Xie, Q. Yin, H. Zhang, A. Nie, W. Li, Y. Wang, G. Ning, W. Wang, and Q. Wang. 2017. Raptor regulates functional maturation of murine beta cells. *Nat Comm*. 8:15755.
Nickerson, M.L., M.B. Warren, J.R. Toro, V. Matrosova, G. Glenn, M.L. Turner, P. Duray, M. Merino, P. Choyke, C.P. Pavlovich, N. Sharma, M. Walther, D. Munroe, R. Hill, E. Maher, C. Greenberg, M.I. Lerman, W.M. Linehan, B. Zbar, and L.S. Schmidt. 2002. Mutations in a novel gene lead to kidney tumors, lung wall defects, and benign tumors of the hair follicle in patients with the Birt-Hogg-Dubé syndrome. *Cancer Cell*. 2:157-64.
Nogueira, V., Y. Park, C. Chen, P. Xu, M. Chen, I. Tonic, T. Unterman, and N. Hay. 2008. Akt determines replicative senescence and oxidative or oncogenic premature senescence and sensitizes cells to oxidative apoptosis. *Cancer Cell*. 14:458-70.
Okosun, J., R.L. Wolfson, J. Wang, S. Araf, L. Wilkins, B.M. Castellano, L. Escudero-Ibarz, A.F. Al Seraihi, J. Richter, S.H. Bernhart, A. Efeyan, S. Iqbal, J. Matthews, A. Clear, J.A. Guerra-Assunção, C. Bödör, H. Quentmeier, C. Mansbridge, P. Johnson, A. Davies, J.C. Strefford, G. Packham, S. Barrans, A. Jack, M. Du, M. Calaminici, T.A. Lister, R. Auer, S. Montoto, J.G. Gribben, R. Siebert, C. Chelala, R. Zoncu, D.M. Sabatini, and J. Fitzgibbon. 2016. Recurrent mTORC1-activating RRAGC mutations in follicular lymphoma. *Nat Genet*. 48:183-8.
Orozco, J.M., P.A. Krawczyk, S.M. Scaria, A.L. Cangelosi, S.H. Chan, T. Kunchok, C.A. Lewis, and D.M. Sabatini. 2020. Dihydroxyacetone phosphate signals glucose availability to mTORC1. *Nat Metab*. 2:893-901.
Pearce, L.R., X. Huang, J. Boudeau, R. Pawlowski, S. Wullschleger, M. Deak, A.F. Ibrahim, R. Gourlay, M.A. Magnuson, and D.R. Alessi. 2007. Identification of Protor as a novel Rictor-binding component of mTOR complex-2. *Biochem J*. 405:513-522.
Peeters, H., P. Debeer, A. Bairoch, V. Wilquet, C. Huysmans, E. Parthoens, J.P. Fryns, M. Gewillig, Y. Nakamura, N. Niikawa, W. Van de Ven, and K. Devriendt. 2003. PA26 is a candidate gene for heterotaxia in humans: identification of a novel PA26-related gene family in human and mouse. *Hum. Genet*. 112, 573–580.
Peng, M., N. Yin, and M.O. Li. 2014. Sestrins function as guanine nucleotide dissociation inhibitors for Rag GTPases to control mTORC1 signaling. *Cell*. 159:122-133.
Peng, M., N. Yin, and M.O. Li. 2017. SZT2 dictates GATOR control of mTORC1 signalling. *Nature*. 543:433-437.
Peterson, T.R., M. Laplante, C.C. Thoreen, Y. Sancak, S.A. Kang, W.M. Kuehl, N.S.

Gray, and D.M. Sabatini. 2009. DEPTOR is an mTOR inhibitor frequently overexpressed in multiple myeloma cells and required for their survival. *Cell*. 137:873-886.

Peterson, T.R., S.S. Sengupta, T.E. Harris, A.E. Carmack, S.A. Kang, E. Balderas, D.A. Guertin, K.L. Madden, A.E. Carpenter, B.N. Finck, and D.M. Sabatini. 2011. mTOR complex 1 regulates lipin 1 localization to control the SREBP pathway. *Cell*. 146:408-420.

Petit, C.S., A. Roczniak-Ferguson, and S.M. Ferguson. 2013. Recruitment of folliculin to lysosomes supports the amino acid-dependent activation of Rag GTPases. *J Cell Biol*. 202:1107-1122.

Powell, J.D., K.N. Pollizzi, E.B. Heikamp, and M.R. Horton. 2012. Regulation of immune responses by mTOR. *Annu. Rev. Immunol*. 30:39-68.

Robitaille, A.M., S. Christen, M. Shimobayashi, M. Cornu, L.L. Fava, S. Moes, C. Prescianotto-Baschong, U. Sauer, P. Jenoe, and M.N. Hall. 2013. Quantitative phosphoproteomics reveal mTORC1 activates de novo pyrimidine synthesis. *Science*. 339:1320-1323.

Polak, P., N. Cybulski, J.N. Feige, J. Auwerx, M.A. Rüegg, and M.N. Hall. 2008. Adipose-specific knockout of raptor results in lean mice with enhanced mitochondrial respiration. *Cell Metab*. 8:399-410.

Roux, P.P., B.A. Ballif, R. Anjum, S.P. Gygi, and J. Blenis. 2004. Tumor-promoting phorbol esters and activated Ras inactivate the tuberous sclerosis tumor suppressor complex via p90 ribosomal S6 kinase. *Proc Natl Acad Sci U S A*. 101:13489-13494.

Sabatini, D.M., H. Erdjument-Bromage, M. Lui, P. Tempst, and S.H. Snyder. 1994. RAFT1: A mammalian protein that binds to FKBP12 in a rapamycin-dependent fashion and is homologous to yeast TORs. *Cell*. 78:35-43.

Sabers, C.J., M.M. Martin, G.J. Brunn, J.M. Williams, F.J. Dumont, G. Wiederrecht, and R.T. Abraham. 1995. Isolation of a Protein Target of the FKBP12-Rapamycin Complex in Mammalian Cells (∗). *Journal of Biological Chemistry*. 270:815-822.

Sancak, Y., L. Bar-Peled, R. Zoncu, A.L. Markhard, S. Nada, and D.M. Sabatini. 2010. Ragulator Rag complex targets mTORC1 to the lysosomal surface and is necessary for its activation by amino acids. *Cell*. 141:290-303.

Sancak, Y., T.R. Peterson, Y.D. Shaul, R.A. Lindquist, C.C. Thoreen, L. Bar-Peled, and D.M. Sabatini. 2008. The Rag GTPases bind raptor and mediate amino acid signaling to mTORC1. *Science*. 320:1496-1501.

Sancak, Y., C.C. Thoreen, T.R. Peterson, R.A. Lindquist, S.A. Kang, E. Spooner, S.A. Carr, and D.M. Sabatini. 2007. PRAS40 is an insulin-regulated inhibitor of the mTORC1 protein kinase. *Mol Cell*. 25:903-915.

Sarbassov, D.D., S.M. Ali, D.H. Kim, D.A. Guertin, R.R. Latek, H. Erdjument-Bromage, P. Tempst, and D.M. Sabatini. 2004. Rictor, a novel binding partner of mTOR, defines a rapamycin insensitive and raptor-independent pathway that regulates the cytoskeleton. *Curr Biol*. 14:1296-1302.

Sarbassov, D.D., S.M. Ali, S. Sengupta, J.H. Sheen, P.P. Hsu, A.F. Bagley, A.L. Markhard, and D.M. Sabatini. 2006. Prolonged rapamycin treatment inhibits mTORC2 assembly and Akt/PKB. *Mol. Cell*. 22:159-168.

Sarbassov, D.D., D.A. Guertin, S.M. Ali, and D.M. Sabatini. 2005. Phosphorylation and

regulation of Akt/PKB by the rictor-mTOR complex. *Science*. 307:1098-1101.
Sardiello, M., M. Palmieri, A. di Ronza, D.L. Medina, M. Valenza, V.A. Gennarino, C. Di Malta, F. Donaudy, V. Embrione, R.S. Polishchuk, S. Banfi, G. Parenti, E. Cattaneo, and A. Ballabio. 2009. A Gene Network Regulating Lysosomal Biogenesis and Function. *Science*. 325:473.
Saxton, R.A., K.E. Knockenhauer, R.L. Wolfson, L. Chantranupong, M.E. Pacold, T. Wang, T.U. Schwartz, and D.M. Sabatini. 2016. Structural basis for leucine sensing by the Sestrin2-mTORC1 pathway. *Science*. 351:53-58.
Schinaman, J.M., A. Rana, W.W. Ja, R.I. Clark, and D.W. Walker. 2019. Rapamycin modulates tissue aging and lifespan independently of the gut microbiota in Drosophila. *Sci Rep*. 9:7824.
Sengupta, S., T.R. Peterson, M. Laplante, S. Oh, and D.M. Sabatini. 2010. mTORC1 controls fasting-induced ketogenesis and its modulation by ageing. *Nature*. 468:1100-1104.
Settembre, C., C. Di Malta, V.A. Polito, M. Garcia Arencibia, F. Vetrini, S. Erdin, S.U. Erdin, T. Huynh, D. Medina, P. Colella, M. Sardiello, D.C. Rubinsztein, and A. Ballabio. 2011. TFEB links autophagy to lysosomal biogenesis. *Science*. 332:1429-1433.
Settembre, C., R. Zoncu, D.L. Medina, F. Vetrini, S. Erdin, S. Erdin, T. Huynh, M. Ferron, G. Karsenty, M.C. Vellard, V. Facchinetti, D.M. Sabatini, and A. Ballabio. 2012. A lysosome to-nucleus signalling mechanism senses and regulates the lysosome via mTOR and TFEB. *Embo j*. 31:1095-1108.
Shaw, R.J., N. Bardeesy, B.D. Manning, L. Lopez, M. Kosmatka, R.A. DePinho, and L.C. Cantley. 2004. The LKB1 tumor suppressor negatively regulates mTOR signaling. *Cancer Cell*. 6:91-99.
Shigeyama, Y., T. Kobayashi, Y. Kido, N. Hashimoto, S. Asahara, T. Matsuda, A. Takeda, T. Inoue, Y. Shibutani, M. Koyanagi, T. Uchida, M. Inoue, O. Hino, M. Kasuga, and T. Noda. 2008. Biphasic response of pancreatic beta-cell mass to ablation of tuberous sclerosis complex 2 in mice. *Mol. Cell. Biol*. 28:2971-2979.
Son, S.M., S.J. Park, H. Lee, F. Siddiqi, J.E. Lee, F.M. Menzies, and D.C. Rubinsztein. 2019. Leucine signals to mTORC1 via its metabolite acetyl-coenzyme A. *Cell Metab*. 29:192-201.e7.
Spilman, P., N. Podlutskaya, M.J. Hart, J. Debnath, O. Gorostiza, D. Bredesen, A. Richardson, R. Strong, and V. Galvan. 2010. Inhibition of mTOR by rapamycin abolishes cognitive deficits and reduces amyloid-beta levels in a mouse model of Alzheimer's disease. *PLoS ONE*. 5:e9979.
Thedieck, K., P. Polak, M.L. Kim, K.D. Molle, A. Cohen, P. Jenö, C. Arrieumerlou, and M.N. Hall. 2007. PRAS40 and PRR5-like protein are new mTOR interactors that regulate apoptosis. *PLoS ONE*. 2: e1217.
Tsun, Z.Y., L. Bar-Peled, L. Chantranupong, R. Zoncu, T. Wang, C. Kim, E. Spooner, and D.M. Sabatini. 2013. The folliculin tumor suppressor is a GAP for the RagC/D GTPases that signal amino acid levels to mTORC1. *Mol Cell*. 52:495-505.
Thomanetz, V., N. Angliker, D. Cloëtta, R.M. Lustenberger, M. Schweighauser, F.

Oliveri, N. Suzuki, and M.A. Rüegg. 2013. Ablation of the mTORC2 component rictor in brain or Purkinje cells affects size and neuron morphology. *J. Cell Biol*. 201: 293-308.

Um, S.H., F. Frigerio, M. Watanabe, F. Picard, M. Joaquin, M. Sticker, S. Fumagalli, P.R. Allegrini, S.C. Kozma, J. Auwerx, and G. Thomas. 2004. Absence of S6K1 protects against age- and diet-induced obesity while enhancing insulin sensitivity. *Nature*. 431:200-205.

Vander Haar, E., S.I. Lee, S. Bandhakavi, T.J. Griffin, and D.H. Kim. 2007. Insulin signalling to mTOR mediated by the Akt/PKB substrate PRAS40. *Nat Cell Biol*. 9:316-323.

Velasco-Miguel, S., L. Buckbinder, P. Jean, L. Gelbert, R. Talbott, J. Laidlaw, B. Seizinger, and N. Kley. 1999. PA26, a novel target of the p53 tumor suppressor and member of the GADD family of DNA damage and growth arrest inducible genes. *Oncogene*. 18:127-37.

Vellai, T., K. Takacs-Vellai, Y. Zhang, A.L. Kovacs, L. Orosz, and F. Müller. 2003. Genetics: Influence of TOR kinase on lifespan in C. elegans. *Nature*. 426:620.

Vézina, C., A. Kudelski, and S.N. Sehgal. 1975. Rapamycin (AY-22,989), a new antifungal antibiotic. I. Taxonomy of the producing streptomycete and isolation of the active principle. *J Antibiot (Tokyo)*. 28:721-726.

Wang, L., T.E. Harris, R.A. Roth R.A., and J.C. Lawrence Jr. 2007. PRAS40 regulates mTORC1 kinase activity by functioning as a direct inhibitor of substrate binding. *J. Biol. Chem*. 282:20036-20044.

Wolfson, R.L., L. Chantranupong, R.A. Saxton, K. Shen, S.M. Scaria, J.R. Cantor, and D.M. Sabatini. 2016. Sestrin2 is a leucine sensor for the mTORC1 pathway. *Science*. 351:43-48.

Wolfson, R.L., L. Chantranupong, G.A. Wyant, X. Gu, J.M. Orozco, K. Shen, K.J. Condon, S. Petri, J. Kedir, S.M. Scaria, M. Abu-Remaileh, W.N. Frankel, and D.M. Sabatini. 2017. KICSTOR recruits GATOR1 to the lysosome and is necessary for nutrients to regulate mTORC1. *Nature*. 543:438-442.

Woo, S.Y., D.H. Kim, C.B. Jun, Y.M. Kim, E.V. Haar, S.I. Lee, J.W. Hegg, S. Bandhakavi, T.J. Griffin, and D.H. Kim. 2007. PRR5, a novel component of mTOR complex 2, regulates platelet-derived growth factor receptor beta expression and signaling. *J. Biol. Chem*. 282: 25604-25612.

Wu, J.J., J. Liu, E.B. Chen, J.J. Wang, L. Cao, N. Narayan, M.M. Fergusson, I.I. Rovira, M. Allen, D.A. Springer, C.U. Lago, S. Zhang, W. DuBois, T. Ward, R. deCabo, O. Gavrilova, B. Mock, and T. Finkel. 2013. Increased mammalian lifespan and a segmental and tissue-specific slowing of aging after genetic reduction of mTOR expression. *Cell Rep*. 4:913-920.

Wyant, G.A., M. Abu-Remaileh, R.L. Wolfson, W.W. Chen, E. Freinkman, L.V. Danai, M.G. Vander Heiden, and D.M. Sabatini. 2017. mTORC1 Activator SLC38A9 Is Required to Efflux Essential Amino Acids from Lysosomes and Use Protein as a Nutrient. *Cell*. 171:642-654.e612.

Xu, D., K.L. Shimkus, H.A. Lacko, L. Kutzler, L.S. Jefferson, and S.R. Kimball. 2019. Evidence for a role for Sestrin1 in mediating leucine-induced activation of mTORC1 in skeletal muscle. *Am J Physiol Endocrinol Metab*. 316:E817-E828.

Yang, Q., K. Inoki, T. Ikenoue, and K.L. Guan. 2006. Identification of Sin1 as an

essential TORC2 component required for complex formation and kinase activity. *Genes Dev.* 20:2820-2832.
Yang, H., D.G Rudge, J.D. Koos, B. Vaidialingam, H.J. Yang, and N.P. Pavletich. 2013. mTOR kinase structure, mechanism and regulation. *Nature*. 497:217-223.
Ye, J., W. Palm, M. Peng, B. King, T. Lindsten, M.O. Li, C. Koumenis, C.B. Thompson. 2015. GCN2 sustains mTORC1 suppression upon amino acid deprivation by inducing Sestrin2. *Genes Dev*. 29:2331-6.
Yilmaz, O.H., P. Katajisto, D.W. Lamming, Y. Gültekin, K.E. Bauer-Rowe, S. Sengupta, K. Birsoy, A. Dursun, V.O. Yilmaz, M. Selig, G.P. Nielsen, M. Mino-Kenudson, L.R. Zukerberg, A.K. Bhan, V. Deshpande, and D.M. Sabatini. 2012. mTORC1 in the Paneth cell niche couples intestinal stem-cell function to calorie intake. *Nature*. 486:490-5.
Yu, Z., Z. Yang, G. Ren, Y. Wang, X. Luo, F. Zhu, S. Yu, L. Jia, M. Chen, P.F. Worley, and B. Xiao. 2022. GATOR2 complex–mediated amino acid signaling regulates brain myelination. *PNAS.* 119:e2110917119.
Yuskaitis, C.J., B.M. Jones, R.L. Wolfson, C.E. Super, S.C. Dhamne, A. Rotenberg, D.M. Sabatini, M. Sahin, A. Poduri. 2018. A mouse model of DEPDC5-related epilepsy: Neuronal loss of Depdc5 causes dysplastic and ectopic neurons, increased mTOR signaling, and seizure susceptibility. *Neurobiol Dis*. 111:91-101.
Zheng, Y., S.L. Collins, M.A. Lutz, A.N. Allen, T.P. Kole, P.E. Zarek, and J.D. Powell. 2007. A role for mammalian target of rapamycin in regulating T cell activation versus anergy. *J. Immunol*. 178:2163-2170.

Chapter 2

Reprinted from *Science*

Zonated leucine sensing by Sestrin-mTORC1 in the liver controls the adaptation to dietary leucine availability

Andrew L. Cangelosi[1,2,3*], Anna M. Puszynska[1,2], Justin M. Roberts[1,2,3], Andrea Armani[1,2,4,5], Thao P. Nguyen[1,2,3], Jessica B. Spinelli[1,2], Tenzin Kunchok[1], Brianna Wang[1], Sze Ham Chan[1, †], Caroline A. Lewis[1], William C. Comb[1,2, ‡], George W. Bell[1], Aharon Helman[6], David M. Sabatini[3]

[1] Whitehead Institute for Biomedical Research, 455 Main Street, Cambridge, MA 02142.
[2] Howard Hughes Medical Institute, Department of Biology, Massachusetts Institute of Technology, Cambridge, MA 02139.
[3] Department of Biology, Massachusetts Institute of Technology, Cambridge, MA 02139.
[4] Veneto Institute of Molecular Medicine, 35129 Padova, Italy.
[5] Department of Biomedical Sciences, University of Padova, 35131 Padova, Italy.
[6] Institute of Biochemistry, Food Science and Nutrition, Robert H. Smith Faculty of Agriculture, Food and Environment, The Hebrew University of Jerusalem, Rehovot, Israel.
[†] Present address: Department of Pharmacology, University of Virginia, Charlottesville, VA 22903.
[‡] Present address: Mythic Therapeutics, Waltham, MA 02453.
* Correspondence: andrewcangelosi1@gmail.com (A.L.C)

Experiments in Fig. 1 were performed by A.L.C.
Experiments in Fig. S1 were performed by A.L.C.
Experiments in Fig. S2a-c were performed by A.L.C.
Experiments in Fig. S2d-f were performed by A.L.C. and A.M.P.
Experiments in Fig. S3 were performed by A.L.C.
Experiments in Fig. 2 were performed by A.L.C. and A.M.P.
Analysis in Fig. 2h was performed by T.K., B.W., S.H.C., and C.A.L.
Experiments in Fig. S4 were performed by A.L.C. and A.M.P.
Experiments in Fig. S5 were performed by A.L.C. and A.M.P.
Experiments in Fig. S6 were performed by A.L.C. and A.M.P.
Experiments in Fig. S7 were performed by A.L.C. and A.M.P.
Experiments in Fig. S8a-f were performed by A.L.C.
Experiment in Fig. S8g was performed by A.L.C. and A.M.P.
Experiment in Fig. S9 was performed by A.L.C. and A.M.P.
Analysis in Fig. S9 was performed by T.K., B.W., S.H.C., and C.A.L.
Experiment in Fig. S10 was performed by A.L.C. and A.M.P.
Experiment in Fig. S11a-d was performed by A.L.C. and A.M.P.
Experiment in Fig. S11e was performed by A.L.C.

Experiments in Fig. 3 were performed by A.L.C. and A.M.P.
Experiments in Fig. S12a-b were performed by A.L.C.
Experiment in Fig. S12c-e was performed by A.L.C. and A.M.P.
Experiment in Fig. S13 was performed by A.L.C.
Analysis in Fig. S13 was performed by T.K., B.W., S.H.C., and C.A.L.
Experiment in Fig. S14a was performed by A.L.C.
Experiment in Fig. S14b-d was performed by A.L.C. and A.M.P.
Experiment in Fig. 4a was performed by A.L.C.
Experiment in Fig. 4b-e was performed by A.L.C., A.M.P., and A.A.
Experiments in Fig. 4f-j were performed by A.L.C.
Analysis in Fig. 4f was performed by G.W.B.
Analysis in Fig. 4h-i was performed by T.K., B.W., S.H.C., and C.A.L.
Experiments in Fig. S15 were performed by A.L.C.
Experiments in Fig. S16 were performed by A.L.C. and A.M.P.
Experiments in Fig. S17 were performed by A.L.C. and A.M.P.
Analysis in Fig. S17 was performed by G.W.B.
Experiments in Fig. S18 were performed by A.L.C.
Analysis in Fig. S18a-c was performed by T.K., B.W., S.H.C., and C.A.L.
Experiments in Fig. S19 were performed by A.L.C.
Experiment in Fig. S20 was performed by A.L.C.
Experiments in Fig. S21 were performed by A.L.C.
Analysis in Fig. S21a was performed by T.K., B.W., S.H.C., and C.A.L.
Experiment in Fig. S22a was performed by J.M.R.
Experiment in Fig. S22b was performed by A.L.C.
Experiments in Fig. S23 were performed by A.L.C.
Analysis in Fig. S23b was performed by T.K., B.W., S.H.C., and C.A.L.
Experiments in Fig. 5 were performed by A.L.C.
Experiments in Fig. S24 were performed by A.L.C.

Abstract

The mTOR Complex 1 (mTORC1) kinase controls growth in response to a variety of nutrients, including the amino acid leucine. In cultured cells, mTORC1 senses leucine through the leucine-binding Sestrin proteins, but the physiological functions and tissue distribution of Sestrin-mediated leucine sensing in mammals are unknown. We find that mice lacking Sestrin1 and Sestrin2 cannot inhibit mTORC1 upon leucine deprivation or adapt to a diet lacking leucine, but respond normally to diets free of other amino acids. When deprived of leucine, these mice suffer a global dysregulation of amino acid homeostasis and rapid loss of white adipose tissue (WAT) and muscle. The WAT loss is driven by increased levels of the hepatokine FGF21 as a result of mTORC1 dysregulation in the liver. In response to leucine limitation, knockin mice expressing a Sestrin2 point mutant with a low affinity for leucine inhibit mTORC1 more strongly and lose less WAT than control animals. Interestingly, Sestrin expression in the liver lobule is zonated, accounting for the zone-specific regulation of mTORC1 activity and FGF21 induction by leucine. These results establish the mammalian Sestrins as leucine sensors *in vivo* and reveal an unexpected intra-tissue spatial organization to nutrient sensing by the mTORC1 pathway.

Introduction

Leucine is an essential amino acid needed to synthesize proteins and metabolites like branched chain fatty acids (Wallace et al., 2018; Crown et al., 2015; Rosenthal et al., 1974). In addition, it has been appreciated for decades that leucine has unique physiological effects, including promoting skeletal muscle growth (Saxton & Sabatini, 2017; Anthony et al., 2000; Duan et al., 2015; Yin et al., 2010; Li et al., 2011), insulin secretion (Moore et al., 2015; de Oliveira et al., 2011; Yang et al., 2010), and immune function (Ananieva et al., 2016; Ren et al., 2017; Torigoe et al., 2019), as well as modulating healthspan and lifespan in mice (Richardson et al., 2021; D'Antona et al., 2010; Solon-Biet et al., 2019). Moreover, plasma leucine levels are also implicated in certain pathological states, such as metabolic syndrome (Newgard et al., 2009; Lynch et al., 2014; Fontana et al., 2016).

A key effector of leucine is thought to be the mTOR Complex 1 (mTORC1) protein kinase, a master regulator of growth and metabolism. Diverse nutrients, growth factors, and stresses regulate mTORC1 (Saxton & Sabatini, 2017; Liu & Sabatini, 2020; Condon & Sabatini, 2019; Valvezan & Manning, 2019) and understanding how it detects so many inputs has been of longstanding interest. A model has started to emerge of the nutrient-sensing mechanisms upstream of mTORC1 in which nutrient-derived signals converge on the heterodimeric Rag GTPase and their many regulators, including the GATOR1, GATOR2, and Ragulator complexes. The Rag heterodimer binds mTORC1 in a nutrient-sensitive manner to control its localization to the lysosomal surface, where it can interact with its kinase activator, the Rheb GTPase (Saxton & Sabatini, 2017; Liu & Sabatini, 2020; Condon & Sabatini, 2019; Valvezan & Manning, 2019).

How the mTORC1 pathway senses leucine has been highly debated (Han et al., 2012; Kim et al., 2017; He et al., 2018; Duran et al., 2012; Linares et al., 2013; Lawrence et al., 2018; Son et al., 2019; Budanov & Karin, 2008). Several years ago we showed that in cultured cells the leucine-binding proteins Sestrin1 and Sestrin2 serve as leucine sensors for the pathway (Wolfson et al., 2006; Saxton et al., 2016). Growing evidence implicates the Sestrins in various facets of organismal function (Fang et al., 2021; Yang et al., 2021; Lee et al., 2012; Segales et al., 2020; Kim et al., 2020; Lu et al., 2021). However, whether the mammalian Sestrins have a leucine sensing role in vivo, and, if so, in which tissues they act and the physiology they control as leucine sensors, is unknown.

Results

To study leucine sensing by mTORC1 in vivo and minimize confounding effects of other nutrient alterations, we tested the response of mice to changes in the leucine content of the diet. We first refed mice with food containing 100%, 10%, or 0% of the leucine content of standard chow (Fig. 1A). Feeding of these diets caused step-wise reductions in plasma leucine concentrations (Fig. 1B) and in the phosphorylation of the mTORC1 substrates S6K1 and 4EBP1 in the liver (Fig. 1C), showing that in our experimental system dietary leucine controls mTORC1 activity in vivo.

In cultured cells Sestrin1 and Sestrin2 inhibit mTORC1 signaling by interacting with and suppressing—in a leucine-sensitive manner—the GATOR2 complex, a positive component of the mTORC1 pathway (Wolfson et al., 2016). To ask whether the same interaction occurs in vivo, we immunoprecipitated, from the liver of mice, GATOR2 using

an antibody to its WDR24 component. Consistent with leucine disrupting the Sestrin1/2-GATOR2 interaction, GATOR2 co-immunoprecipitated greater amounts of Sestrin1 and Sestrin2 in mice refed the leucine-free than control diet (Fig. 1D). Importantly, the addition of leucine, but not arginine, to the immunopurified complexes disrupted the Sestrin1/2-GATOR2 interaction (Fig. 1D). Thus, like in cultured cells, in mouse tissues in vivo leucine regulates the binding of Sestrin1 and Sestrin2 to GATOR2.

To determine if the regulation of mTORC1 by dietary leucine requires Sestrin1 and Sestrin2, we generated mice that lack both (DKO mice) and fasted and refed them with the control or leucine-free diet. While mTORC1 activity in the liver was low in wildtype mice refed with the leucine-free diet, in DKO mice mTORC1 activity was high, irrespective of the leucine content of the diet in both males (Fig. 1E) and females (fig. S1A). Sestrin expression did not impact food consumption (fig. S2A). Loss of either Sestrin1 or Sestrin2 alone had no impact on the sensitivity of mTORC1 to leucine deprivation (fig. S3A-B), consistent with Sestrin1 and Sestrin2 having redundant functions in cultured cells (Wolfson et al., 2016). Like in the liver, leucine regulates mTORC1 activity in white adipose tissue (WAT) in a Sestrin-dependent manner in males (Fig. 1F) and females (fig. S1B).

Loss of the Sestrins impacts the response of mTORC1 specifically to leucine deprivation. mTORC1 signaling remained sensitive to fasting in the liver and WAT of DKO mice (fig. S2B-C) and to starvation of all amino acids (but not of only leucine) in primary hepatocytes and WAT explants obtained from DKO mice (fig. S2D-E).

The Sestrins have been proposed to impinge on the mTORC1 pathway via regulation of AMPK (Lee et al., 2012). However, liver-specific deletion of both AMPK

catalytic subunits (AMPKα1 and α2) did not affect the activation of hepatic mTORC1 by dietary leucine despite eliminating AMPK activity, as indicated by the absence of phosphorylation of ACC, a canonical AMPK substrate (fig. S3C).

Lastly, based on the structure of the leucine-binding pocket of Sestrin2, we previously identified a point mutation (W444L) that reduces, but does not abolish, the affinity of Sestrin2 for leucine (Saxton et al., 2016). To ask how this mutation impacts the activation of mTORC1 by leucine in vivo, we generated knockin mice expressing Sestrin2 W444L from the endogenous Sesn2 locus (Sesn2W444L mice). Leucine—over a range of concentrations—activated mTORC1 to a lesser degree in primary hepatocytes from Sesn2W444L than control (Sesn2WT) mice (fig. S2F). Similarly, food containing 10% of the leucine content of normal chow activated mTORC1 to a lesser extent in the livers of Sesn2W444L than Sesn2WT mice (Fig. 1G). Thus, the affinity of Sestrin2 for leucine determines the sensitivity of mTORC1 to the leucine content of the diet. Taken together, our results establish that, like in cultured cells, Sestrin1 and Sestrin2 transmit leucine availability to the mTORC1 pathway in vivo.

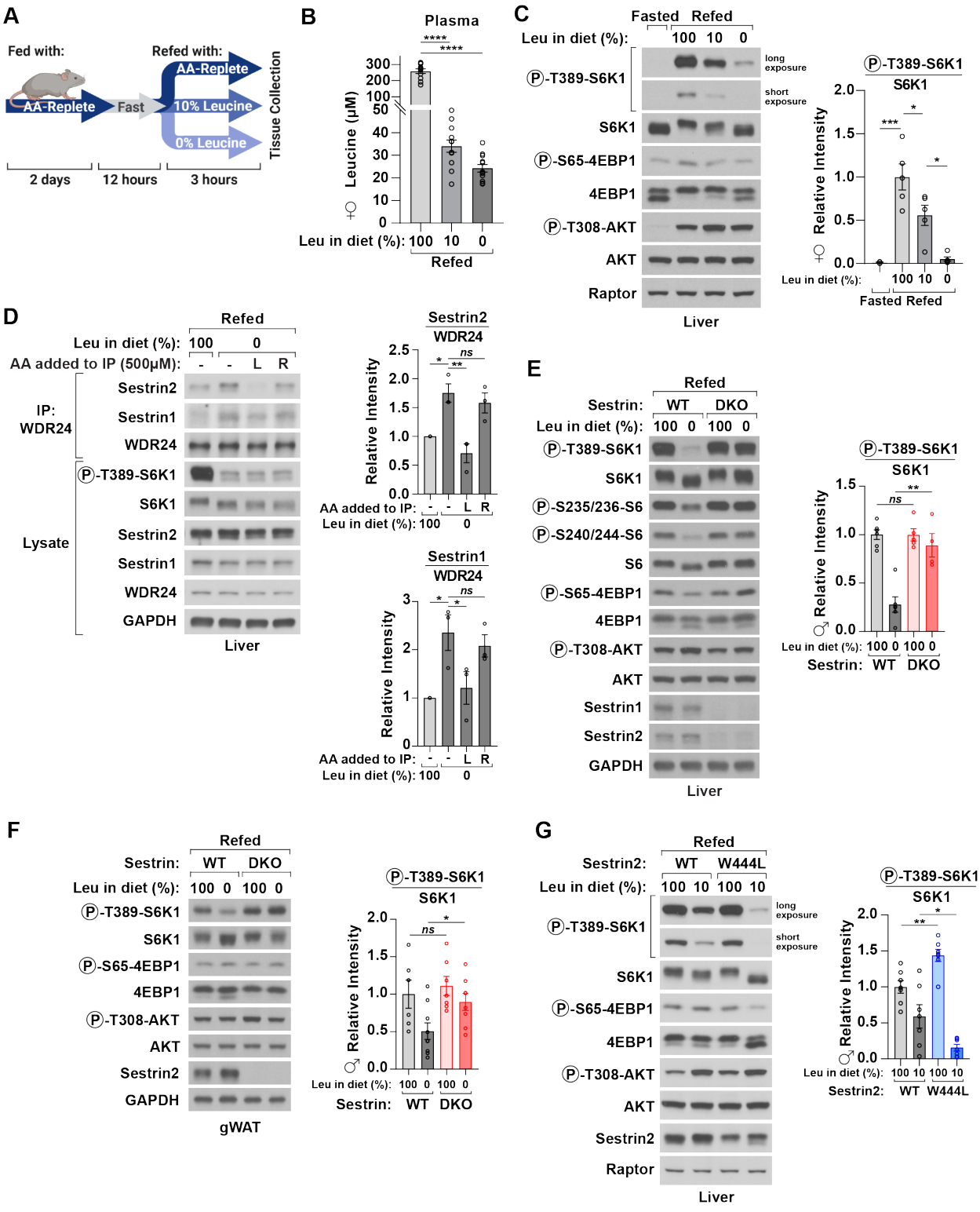

Figure 1: The Sestrins control leucine sensing by mTORC1 in vivo. (A) Schematic of the experimental setup for studying leucine sensing in vivo. Mice maintained on an

amino acid-replete control diet for 2 days were fasted overnight for 12 hours, refed with food containing the indicated leucine contents, and tissues collected 3 hours after the start of the feeding period. Created using Biorender.com. (B) Plasma leucine concentrations in wildtype female mice 3 hours after eating the indicated diets (n=11-12). (C) Phosphorylation state and levels of indicated proteins in liver lysates from wildtype female mice refed with the indicated diets for 3 hours (n=3-5). (D) Dietary leucine regulates Sestrin-GATOR2 interactions. Endogenous WDR24 immunoprecipitates (IPs) were prepared from liver lysates from wildtype male mice refed with the indicated diets for 3 hours. In lanes 2-4, IPs were prepared from equal volumes of the same liver lysate, and, where noted, indicated amino acids were added during washes. IPs and liver lysates were analyzed by immunoblotting for the phosphorylation states and levels of the indicated proteins (n=3). (E) Male mice with indicated genotypes were refed with the indicated diets for 3 hours. Liver lysates were analyzed by immunoblotting for the phosphorylation state and levels of the indicated proteins. (n=4-6). (F) Gonadal WAT lysates from male mice treated as in (E) were analyzed by immunoblotting for the phosphorylation states and levels of the indicated proteins (n=6-9). (G) Female mice with the indicated liver genotypes were refed with diets with different leucine contents for 3 hours and liver lysates analyzed by immunoblotting for the phosphorylation state and levels of the indicated proteins (n=7). Data are the mean ± s.e.m. P values were determined using two-tailed t-tests (B, E-G), one-way ANOVA with Tukey test (B, C), or one-way ANOVA with Dunnett test (D). * $p < 0.05$, ** $p < 0.01$, *** $p < 0.001$, **** $p < 0.0001$.

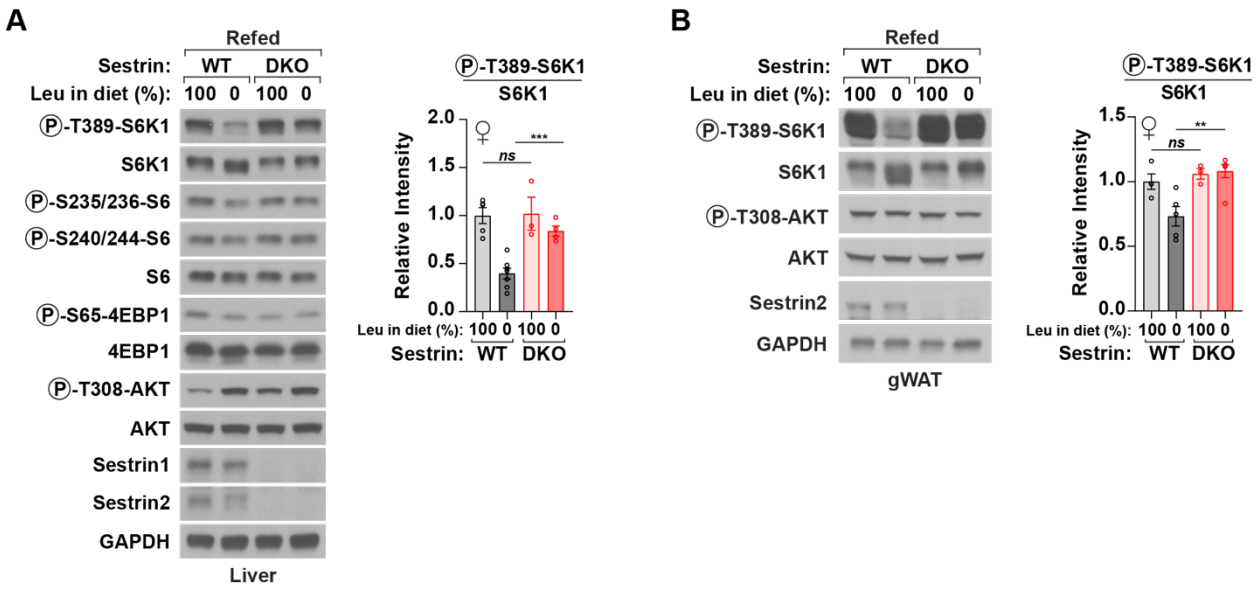

Figure S1: In female Sestrin DKO mice the mTORC1 pathway is insensitive to dietary leucine deprivation in the liver and WAT. (A) Female mice with the indicated genotypes were fasted and refed with the indicated diets for 3 hours. Liver lysates were analyzed by immunoblotting for the phosphorylation state and levels of the indicated proteins. (n=3-7). (B) Female mice with the indicated genotypes were fasted and refed with the indicated diets for 3 hours. Gonadal WAT lysates were analyzed by immunoblotting for the phosphorylation state and levels of the indicated proteins. (n=3-6). Data are the mean ± s.e.m. P values were determined using two-tailed t-test. ** $p < 0.01$, *** $p < 0.001$.

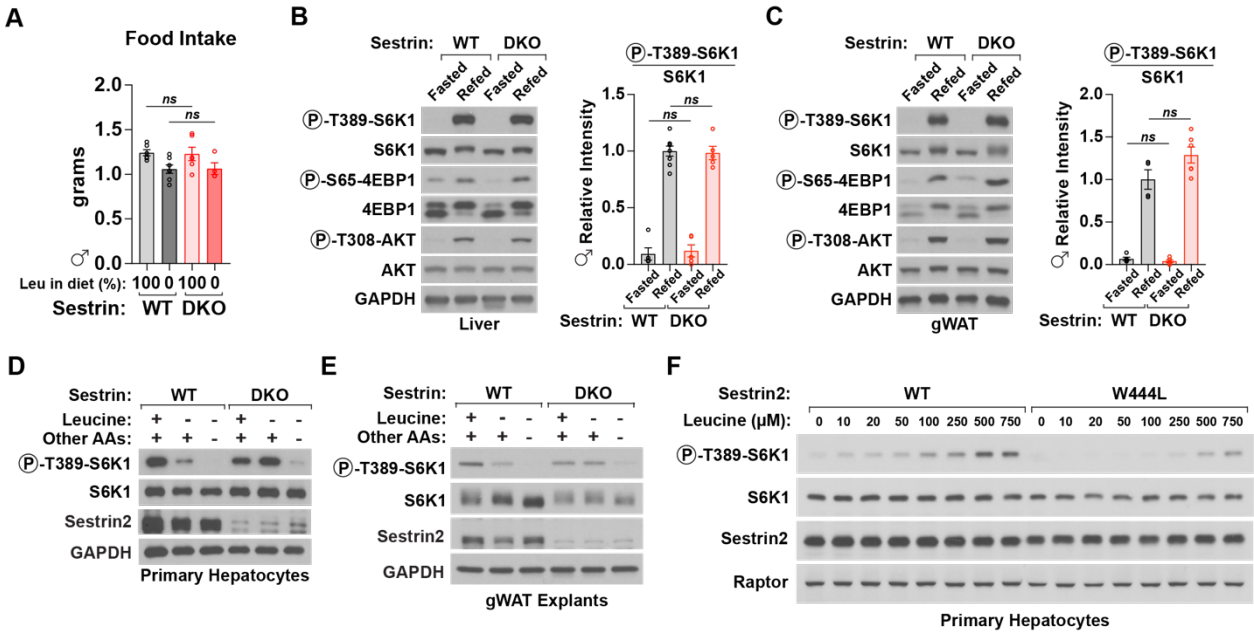

Figure S2: Sestrin DKO mice have normal food intake and retain mTORC1 sensitivity to fasting and to other amino acids in the liver and WAT. (A) Male mice with the indicated genotypes were fasted and refed with the indicated diets for 3 hours, and the amount of food eaten over the 3-hour refeeding period was measured (n=4-6). (B) Male mice with the indicated genotypes were fasted overnight for 12 hours. Liver lysates were analyzed by immunoblotting for the phosphorylation states and levels of the indicated proteins (n=5-8). (C) Male mice with the indicated genotypes were fasted overnight for 12 hours. Gonadal WAT lysates were analyzed by immunoblotting for the phosphorylation states and levels of the indicated proteins (n=4-6). (D-E) Primary hepatocytes or gonadal WAT explants isolated from wildtype or DKO mice were starved of leucine or all amino acids for 1 hour. Lysates were analyzed by immunoblotting for the phosphorylation states and levels of the indicated proteins. (F) Primary hepatocytes isolated from *Sesn2*^{WT} or *Sesn2*^{W444L} mice were starved of leucine for 50 minutes and restimulated with the indicated concentrations of leucine for 10 minutes. Lysates were

analyzed by immunoblotting for the phosphorylation state and levels of the indicated proteins. Data are the mean ± s.e.m. P values were determined using two-tailed t-test.

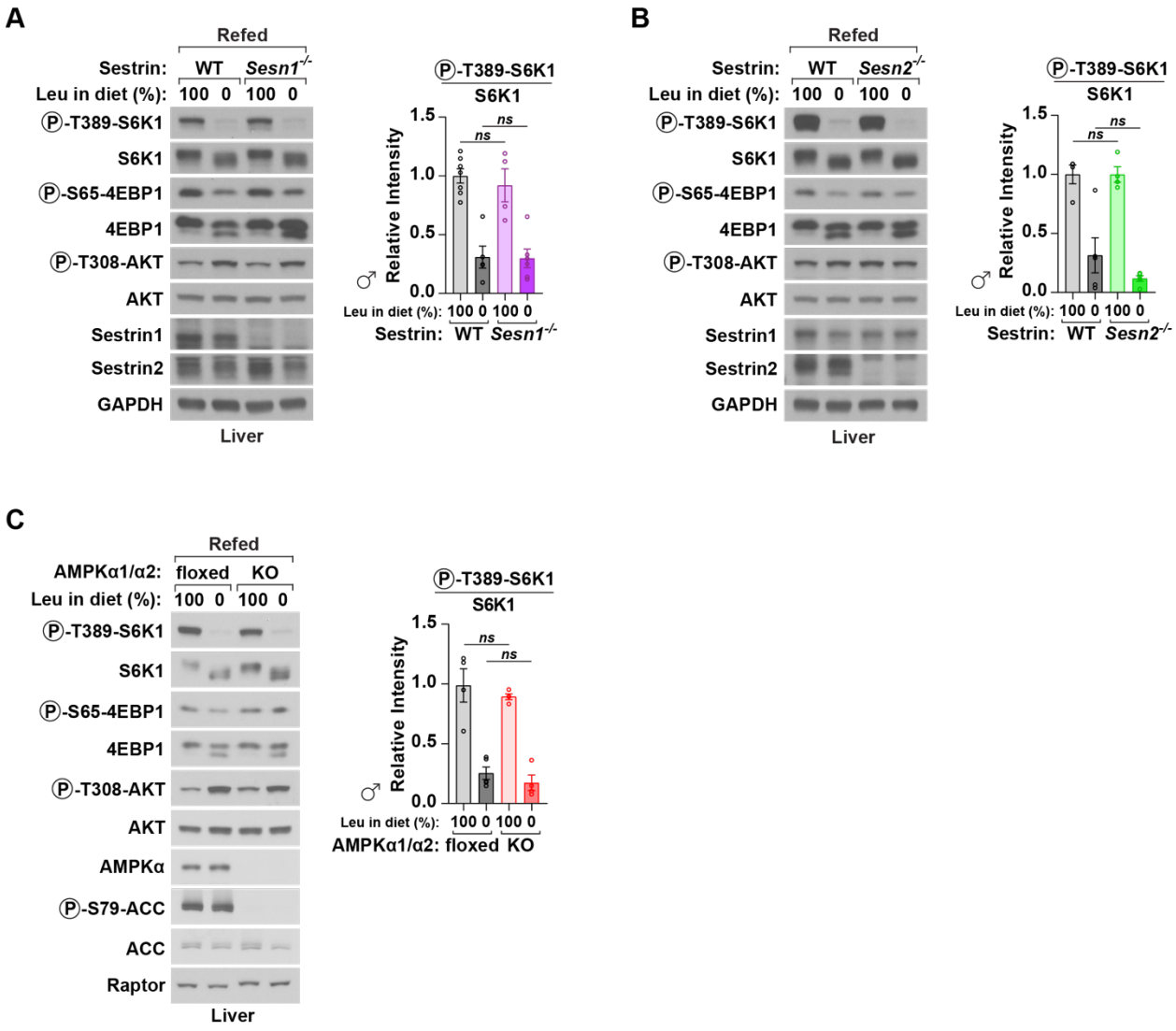

Figure S3: Deletion of only Sestrin1, only Sestrin2, or AMPK activity does not impact the leucine sensitivity of mTORC1 in the liver. (A) Male mice with the indicated genotypes (WT = *Sesn1*$^{+/-}$*; Sesn2*$^{-/-}$, *Sesn1*$^{-/-}$ = *Sesn1*$^{-/-}$*; Sesn2*$^{-/-}$) were fasted and refed with the indicated diets for 3 hours. Liver lysates were analyzed by immunoblotting for the phosphorylation state and levels of the indicated proteins. (n=4-

7). (B) Male mice with the indicated genotypes were fasted and refed with the indicated diets for 3 hours. Liver lysates were analyzed by immunoblotting for the phosphorylation state and levels of the indicated proteins. (n=4-5). (C) Male mice with the indicated genotypes were fasted and refed with the indicated diets for 3 hours. Liver lysates were analyzed by immunoblotting for the phosphorylation state and levels of the indicated proteins. (n=4-5). Data are the mean ± s.e.m. P values were determined using two-tailed t-test.

To examine the physiological importance of leucine sensing by mTORC1, we fed wildtype and DKO mice lacking Sestrin1 and Sestrin2 the leucine-free diet for 8 days (Fig. 2A). DKO mice, but not Sesn1-/- mice or Sesn2-/- mice, lost more body weight than wildtype controls (Fig. 2B and fig. S4A-F), despite eating similar amounts of the leucine-free food (fig. S5A-B). The greater reduction in body weight in DKO mice was a consequence of a severe loss of WAT, as evident in gross and microscopic examinations of several fat depots (Fig. 2C and Fig. 2E-G), as well as a reduction in skeletal muscle mass (Fig. 2D). We saw these phenotypes in both sexes (fig. S6A-D), although the WAT loss was more pronounced in female mice. Liver mass did not contribute to the difference in body weight, as it was unaffected by Sestrin loss (fig. S5C and fig. S6E). The reductions in body weight, WAT, and skeletal muscle occurred in leucine-deprived DKO mice regardless of whether or not they were fasted prior to feeding with the leucine-free diet (fig. S7A-C). As mTORC1 activity and leucine deprivation can both impact insulin signaling and glucose homeostasis (Saxton & Sabatini, 2017; Xiao et al., 2011; Wei et al., 2018), we assessed glucose tolerance,

insulin secretion, and hepatic insulin sensitivity but found no alterations in the DKO mice (fig. S8A-G). On the leucine-free diet, wildtype and DKO mice had similarly low levels of plasma leucine (Fig. 2H and fig. S9A). However, while wildtype mice maintained and in some cases even increased the plasma levels of several other amino acids, DKO mice did not and instead had reduced levels of the same amino acids (Fig. 2H and fig. S9B-S).

Treatment with rapamycin, an mTORC1 inhibitor, restored the total body weight and WAT mass of DKO mice to those of wildtype animals (fig. S10A-D), indicating that aberrant mTORC1 activity underlies their inappropriate response to leucine deprivation.

Importantly, on diets lacking valine or methionine, DKO and wildtype mice lost equal amounts of total body weight, WAT, and skeletal muscle (Fig. 2I-N), consistent with the Sestrins being specific sensors of leucine at physiological amino acid concentrations (Wolfson et al., 2016). Furthermore, wildtype and DKO mice ate a similarly reduced amount of the leucine-free than control food (fig. S5A-B), but this reduction in food intake does not account for the different responses of wildtype and DKO mice to leucine-free feeding (fig. S7D-F).

Lastly, Sesn2W444L mice, in which mTORC1 is inhibited more strongly upon limitations in leucine than in wildtype animals (Fig. 1G), lost—over an extended period of leucine deprivation (16 days)—less WAT mass than control Sesn2WT mice (Fig. 2O-Q), showing that the leucine binding capacity of Sestrin2 modulates the physiological response to leucine deprivation even when the intake of the leucine-free food is the same (fig. S11A). In contrast, leucine-deprived Sesn2W444L and Sesn2WT mice lost similar amounts of skeletal muscle (fig. S11B-D), consistent with muscle not expressing

detectable levels of Sestrin2 (fig. S11E)(Xu et al., 2019). Thus, mice require the Sestrin-mediated regulation of mTORC1 to maintain homeostasis specifically in response to limited leucine availability.

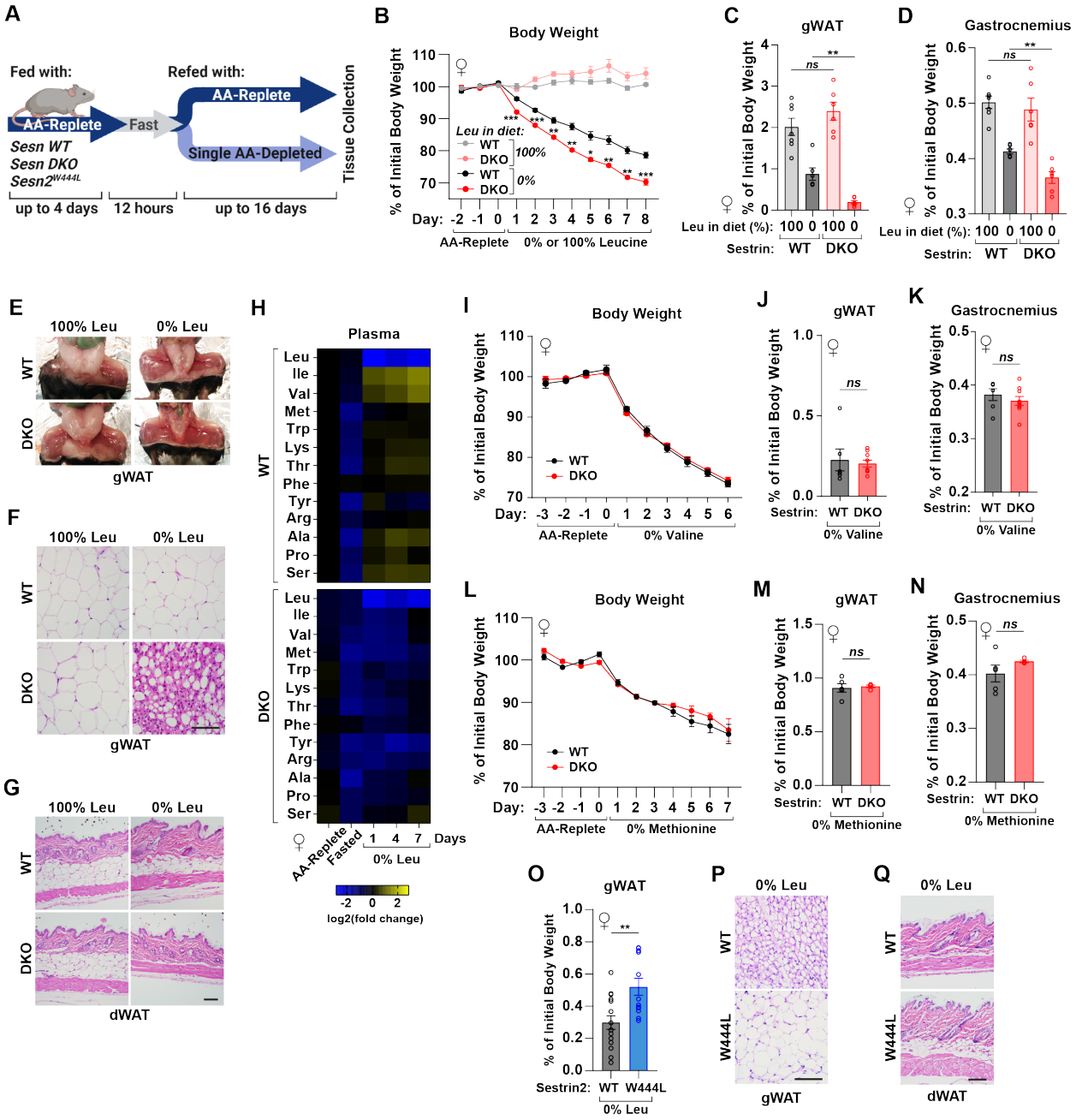

Figure 2: Mice require Sestrin1 and Sestrin2 to adapt to limitations in dietary leucine. (A) Experimental setup for studying the long-term impact of depriving mice of individual amino acids. Mice of the indicated genotypes were maintained on an amino acid-replete control diet for up to 4 days, and then fasted overnight for 12 hours and refed with the control diet or food lacking an essential amino acid for up to 16 days. Created using Biorender.com. (B) Body weights of female mice of the indicated genotypes during feeding with the indicated diets (n=6-7). The daily body weight measurements of each mouse during initial maintenance on an amino acid-replete control diet was averaged; the % change from this average is depicted. (C-D) Gonadal WAT and gastrocnemius muscle weights in female mice of the indicated genotypes after 8 days on the indicated diets (n=6-7). Tissue weights for each mouse are presented as % of the average body weight while on an amino acid-replete control diet. (E) Representative images of gonadal WAT from female mice of the indicated genotypes after 8 days on the indicated diets (n=6-7). (F-G) H&E stain of gonadal and dermal WAT pad sections from female mice of the indicated genotypes after 8 days on the indicated diets. Images are representative of n=6-7 mice. Scale bar = 50 μm. (H) Relative plasma abundances of amino acids from serial blood sampling of female mice of the indicated genotypes, which were kept on an amino acid-replete diet, fasted for 12 hours overnight, and then refed with a leucine-free diet for up to 7 days. Data are presented as log2 fold change of mean values relative to those in wildtype mice on the control diet (n=3-5). Amino acids with significant changes during leucine-free feeding are shown. See Fig S8 for all amino acids and statistical analyses. (I) Body weights of female mice of the indicated genotypes on a valine-free diet (n=6-9). The daily body

weight measurements of each mouse during initial maintenance on an amino acid-replete control diet was averaged; the % change from this average is depicted. (J-K) Gonadal WAT and gastrocnemius muscle weight of female mice of the indicated genotypes after 8 days of feeding on a valine-free diet (n=6-9). Tissue weight for each mouse is presented as % of the average body weight while on the amino acid-replete control diet. (L-N) Same analyses as in I-K except mice were fed a methionine-free diet (n=4-5). (O) Gonadal WAT weight of female mice of the indicated genotypes after 16 days of feeding with a leucine-free diet (n=12-15). Tissue weight for each mouse is presented as % of the average body weight while initially kept on the amino acid-replete control diet for 4 days. (P-Q) H&E stain of gonadal and dermal WAT pad sections from female mice of the indicated genotypes after 16 days of feeding with a leucine-free diet. Images are representative of n=6-8 mice. Scale bar = 50 μm. Data are the mean ± s.e.m. P values were determined using repeated measures two-way ANOVA with Sidak test (B, I, L) or two-tailed t-tests (C, D, J, K, M-O). * $p < 0.05$, ** $p < 0.01$, *** $p < 0.001$.

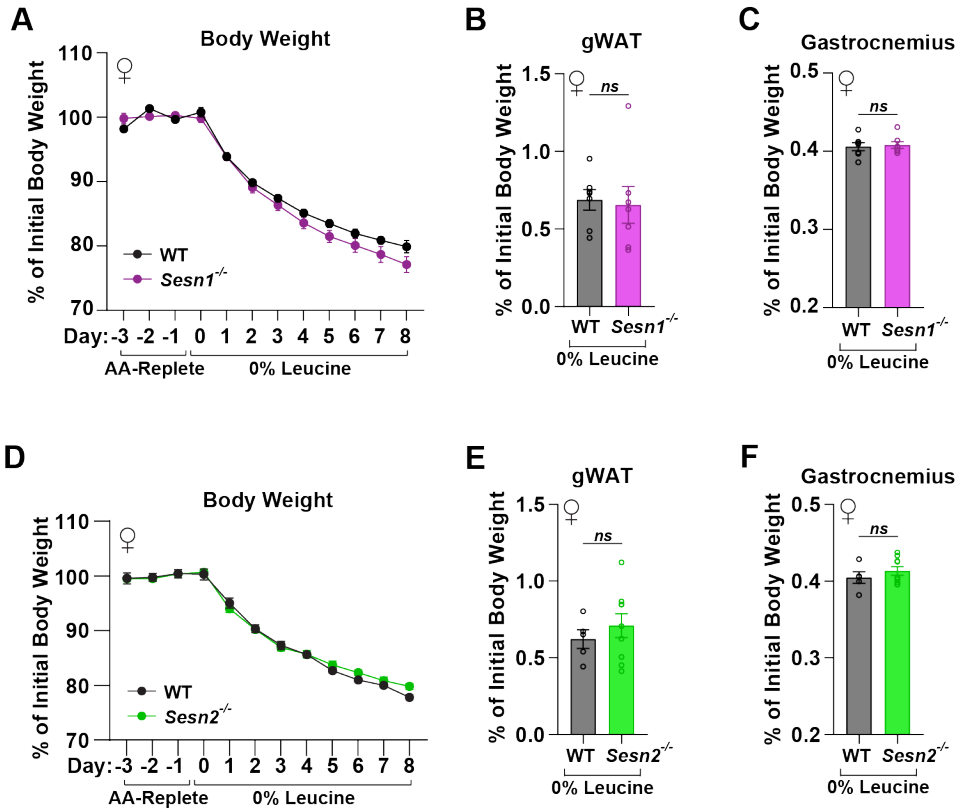

Figure S4: Loss of either Sestrin1 or Sestrin2 alone does not impact the adaptation to dietary leucine deficiency. (A) Body weights of female mice of the indicated genotypes (WT = *Sesn1*$^{+/-}$*; Sesn2*$^{-/-}$, *Sesn1*$^{-/-}$ = *Sesn1*$^{-/-}$*; Sesn2*$^{-/-}$) on a leucine-free diet (n=7). The daily body weight measurements of each mouse during initial maintenance on an amino acid-replete control diet was averaged; the % change from this average is depicted. The data for the wildtype and *Sesn2*$^{-/-}$ mice shown here are the same as in Fig S12. (B-C) Gonadal WAT and gastrocnemius muscle weight of female mice of the indicated genotypes (WT = *Sesn1*$^{+/-}$*; Sesn2*$^{-/-}$, *Sesn1*$^{-/-}$ = *Sesn1*$^{-/-}$*; Sesn2*$^{-/-}$) after 8 days of feeding on a leucine-free diet (n=7). Tissue weights for each mouse are presented as % of the average body weight while on the amino acid-replete control diet. (D) Body weights of female mice of the indicated genotypes on a leucine-free diet (n=5-9). The daily body weight measurements of each mouse during initial maintenance on

an amino acid-replete control diet was averaged; the % change from this average is depicted. The data for the wildtype and *Sesn2*$^{-/-}$ mice shown here are duplicated from that in Fig S12C. (E-F) Gonadal WAT and gastrocnemius muscle weight of female mice of the indicated genotypes after 8 days of feeding on a leucine-free diet (n=5-9). Tissue weights for each mouse are presented as % of the average body weight while on the amino acid-replete control diet. The gWAT weight data shown in E are the same as that in Fig S12D. Data are the mean ± s.e.m. P values were determined using repeated measures two-way ANOVA with Sidak test (A, D) or two-tailed t-tests (B, C, E, F).

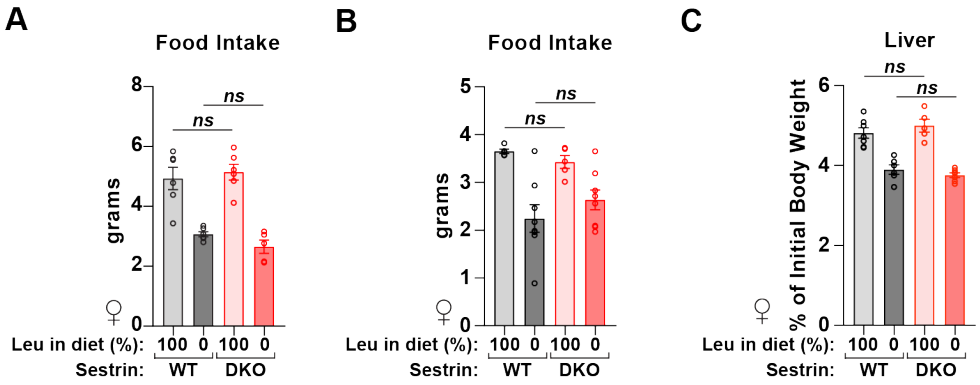

Figure S5: Sestrin loss does not impact food intake or liver weight during dietary leucine deprivation in female mice. (A) Food intake of female mice with the indicated genotypes during the initial 24-hour period of feeding with the indicated diets (n=5-6). (B) Food intake of female mice with the indicated genotypes during a 24-hour period after 6 days of feeding with the indicated diets (n=5-8). (C) Liver weights in female mice of the indicated genotypes after 8 days on the indicated diets (n=5-7). Tissue weight for each mouse is presented as % of the average body weight while on an amino acid-replete control diet. Data are the mean ± s.e.m. P values were determined using two-tailed t-test.

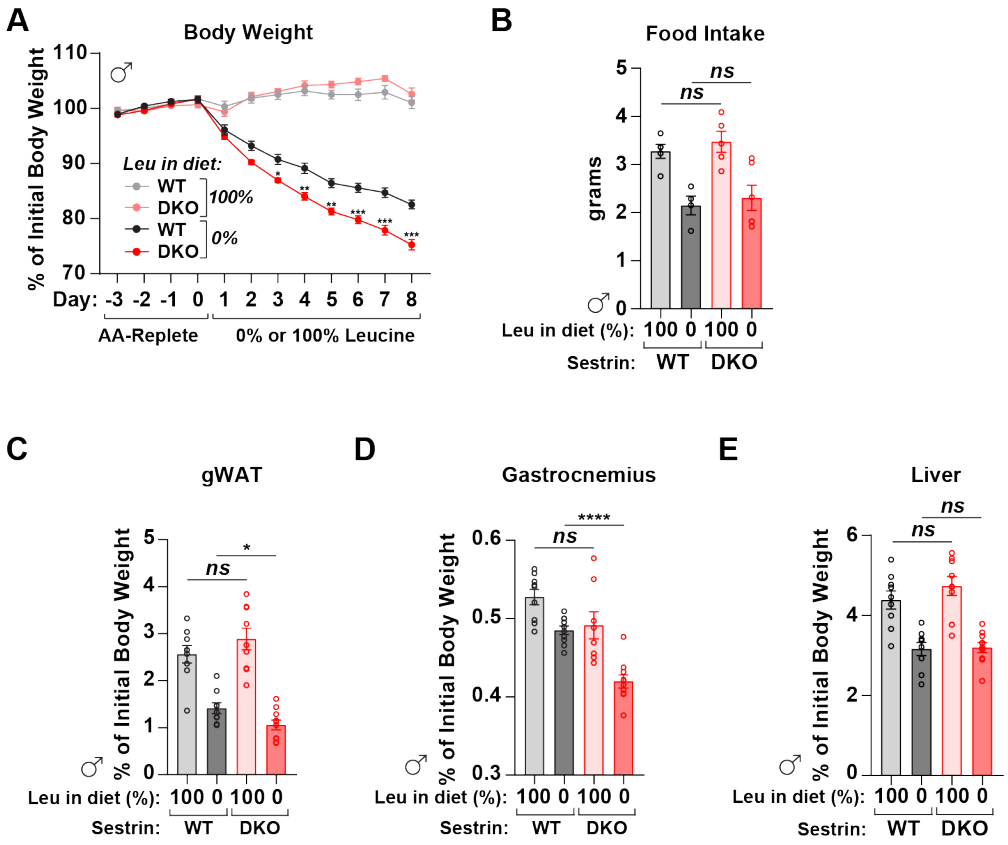

Figure S6: Sestrin1 and Sestrin2 control the maintenance of body weight, gWAT, and muscle during leucine deprivation in male mice. (A) Body weights of male mice with the indicated genotypes on the indicated diets (n=9-10). The daily body weight measurements of each mouse during initial maintenance on an amino acid-replete control diet was averaged; the % change from this average is depicted. (B) Food intake of male mice with the indicated genotypes during a 24-hour period after 7 days of feeding with the indicated diets (n=4-5). (C-E) Gonadal WAT, gastrocnemius muscle, and liver weights in male mice with the indicated genotypes following 8 days on the indicated diets (n=9-10). Tissue weights for each mouse are presented as % of the average body weight while initially maintained on an amino acid-replete control diet. Data are the mean ± s.e.m. P values were determined using repeated measures two-

way ANOVA with Sidak test (A) or two-tailed t-tests (B-E). * $p < 0.05$, ** $p < 0.01$, *** $p < 0.001$, **** $p < 0.0001$.

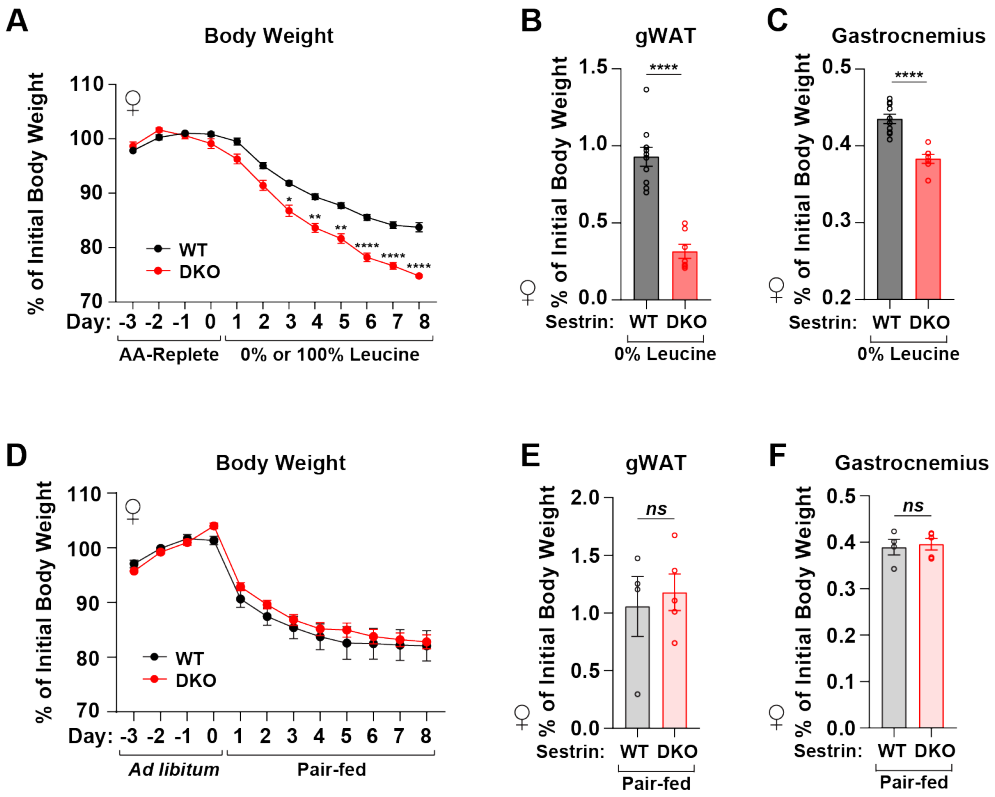

Figure S7: The effects of leucine deprivation on DKO mice are not due to the fasting period or reduced food intake. (A) Body weights of female mice with the indicated genotypes on a leucine-free diet (n=7-10). The mice were switched to the leucine-free diet without a prior fasting period. The daily body weight measurements of each mouse during initial maintenance on an amino acid-replete control diet was averaged; the % change from this average is depicted. (B-C) Gonadal WAT and gastrocnemius muscle weights of female mice of the indicated genotypes after 8 days of feeding on a leucine-free diet (n=7-10). Tissue weights for each mouse are presented as % of the average body weight while on the amino acid-replete control diet. (D) Body

weights of female mice of the indicated genotypes pair-fed with an amino acid-replete diet to match food intake on the leucine-free diet (n=4-5). The daily body weight measurements of each mouse during initial *ad libitum* feeding of the amino acid-replete control diet was averaged; the % change from this average is depicted. (E-F) Gonadal WAT weight and gastrocnemius muscle weight in female mice with the indicated genotypes following 8 days of pair-feeding as described in (D) (n=4-5). Tissue weights for each mouse are depicted as % of the average body weight while initially maintained on *ad libitum* feeding. Data are the mean ± s.e.m. P values were determined using repeated measures two-way ANOVA with Sidak test (A, D) or two-tailed t-tests (B, C, E, F). * $p < 0.05$, ** $p < 0.01$, *** $p < 0.001$, **** $p < 0.0001$.

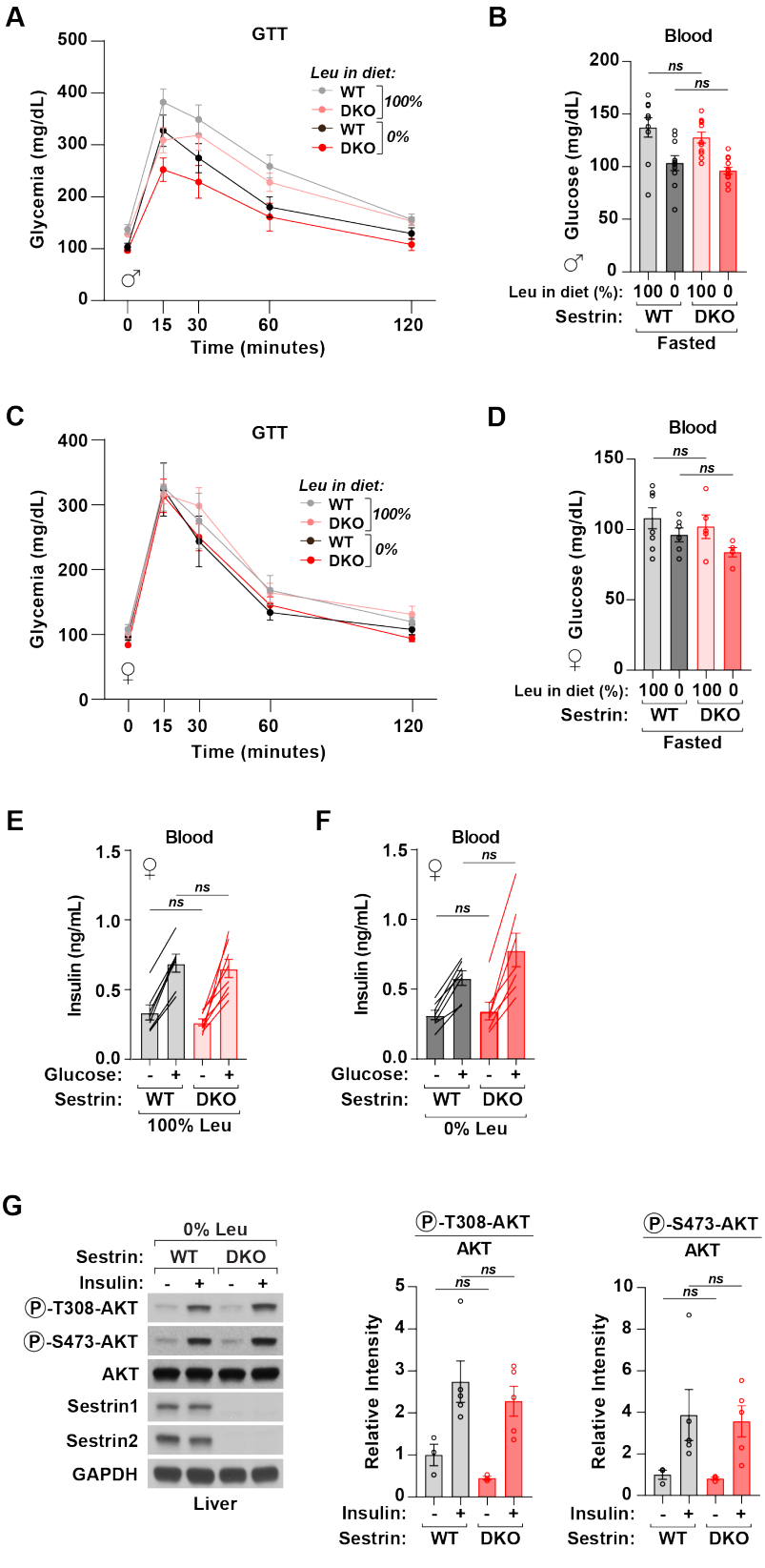
A
GTT
Leu in diet:
WT
DKO
100%
WT
DKO
0%
Glycemia (mg/dL)
Time (minutes)
B
Blood
Glucose (mg/dL)
ns
Leu in diet (%): 100 0 100 0
Sestrin: WT DKO
Fasted
C
GTT
Leu in diet:
Glycemia (mg/dL)
Time (minutes)
D
Blood
Glucose (mg/dL)
Leu in diet (%): 100 0 100 0
Sestrin: WT DKO
Fasted
E
Blood
Insulin (ng/mL)
Glucose:
Sestrin: WT DKO
100% Leu
F
Blood
Insulin (ng/mL)
Glucose:
Sestrin: WT DKO
0% Leu
G
0% Leu
Sestrin: WT DKO
Insulin:
Ⓟ-T308-AKT
Ⓟ-S473-AKT
AKT
Sestrin1
Sestrin2
GAPDH
Liver
Ⓟ-T308-AKT
AKT
Relative Intensity
Insulin:
Sestrin: WT DKO
Ⓟ-S473-AKT
AKT
Relative Intensity
Insulin:
Sestrin: WT DKO

Figure S8: Glucose homeostasis and insulin sensitivity are not impacted by Sestrin loss. (A) Intraperitoneal glucose tolerance test in male mice with the indicated genotypes following 4 days of feeding with the indicated diets (n=10-12). (B) 6-hour fasted blood glucose levels in male mice with the indicated genotypes following 4 days of feeding with the indicated diets (n=10-12). Blood glucose measurements shown here are the same as those at t=0 in A. (C) Intraperitoneal glucose tolerance test in female mice with the indicated genotypes following 4 days of feeding with the indicated diets (n=5-8). (D) 6-hour fasted blood glucose levels in female mice with the indicated genotypes following 4 days of feeding with the indicated diets (n=5-8). Blood glucose measurements shown here are the same as those depicted at t=0 in C. (E) Plasma insulin levels in female mice of the indicated genotypes (n=7-8). Mice were fed an amino-acid replete control diet for 4 days, fasted for 6 hours, and injected with glucose. Insulin levels were measured before and 15 minutes after the glucose injections. (F) Plasma insulin levels in female mice of the indicated genotypes (n=7). Mice were fed a leucine-free diet for 4 days, fasted for 6 hours, and injected with glucose. Insulin levels were measured before and 15 minutes after the glucose injections. (G) Female mice with indicated genotypes were fed a leucine-free diet for 7 days, fasted for 6 hours, and injected with insulin. Liver lysates were analyzed by immunoblotting for the phosphorylation state and levels of the indicated proteins (n=3-5). Data are the mean ± s.e.m. P values were determined using two-tailed t-tests.

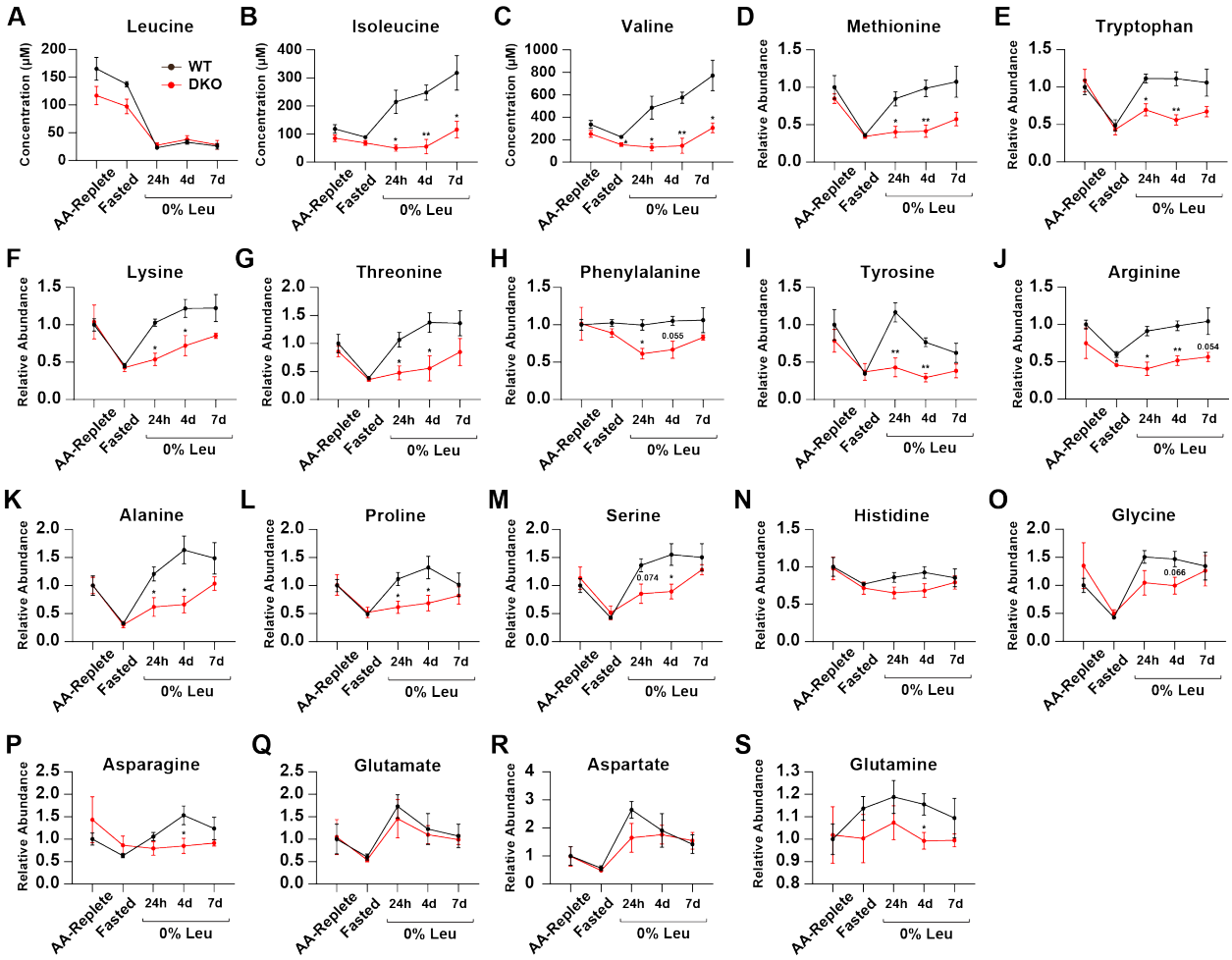

Figure S9: Reduced amino acid levels in the plasma of Sestrin DKO mice during dietary leucine deficiency. (A-S) Amino acid levels in the plasma of female mice of the indicated genotypes on an amino acid-replete control diet, following a 12-hour overnight fast, or fasted and refed for the indicated days with a leucine-free diet (n=3-5). The mean values of the same data are presented as log_2-transformed heatmaps in Fig 2H. Absolute quantification is shown for leucine, isoleucine, and valine (A-C); all other amino acids are shown as relative abundances. Data are the mean ± s.e.m. P values were determined using repeated measures two-way ANOVA with Fisher's LSD test. * $p < 0.05$, ** $p < 0.01$.

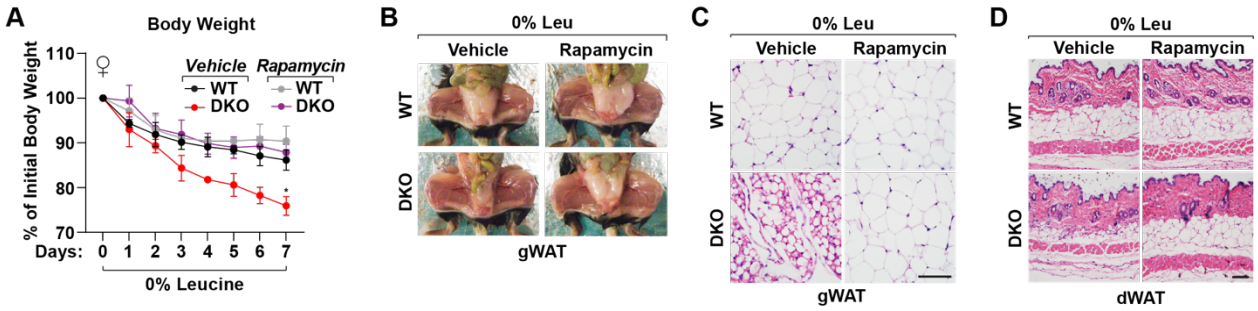

Figure S10: Pharmacological mTORC1 inhibition prevents the maladaptive responses of Sestrin DKO mice to leucine deprivation. (A) Body weights of female mice with the indicated genotypes treated with rapamycin or vehicle during deprivation of dietary leucine (n=3-4). The daily body weight measurements are depicted as the % change from the initial body weight of each mouse on an amino acid-replete control diet. (B) Images showing gonadal WAT of female mice with the indicated genotypes following 7 days of dietary leucine deprivation with or without rapamycin treatment. Images are representative of n=3-4 mice. (C-D) H&E analyses of gonadal WAT and dermal WAT sections from female mice with the indicated genotypes following 7 days of dietary leucine deprivation with or without rapamycin treatment. Images are representative of n=3-4 mice. Scale bar = 50 μm. Data are the mean ± s.e.m. P values were determined using repeated measures two-way ANOVA with Tukey test.

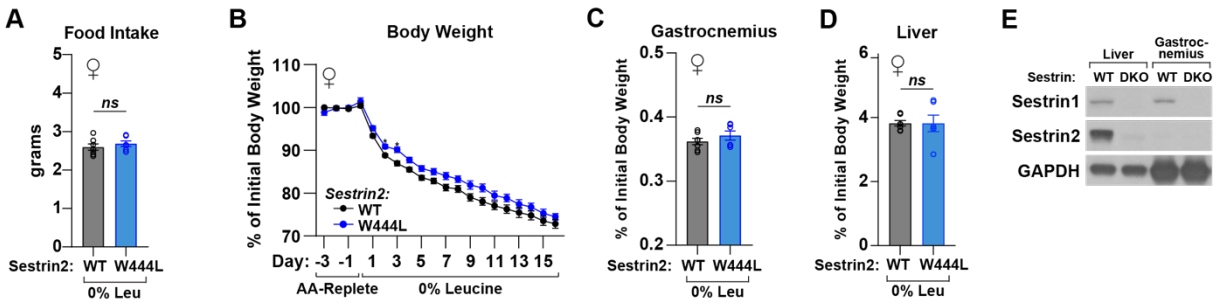

Figure S11: During dietary leucine deprivation Sesn2^{W444L} mice do not have alterations in food intake or muscle or liver weight. (A) Food intake of female mice with the indicated genotypes during a 24-hour period following 15 days of feeding with a leucine-free diet (n=6-7). (B) Body weights of female mice with the indicated genotypes on a leucine-free diet (n=12-15). The daily body weight measurements of each mouse during initial maintenance on an amino acid-replete control diet was averaged; the % change from this average is depicted. (C-D) Gastrocnemius and liver weights of female mice of the indicated genotypes after 16 days of feeding with a leucine-free diet (n=6-7). Tissue weight for each mouse is presented as % of the average body weight while initially kept on the amino acid-replete control diet for 4 days. (E) Livers and gastrocnemius muscles from mice of the indicated genotypes were lysed and analyzed by immunoblotting for levels of the indicated proteins. Data are the mean ± s.e.m. P values were determined using repeated measures two-way ANOVA with Sidak test (B) or two-tailed t-tests (A, C-D). * $p < 0.05$.

Because adipocyte-specific hyperactivation of mTORC1 can lead to a reduction in WAT mass (Magdalon et al., 2016), we considered the possibility that mTORC1 deregulation in the adipocytes of the WAT itself (Fig. 1F, fig. S1B, and fig. S2E) might

cause its loss in DKO mice on the leucine-free diet. While mice lacking both Sestrin1 and Sestrin2 only in adipose tissue (AdiDKO mice) lack mTORC1 regulation in the WAT in response to leucine (fig. S12A-B), they did not phenocopy DKO mice when fed the leucine-free diet (fig. S12C-E), indicating that Sestrin loss impacts WAT mass through a tissue-nonautonomous mechanism.

Given that hepatic mTORC1 can regulate organismal physiology (Sengupta et al., 2010; Koketsu et al., 2008; Cornu et al., 2014) and is sensitive to dietary leucine in a Sestrin-dependent manner (Fig. 1E and fig. S1A), we hypothesized a central role for the Sestrins in the liver in the response to leucine limitation. Indeed, in mice lacking both Sestrins in the liver (LiDKO mice), leucine deprivation caused a greater loss of body weight than in wildtype and Sesn2-/- mice, albeit not as pronounced as in DKO mice (Fig. 3A). As DKO mice lose both WAT and muscle mass upon leucine deprivation (Fig. 2C-G), we determined what accounted for the reduction in body weight of LiDKO mice. Remarkably, on the leucine-free diet LiDKO mice phenocopied the severe WAT loss of DKO mice (Fig. 3B-D), but had muscle mass and plasma amino acid levels similar to those in wildtype animals (Fig. 3E and fig. S13A-H). The WAT loss of DKO and LiDKO mice is unlikely the consequence of an unrecognized developmental defect, as the AAV-Cre-mediated acute deletion of Sestrin1 and Sestrin2 in the livers of adult mice conferred the same phenotype (fig. S14A-D).

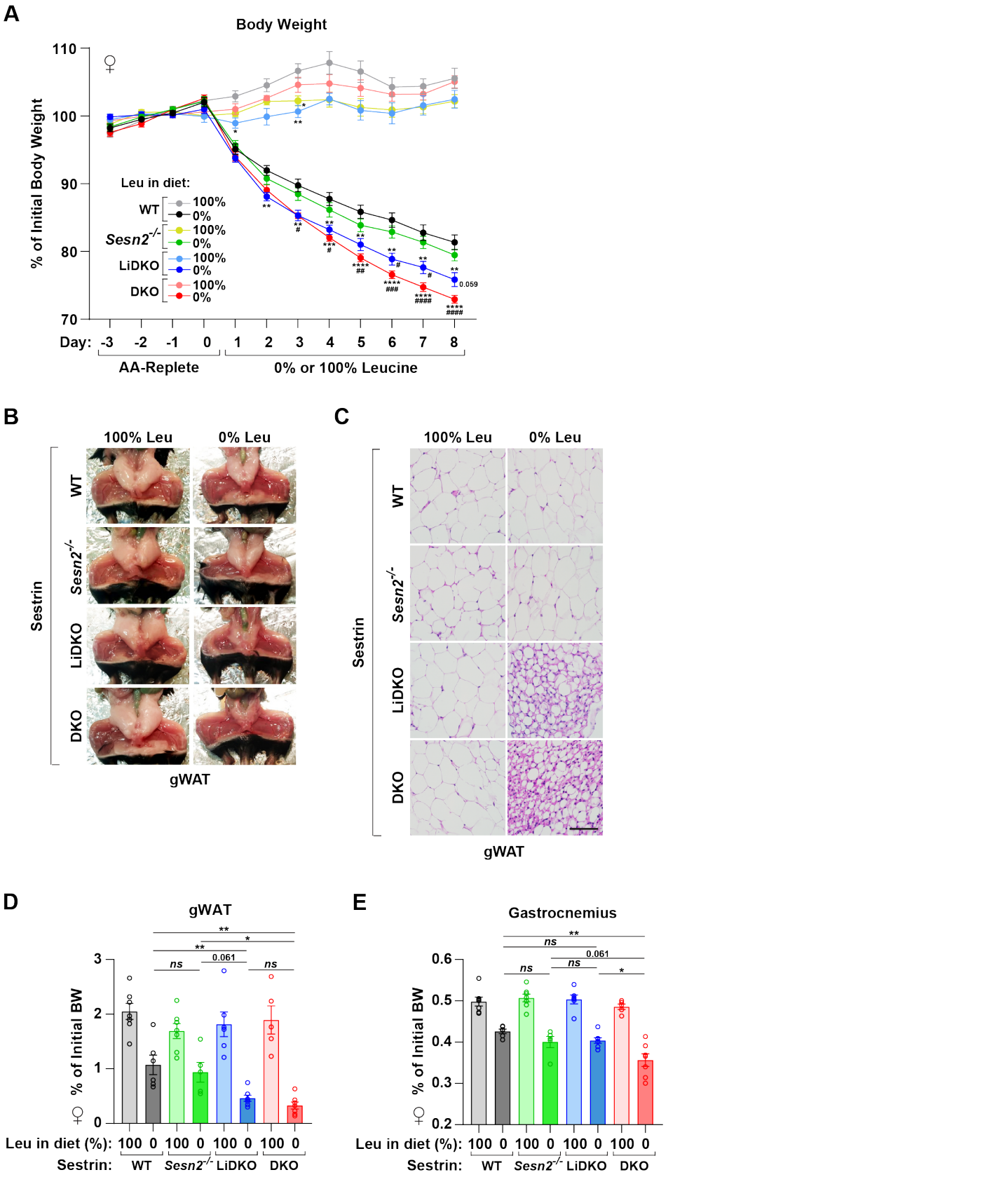
A
Body Weight
% of Initial Body Weight
Leu in diet:
WT
100%
0%
Sesn2-/-
LiDKO
DKO
Day: -3 -2 -1 0 1 2 3 4 5 6 7 8
AA-Replete
0% or 100% Leucine
B
100% Leu
0% Leu
Sestrin
gWAT
C
gWAT
D
gWAT
% of Initial BW
Leu in diet (%): 100 0 100 0 100 0 100 0
Sestrin: WT Sesn2-/- LiDKO DKO
E
Gastrocnemius

Figure 3: Liver Sestrins control WAT remodeling upon deprivation of dietary leucine. (A) Body weights of female mice of the indicated genotypes fed the indicated diets (n=5-12). The daily body weight measurements of each mouse during initial maintenance on an amino acid-replete control diet was averaged; the % change from this average is depicted. (B) Images of gonadal WAT in female mice of the indicated genotypes after 8 days on the indicated diets. Images are representative of n=3-4 mice. (C) H&E analyses of gonadal WAT sections from female mice of the indicated genotypes after 8 days on the indicated diets. Images are representative of n=3-4 mice. Scale bar = 50 μm. (D-E) Gonadal WAT (D) and gastrocnemius muscle (E) weights of female mice with the indicated genotypes after 8 days on a leucine-free diet (n=5-7). Tissue weights of each mouse are presented as % of the average body weight on the amino acid-replete control diet. Data are the mean ± s.e.m. P values were determined using repeated measures two-way ANOVA with Tukey test (A) or one-way ANOVA with Tukey test (D, E). * $p < 0.05$, ** $p < 0.01$.

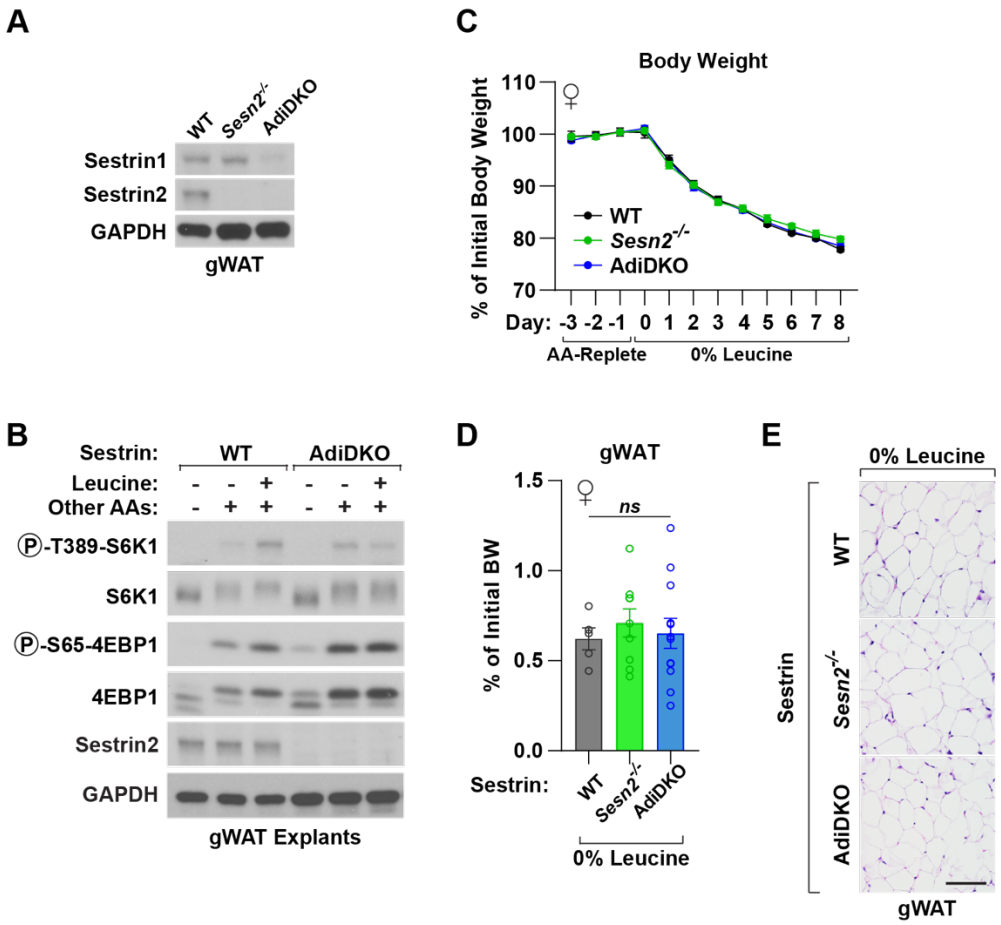

Figures S12: Sestrin loss in adipose tissue does not recapitulate the phenotypes of leucine-deprived Sestrin DKO mice. (A) Gonadal WAT from mice of the indicated genotypes were lysed and analyzed by immunoblotting for levels of the indicated proteins. (B) Gonadal WAT explants isolated from wildtype or AdiDKO mice were starved of leucine or all amino acids for 1 hour. Lysates were analyzed by immunoblotting for the phosphorylation states and levels of the indicated proteins. (C) Body weights of female mice with the indicated genotypes during feeding with a leucine-free diet (n=5-12). The daily body weight measurements of each mouse during initial maintenance on an amino acid-replete control diet was averaged; the % change from this average is depicted. The data for the wildtype and *Sesn2*$^{-/-}$ mice are also shown in Fig S4D. (D) Gonadal WAT weight of female mice with the indicated genotypes

following 8 days of feeding with a leucine-free diet (n=5-12). Tissue weight for each mouse is depicted as % of the average body weight while initially maintained on an amino acid-replete control diet. The data for the wildtype and *Sesn2*$^{-/-}$ mice are also shown in Fig S4E. (E) H&E analyses of gonadal WAT sections from female mice with the indicated genotypes following 8 days of feeding with a leucine-free diet. Images are representative of n=5-6 mice. Scale bar = 50 μm. Data are the mean ± s.e.m. P values were determined using repeated measures two-way ANOVA with Tukey test (C) or one-way ANOVA with Tukey test (D).

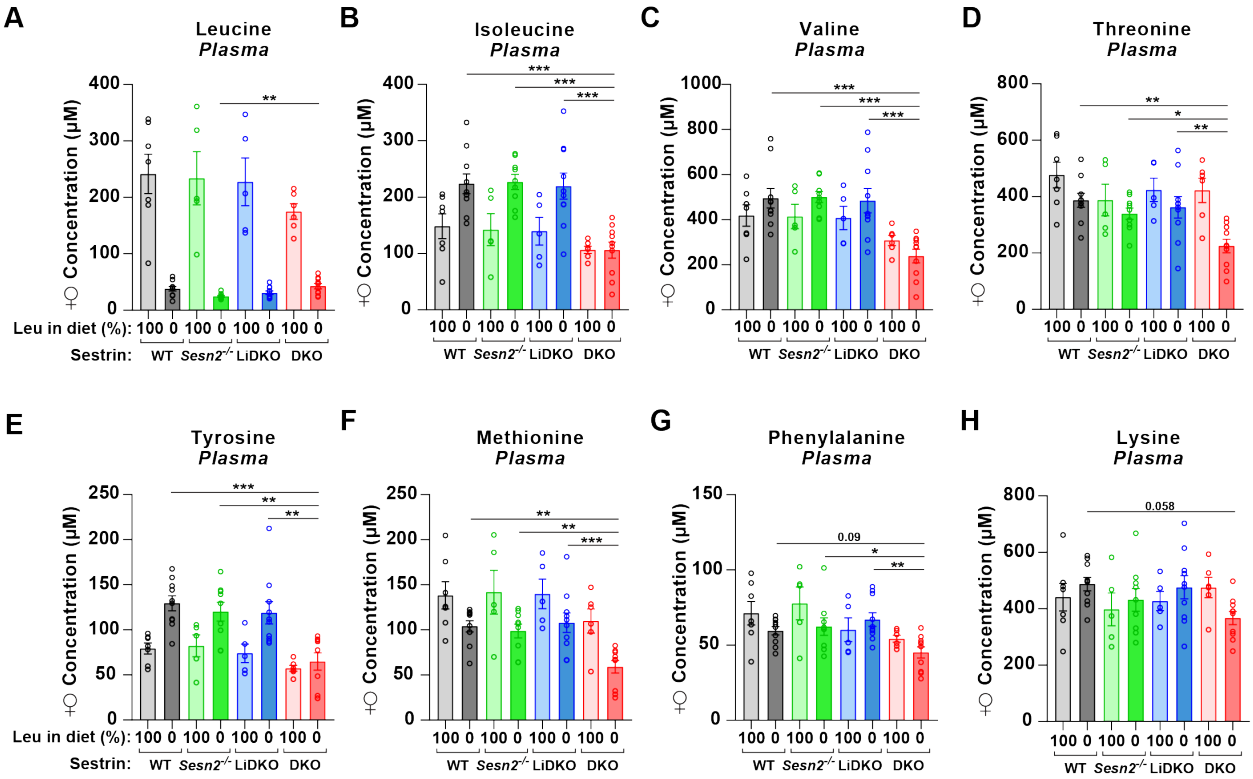

Figure S13: Sestrin loss in the liver is not responsible for reduced plasma amino acids in leucine-deprived Sestrin DKO mice. (A-H) Absolute quantification of amino acids in the plasma of female mice with the indicated genotypes following 24 hours of feeding on an amino acid-replete or leucine-free diet (n=5-10). Data are the mean ± s.e.m. P values were determined using one-way ANOVA with Tukey test. * $p < 0.05$, ** $p < 0.01$, *** $p < 0.001$.

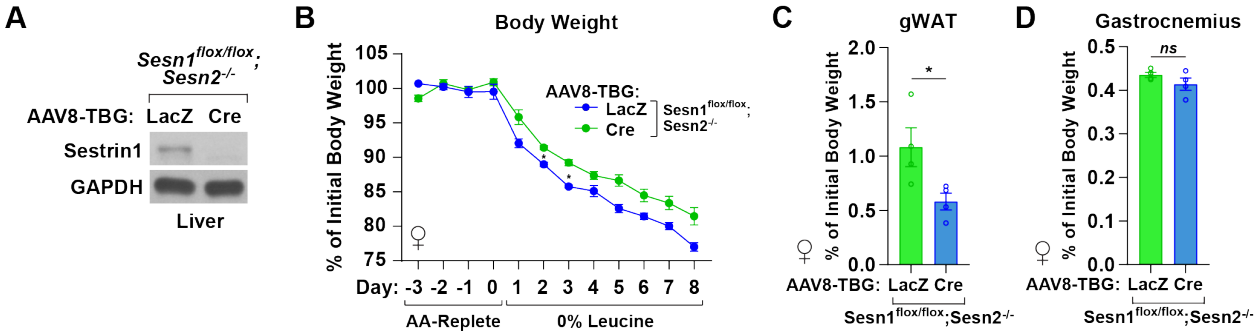

Figure S14: Acute Sestrin deletion in the liver recapitulates the phenotypes of leucine-deprived LiDKO mice. (A) Female *Sesn1*$^{flox/flox}$; *Sesn2*$^{-/-}$ mice were administered the indicated AAVs, and after 30 days livers were lysed and analyzed by immunoblotting for levels of the indicated proteins. (B) Body weights of female *Sesn1*$^{flox/flox}$; *Sesn2*$^{-/-}$ mice and administered the indicated AAVs after feeding with a leucine-free diet (n=4). The daily body weight measurements of each mouse during initial maintenance on an amino acid-replete control diet was averaged; the % change from this average is depicted. (C-D) Gonadal WAT and gastrocnemius muscle weight of female *Sesn1*$^{flox/flox}$; *Sesn2*$^{-/-}$ and administered the indicated AAVs following 8 days of feeding with a leucine-free diet (n=4). Tissue weights for each mouse are presented as

% of the average body weight while initially maintained on an amino acid-replete control diet. Data are the mean ± s.e.m. P values were determined using repeated measures two-way ANOVA with Sidak test (B) or two-tailed t-tests (C-D). * $p < 0.05$.

Together, our results indicate that hepatic Sestrin-mTORC1 plays a key role in the organismal response to leucine deprivation and suggest that liver-to-WAT communication controls the WAT loss observed in DKO mice. The two other phenotypes we documented in DKO mice—loss of muscle mass and deregulation of plasma amino acid levels upon leucine starvation—are independent of Sestrin function in the liver, and perhaps mediated by the Sestrins in muscle given its importance for maintaining circulating amino acid levels (Pozefsky et al., 1976; Vendelbo et al., 2014; Cahill, 1970; Wolfe, 2006). Thus, mice require leucine-sensitive Sestrin function in several tissues to maintain homeostasis upon limitations in dietary leucine.

Among its many functions, the liver is a source of circulating factors, or hepatokines, that promote metabolic homeostasis. Amongst these, we focused on FGF21 as it is implicated in the response to amino acid starvation and WAT remodeling (De Sousa-Coelho et al., 2012; De Sousa-Coelho et al., 2013; Laeger et al., 2014). Indeed, upon leucine deprivation, plasma FGF21 levels were significantly higher in DKO than wildtype mice (Fig 4A), but similar when mice were fed an amino acid-replete diet (Fig. 4A) or fasted (fig. S15A). In DKO mice, FGF21 mediates the exacerbated loss of body weight and WAT during leucine deprivation, as its deletion prevented these effects (Fig. 4B-E, fig. S16A-C). When deprived of leucine, DKO and LiDKO mice had similar increases in plasma FGF21 (Fig. 4A), pinpointing the liver as the likely source of the

FGF21. Correspondingly, leucine deprivation increased the amount of Fgf21 mRNA in the liver of DKO mice (fig. S15B), resulting in a boost in hepatic FGF21 protein levels that strongly correlated with those in the plasma (fig. S15C). Consistent with estrogen signaling potentiating hepatic FGF21 production (Allard et al., 2019), FGF21 levels increased less in male than female DKO mice deprived of leucine (fig. S15D), perhaps accounting for the more modest loss of WAT observed in males (fig. S2D).

Fgf21 expression in the liver is transcriptionally regulated by several mechanisms, including the transcription factor ATF4 (Lundasen et al., 2007; Kim et al., 2013; Maruyama et al., 2016). Transcriptome analysis revealed that during leucine deprivation DKO mice strongly induced ATF4 activity in the liver, as they had increased expression of many ATF4 target genes compared to leucine-deprived wildtype controls at short (24 hours) and long (8 days) timepoints after the start of the leucine-free diet (Fig. 4F and fig. S17A-D). ATF4 expression is induced by eIF2α phosphorylation during the integrated stress response (ISR) (Harding et al., 2000). Consistent with activation of the ISR in the livers of DKO mice, leucine starvation led to an increase in eIF2α phosphorylation and ATF4 protein (Fig. 4G). Independently of eIF2α, mTORC1 itself can also promote ATF4 mRNA translation (Torrence et al., 2021; Ben-Sahra et al., 2016) and so may contribute to the observed increase in ATF4 levels. Oxidative stress can also induce ATF4 (Lange et al., 2008; Miyamoto et al., 2011), but we observed no differences in redox state between wildtype and DKO livers during leucine deprivation, as indicated by the ratios of GSH:GSSG, NADH:NAD+, and AMP:ATP (fig. S18A-C).

Several stress-activated kinases can phosphorylate eIF2α, including PERK, which responds to ER stress, and GCN2, which is activated by the uncharged tRNAs

that accumulate when amino acids are limiting for tRNA aminoacylation. Leucine starvation did not increase PERK autophosphorylation, a marker of its activity, as compared to treatment with tunicamycin, the canonical activator of ER stress (fig. S18D). In contrast, leucine deprivation initially boosted GCN2 activity (indicated by its autophosphorylation) and ATF4 target gene expression in the liver (fig. S19A-D and fig. S20A). Notably, while wildtype mice largely suppressed this initial ISR induction within 24 hours of leucine starvation, DKO mice retained elevated GCN2 activity (Fig. 4G), suggesting that the Sestrins are required for the liver to sustain amino acid homeostasis during leucine deprivation. Indeed, while leucine starvation reduced leucine to equally low levels in the livers of both wildtype and DKO mice (Fig. 4H and fig. S21A), wildtype mice largely maintained or even increased the levels of other proteogenic amino acids in the liver, but DKO mice did not and had significantly lower hepatic levels of several amino acids (Fig. 4I and fig. S21A).

A major source of amino acids in the liver is from the degradation of proteins by autophagy (Madrigal-Matute & Cuervo, 2016; Ezaki et al., 2011), a process suppressed by mTORC1 via inhibitory phosphorylation of the kinase ULK1 (Saxton & Sabatini, 2017; Liu & Sabatini, 2020; Condon & Sabatini, 2019; Valvezan & Manning, 2019). Notably, the reduced hepatic amino acids in DKO mice, particularly isoleucine, valine, threonine, tyrosine, and serine, closely resemble those reported in the livers of mice with hepatic autophagy disruption (Ezaki et al., 2011). We therefore examined autophagic flux by measuring LC3B lipidation after treating mice with the lysosomal protease inhibitor leupeptin (Moulis & Vindis, 2017; Haspel et al., 2011). Compared to a control diet, leucine deprivation increased autophagic flux in wildtype livers (fig. S21B).

In contrast, leucine deprivation did not relieve the inhibitory phosphorylation of ULK1 by mTORC1 (fig. S21C) or induce autophagic flux in DKO mice (Fig. 4J), providing a likely explanation for their activation of GCN2 and expression of ATF4 and FGF21.

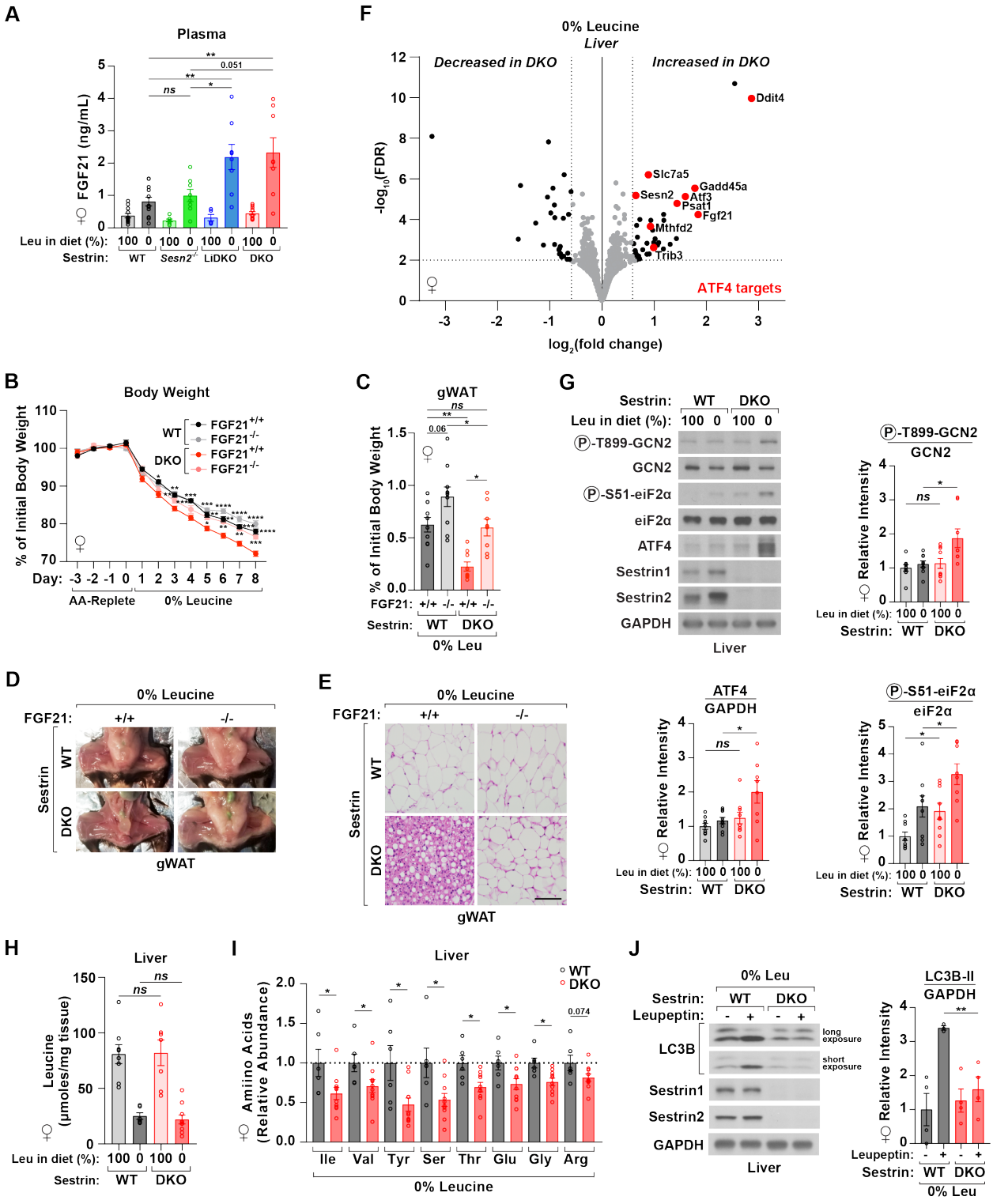

Figure 4: During dietary leucine deprivation Sestrins in the liver control WAT maintenance via FGF21 production. (A) Plasma FGF21 levels in female mice of the

indicated genotypes 24 hours after feeding with the indicated diets (n=5-12). (B) Body weights of female mice of the indicated genotypes during feeding with a leucine-free diet (n=5-10). The daily body weight measurements of each mouse during initial maintenance on an amino acid-replete control diet was averaged; the % change from this average is depicted. Statistical comparisons to the DKO group are shown. (C) Gonadal WAT weight of female mice with the indicated genotypes after 8 days on a leucine-free diet (n=5-10). Tissue weights of each mouse are presented as % of the average body weight on the amino acid-replete control diet. (D) Images of gonadal WAT in female mice of the indicated genotypes after 8 days on a leucine-free diet. Images are representative of n=5-10 mice. (E) H&E analyses of gonadal WAT sections from female mice of the indicated genotypes after 8 days on a leucine-free diet. Images are representative of n=5-10 mice. Scale bar = 50 μm. (F) Volcano plot of genes differentially expressed in WT and DKO livers following 24 hours of leucine-free feeding (n=7-18). Transcripts that are differentially expressed >1.5-fold with FDR < 0.01 are depicted in black. Among these, ATF4 target genes are depicted in red. For better visualization, Sesn1 (log2(fold change) = -1.60; -log10(FDR) = 79.87) was excluded from the plot. Note: Sesn2 reads in DKO mice are derived from nonfunctional transcripts generated by the Sesn2 null allele. See Fig S17 for additional analysis. (G) Female mice of the indicated genotypes were fed with the indicated diets for 24 hours and liver lysates analyzed by immunoblotting for the phosphorylation state and levels of the indicated proteins (n=8-9). (H) Quantification of leucine in the livers of female mice of the indicated genotypes following 24 hours of feeding with the indicated diets (n=6-10). Molar quantities are normalized to tissue weights. (I) Relative abundances of amino

acids in the livers of female mice of the indicated genotypes following 24 hours of feeding with a leucine-free diet. Abundances are normalized to tissue weights and shown relative to the average abundances in wildtype livers (n=6-10). Data was acquired from the same samples as in (H). Amino acids with significant changes are shown. See Fig S22A for data for all amino acids and experimental groups. (J) Female mice of the indicated genotypes were treated with leupeptin or vehicle for 4 hours after 24 hours of feeding with a leucine-free diet. Liver lysates were analyzed by immunoblotting for levels of the indicated proteins (n=3-4). Data are the mean ± s.e.m. P values were determined using one-way ANOVA with Tukey test (A, C), repeated measures two-way ANOVA with Tukey test (B), or two-tailed t-test (G-J). * $p < 0.05$, ** $p < 0.01$, *** $p < 0.001$, **** $p < 0.0001$.

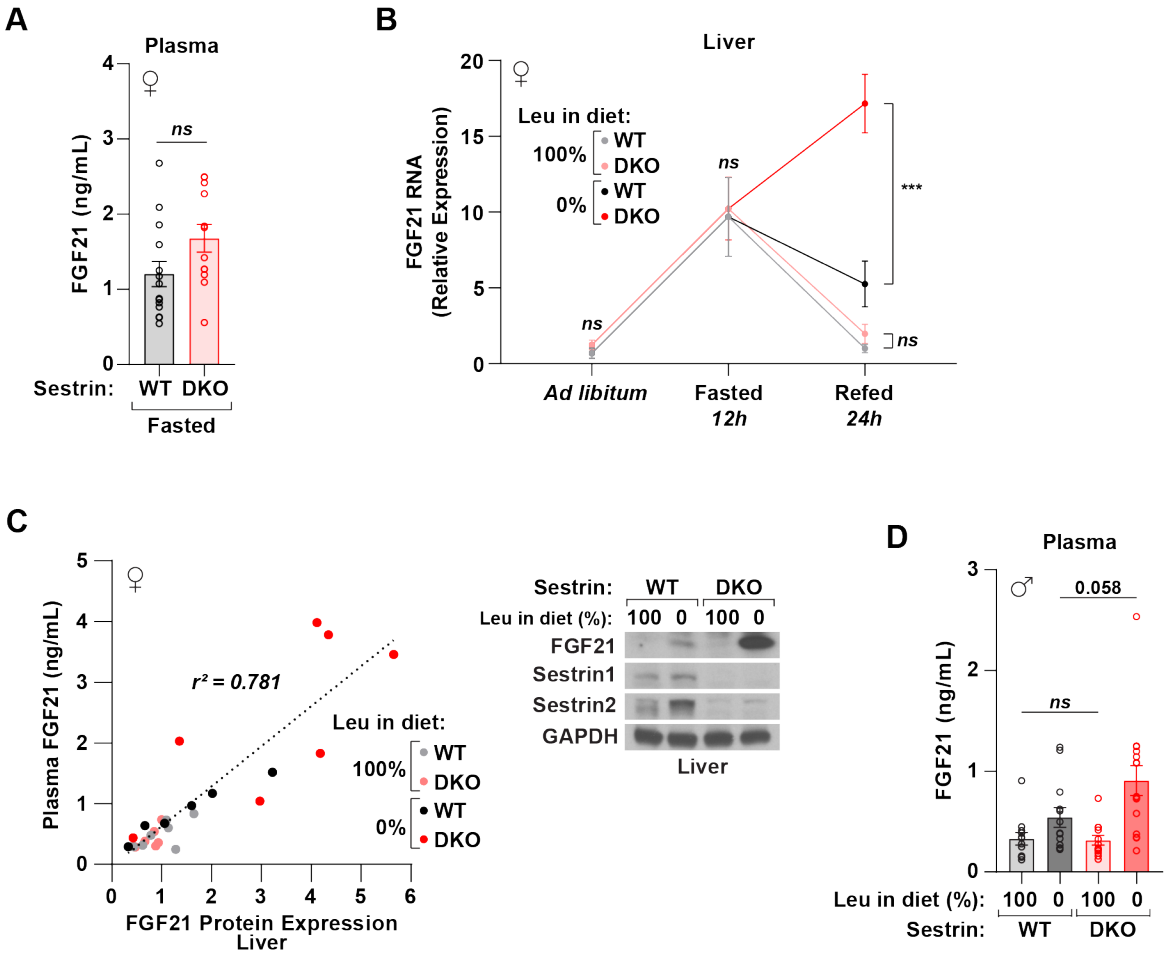

Figure S15: Additional characterization of FGF21 levels in Sestrin DKO mice.

(A) Plasma FGF21 levels in female mice of the indicated genotypes following a 12-hour overnight fast (n=12-14). (B) *Fgf21* mRNA expression, measured by qPCR and normalized to that of the *36B4* mRNA, in the livers of female mice of the indicated genotypes during *ad libitum* feeding on an amino acid-replete control diet, following a 12-hour overnight fast, and following 24 hours of feeding with the indicated diets (n=4-17). (C) Scatterplot of plasma FGF21 levels vs. hepatic FGF21 protein expression (normalized to GAPDH levels) in female mice of the indicated genotypes following 24 hours of feeding with the indicated diets (n=6-7). Representative immunoblot of hepatic FGF21 protein expression is shown. (D) Plasma FGF21 levels in male mice of the

indicated genotypes following 24 hours of feeding with the indicated diets (n=12-15). Data are the mean ± s.e.m. P values were determined using two-tailed t-tests. *** p < 0.001.

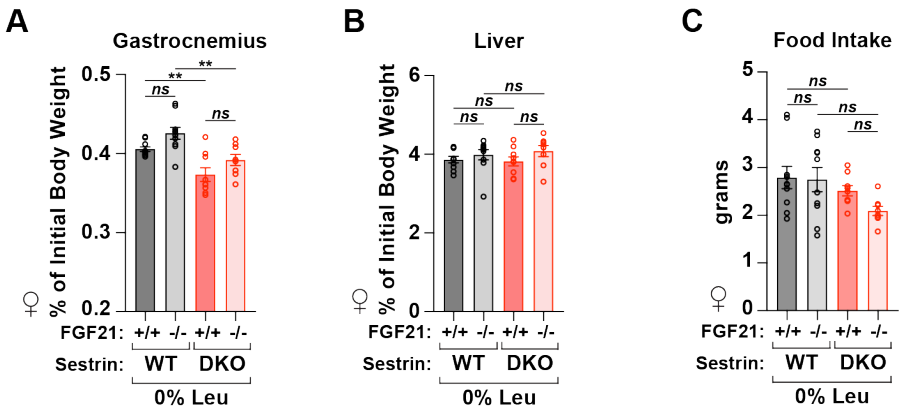

Figure S16: FGF21 deletion does not prevent muscle loss or impact food intake in leucine-deprived Sestrin DKO mice. (A-B) Gastrocnemius and liver weight of female mice with the indicated genotypes after 8 days on a leucine-free diet (n=8-10). Tissue weights of each mouse are presented as % of the average body weight on the amino acid-replete control diet. (C) Food intake of female mice with the indicated genotypes during a 24-hour period following 7 days of feeding with a leucine-free diet (n=8-10). Data are the mean ± s.e.m. P values were determined using one-way ANOVA with Tukey test. ** p < 0.01.

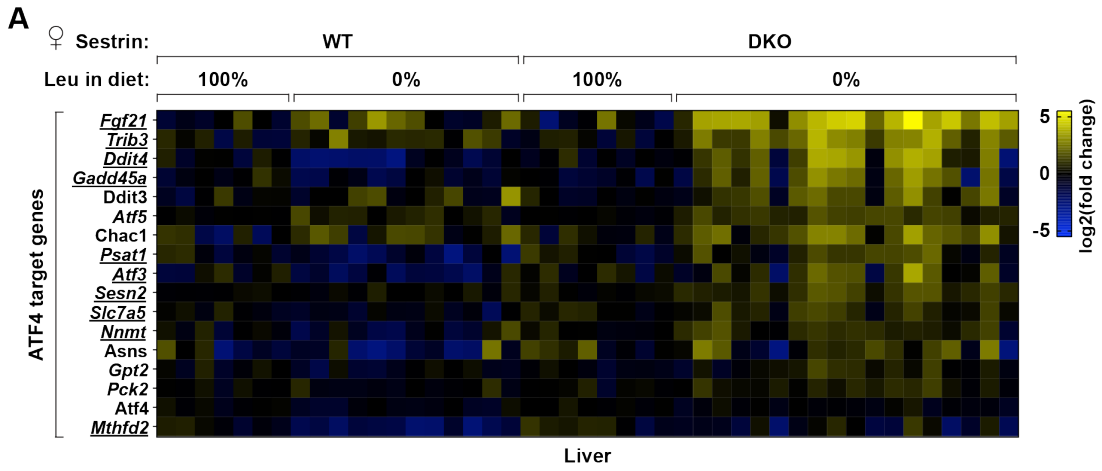
A
♀ Sestrin:
WT
DKO
Leu in diet:
100%
0%
100%
0%
ATF4 target genes
Fgf21
Trib3
Ddit4
Gadd45a
Ddit3
Atf5
Chac1
Psat1
Atf3
Sesn2
Slc7a5
Nnmt
Asns
Gpt2
Pck2
Atf4
Mthfd2
5
0
-5
log2(fold change)
Liver

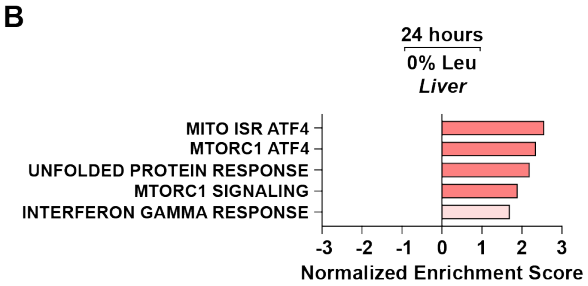
B
24 hours
0% Leu
Liver
MITO ISR ATF4
MTORC1 ATF4
UNFOLDED PROTEIN RESPONSE
MTORC1 SIGNALING
INTERFERON GAMMA RESPONSE
-3
-2
-1
0
1
2
3
Normalized Enrichment Score

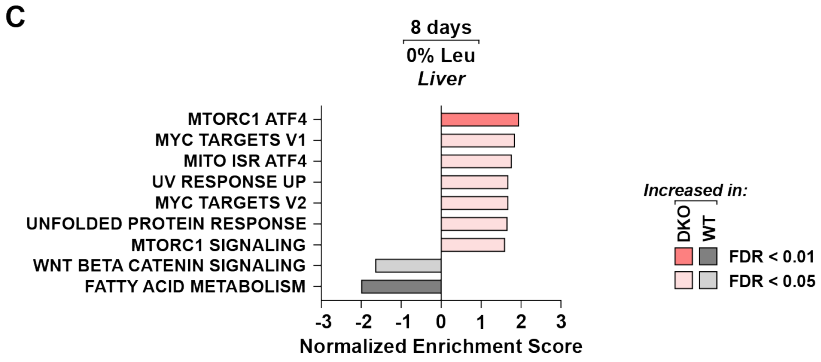
C
8 days
0% Leu
Liver
MTORC1 ATF4
MYC TARGETS V1
MITO ISR ATF4
UV RESPONSE UP
MYC TARGETS V2
UNFOLDED PROTEIN RESPONSE
MTORC1 SIGNALING
WNT BETA CATENIN SIGNALING
FATTY ACID METABOLISM
-3
-2
-1
0
1
2
3
Normalized Enrichment Score
Increased in:
DKO
WT
FDR < 0.01
FDR < 0.05

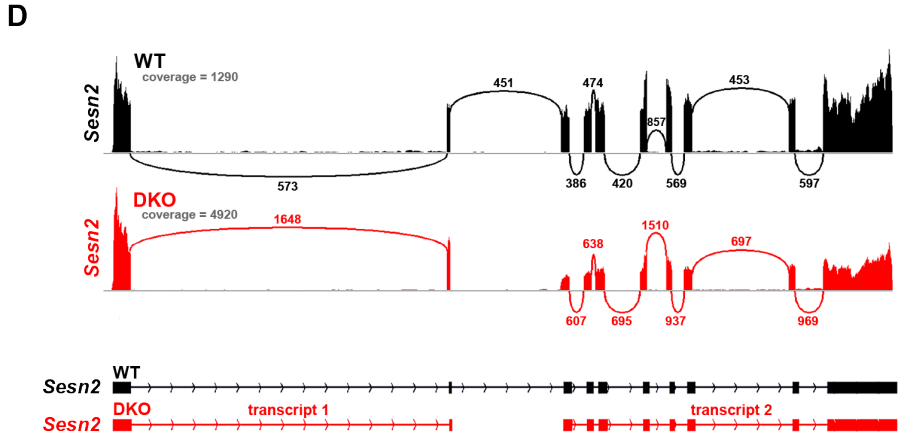
D
WT
coverage = 1290
Sesn2
451
474
857
453
573
386
420
569
597
DKO
coverage = 4920
Sesn2
1648
638
1510
697
607
695
937
969
WT
Sesn2
DKO
Sesn2
transcript 1
transcript 2

Figure S17: Sestrin loss alters the liver transcriptome during leucine deprivation primarily by increasing Atf4 target gene expression. (A) Expression of Atf4 target genes in female mice of the indicated genotypes following 24 hours of feeding with the indicated diets (n=7-18). Data are presented as $\log_2$ fold change relative to the average expression in wildtype mice on the control diet. Genes differentially expressed between genotypes on the leucine-free diet are underlined (FDR $\leq$ 0.01) or italicized (FDR $\leq$ 0.05). Note: *Sesn2* reads in DKO mice are derived from nonfunctional transcripts generated by the *Sesn2* null allele, which are detailed in D. (B) Gene Set Enrichment Analysis of RNA sequencing data from DKO and WT livers after 24 hours of leucine deprivation (the same leucine-deprived mice as shown in (A), queried with the molecular signature database (MSigDB) hallmark gene set collection and curated ATF4 gene signatures (Bao et al., 2016; Guo et al., 2020; Quiros et al., 2017). All gene sets found to be significantly different (FDR < 0.05) between genotypes are shown. No gene sets were detected as significantly different between WT and DKO mice fed the control diet for 24 hours. FDR=false discovery rate. (C) Same analysis as in B was performed on RNA sequencing data from DKO and WT livers after 8 days of leucine deprivation (n=5-6). All gene sets found to be significantly different (FDR < 0.05) between genotypes are shown. No gene sets were detected as significantly different between WT and DKO mice fed the control diet for 8 days. FDR=false discovery rate. (D) Sashimi plot and transcript alignment demonstrating truncated *Sesn2* transcripts in DKO livers. Plots were generated using the reads of all WT and DKO samples in the RNA sequencing data. To avoid mis-mapped reads, only exon-exon junctions supported by >20 reads are included.

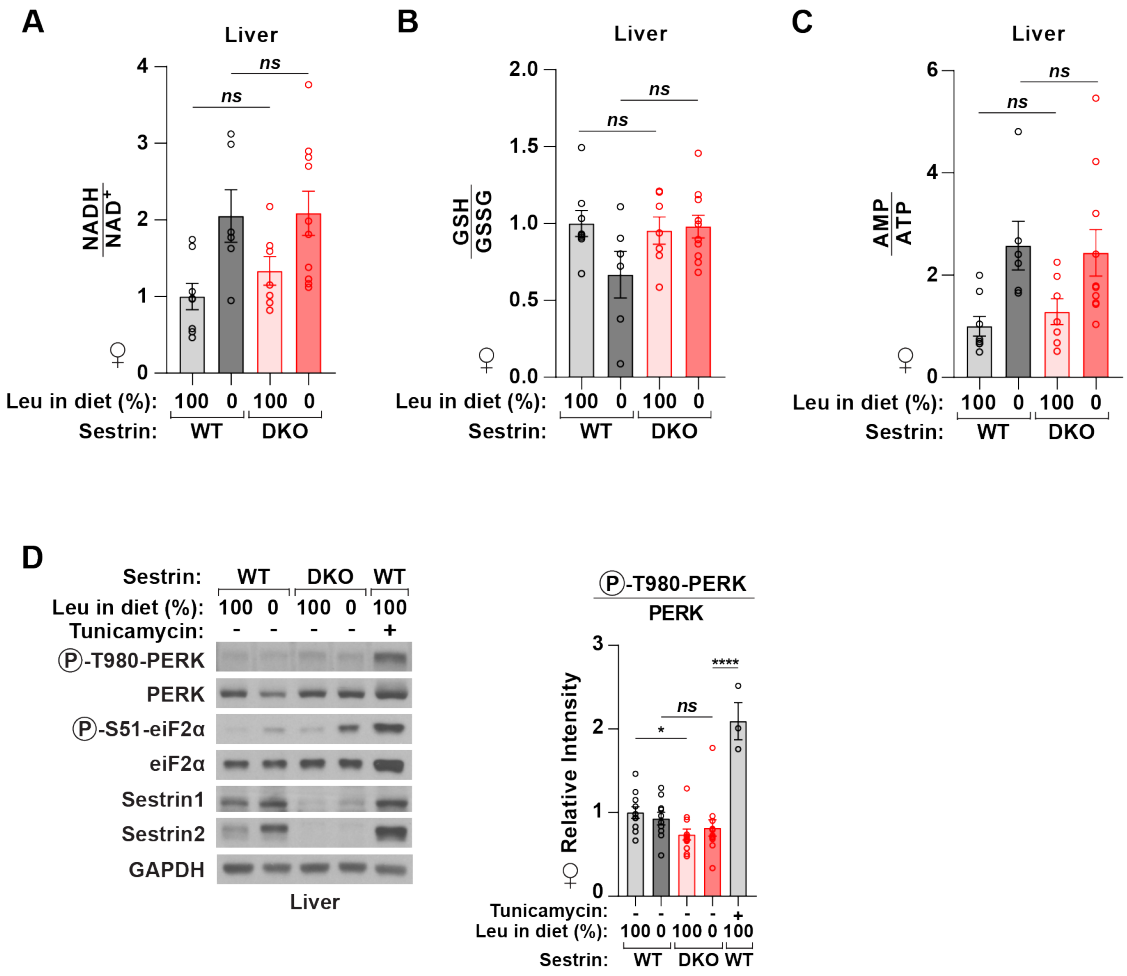

Figure S18: PERK activity and redox balance are not affected by Sestrin loss.

(A-C) Ratio of NADH:NAD$^+$ (A), GSH:GSSG (B), and AMP:ATP (C) in the livers of female mice of the indicated genotypes following 24 hours of feeding with the indicated diets (n=6-10). Relative abundances that were used to calculate ratios were normalized to tissue weight. Data analyzed from same samples as in Fig 4H. (D) Female mice of the indicated genotypes were fed with the indicated diets for 24 hours, with or without tunicamycin treatment. Liver lysates were analyzed by immunoblotting for the phosphorylation states and levels of the indicated proteins (n=3-12). Data are the mean ± s.e.m. P values were determined using two-tailed t-test. * $p < 0.05$, **** $p < 0.0001$.

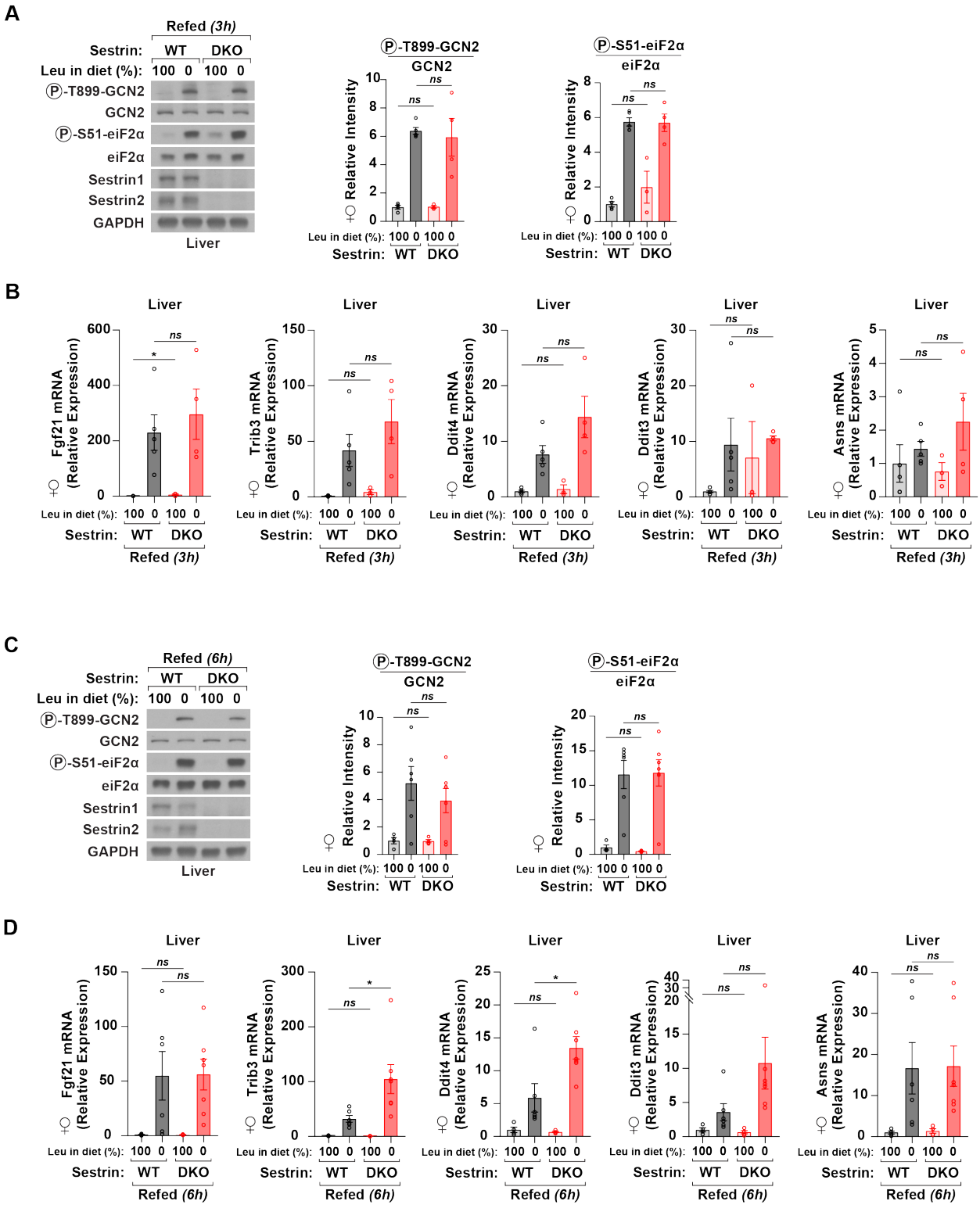
A
Refed (3h)
Sestrin: WT DKO
Leu in diet (%): 100 0 100 0
Ⓟ-T899-GCN2
GCN2
Ⓟ-S51-eiF2α
eiF2α
Sestrin1
Sestrin2
GAPDH
Liver
Ⓟ-T899-GCN2 / GCN2
Ⓟ-S51-eiF2α / eiF2α
Relative Intensity
ns
B
Liver
Fgf21 mRNA (Relative Expression)
Trib3 mRNA (Relative Expression)
Ddit4 mRNA (Relative Expression)
Ddit3 mRNA (Relative Expression)
Asns mRNA (Relative Expression)
Refed (3h)
C
Refed (6h)
D
Refed (6h)

Figure S19: Dietary leucine deprivation acutely activates GCN2 upstream of the integrated stress response in the liver in females. (A) Female mice with indicated genotypes were refed with the indicated diets for 3 hours. Liver lysates were analyzed by immunoblotting for the phosphorylation state and levels of the indicated proteins. (n=3-5). (B) mRNA expression of the indicated Atf4 target genes, measured by qPCR and normalized to that of the *36B4* mRNA, in the livers of female mice of the indicated genotypes refed with the indicated diets for 3 hours (n=3-5). (C) Female mice with indicated genotypes were refed with the indicated diets for 6 hours. Liver lysates were analyzed by immunoblotting for the phosphorylation state and levels of the indicated proteins. (n=4-7). (D) mRNA expression of the indicated Atf4 target genes, measured by qPCR and normalized to that of the *36B4* mRNA, in the livers of female mice of the indicated genotypes refed with the indicated diets for 6 hours (n=4-7). Data are the mean ± s.e.m. P values were determined using two-tailed t-test. * $p < 0.05$.

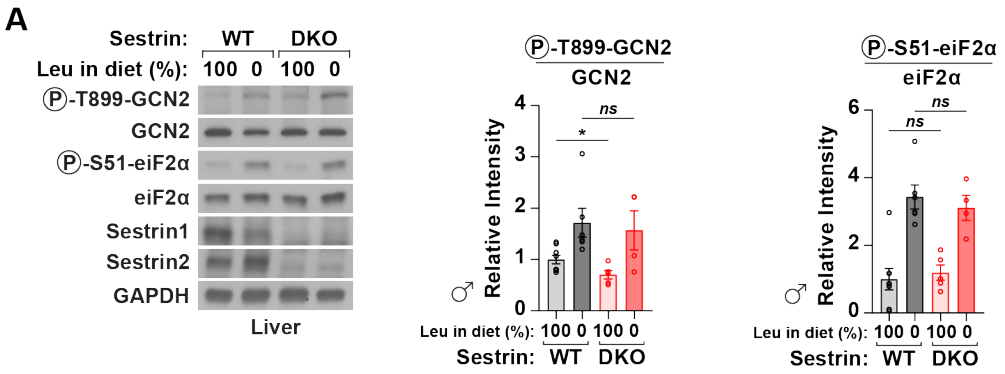

Figure S20: Dietary leucine deprivation acutely activates GCN2 in the livers of male mice. (A) Male mice with indicated genotypes were fasted and refed with the indicated diets for 3 hours. Liver lysates were analyzed by immunoblotting for the phosphorylation state and levels of the indicated proteins. (n=4-8). Data are the mean ± s.e.m. P values were determined using two-tailed t-test. * $p < 0.05$.

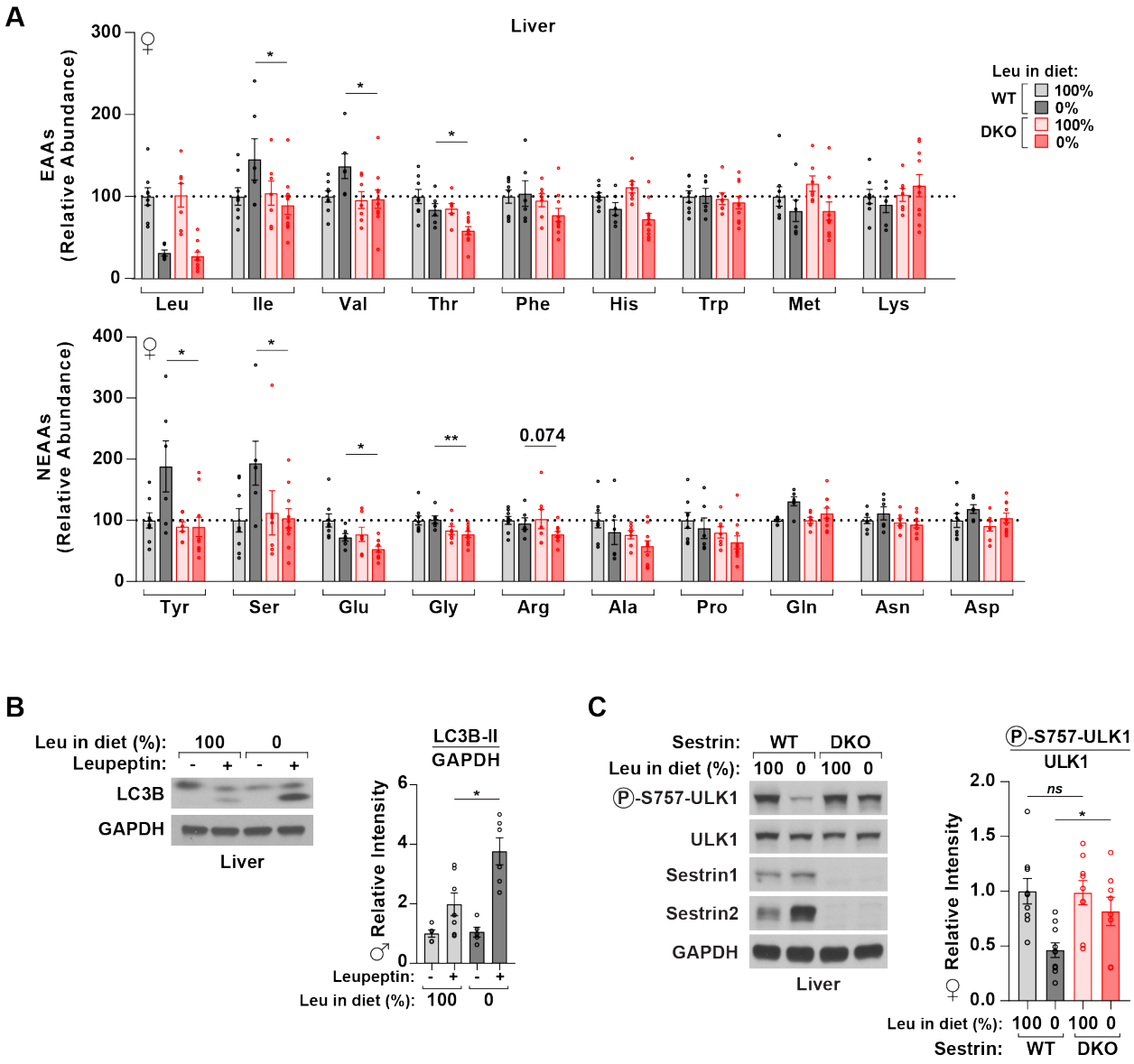

Figure S21: Amino acid homeostasis and autophagy induction during leucine deprivation are impaired by Sestrin loss. (A) Relative abundances of essential amino acids (EAAs) and nonessential amino acids (NEAAs) in the livers of female mice of the indicated genotypes following 24 hours of feeding with the indicated diets. Abundances are normalized to tissue weights and shown relative to the average abundances in control-fed wildtype livers (n=6-10). Data was acquired from the same samples as in Fig 4H. (B) Male wildtype mice were treated with leupeptin or vehicle for 4 hours after 24

hours of feeding with the indicated diets. Liver lysates were analyzed by immunoblotting for levels of the indicated proteins (n=5-7). (C) Female mice of the indicated genotypes were fed with the indicated diets for 24 hours and liver lysates analyzed by immunoblotting for the phosphorylation state and levels of the indicated proteins (n=8-10). Data are the mean ± s.e.m. P values were determined using two-tailed t-test. * $p < 0.05$, ** $p < 0.01$.

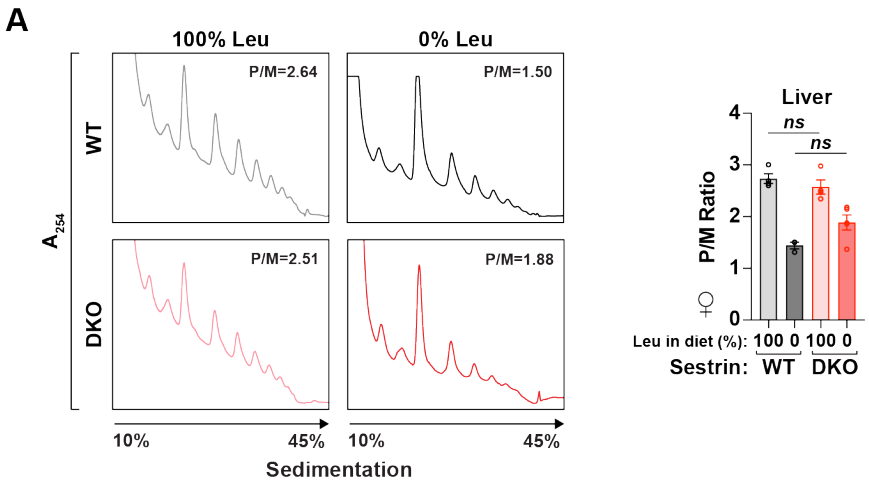

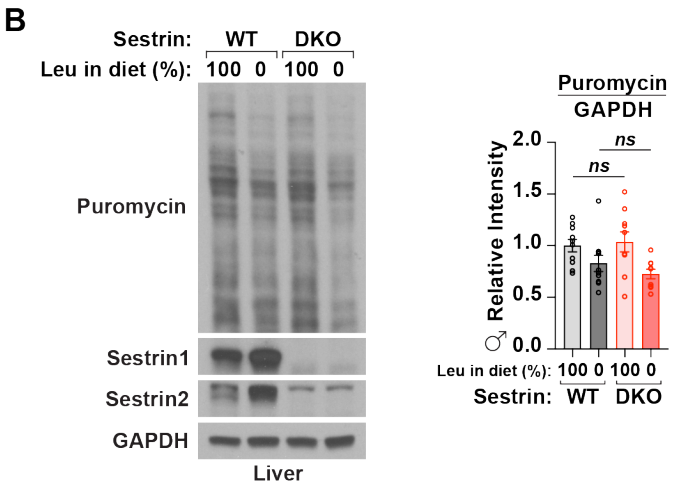

Figure S22: Sestrin loss does not have a detectable impact on whole liver protein synthesis. (A) Female mice of the indicated genotypes were fed with the indicated diets for 24 hours. Livers were analyzed by polysome profiling (n=3-5). P/M indicates the polysome/monosome ratio. (B) Male mice of the indicated genotypes were fed with the indicated diets for 24 hours and then administered 40 μmol/kg puromycin 30 minutes prior to tissue collection. Liver lysates were analyzed by immunoblotting for the levels of the indicated proteins (n=9-10). Data are the mean ± s.e.m. P values were determined using two-tailed t-test.

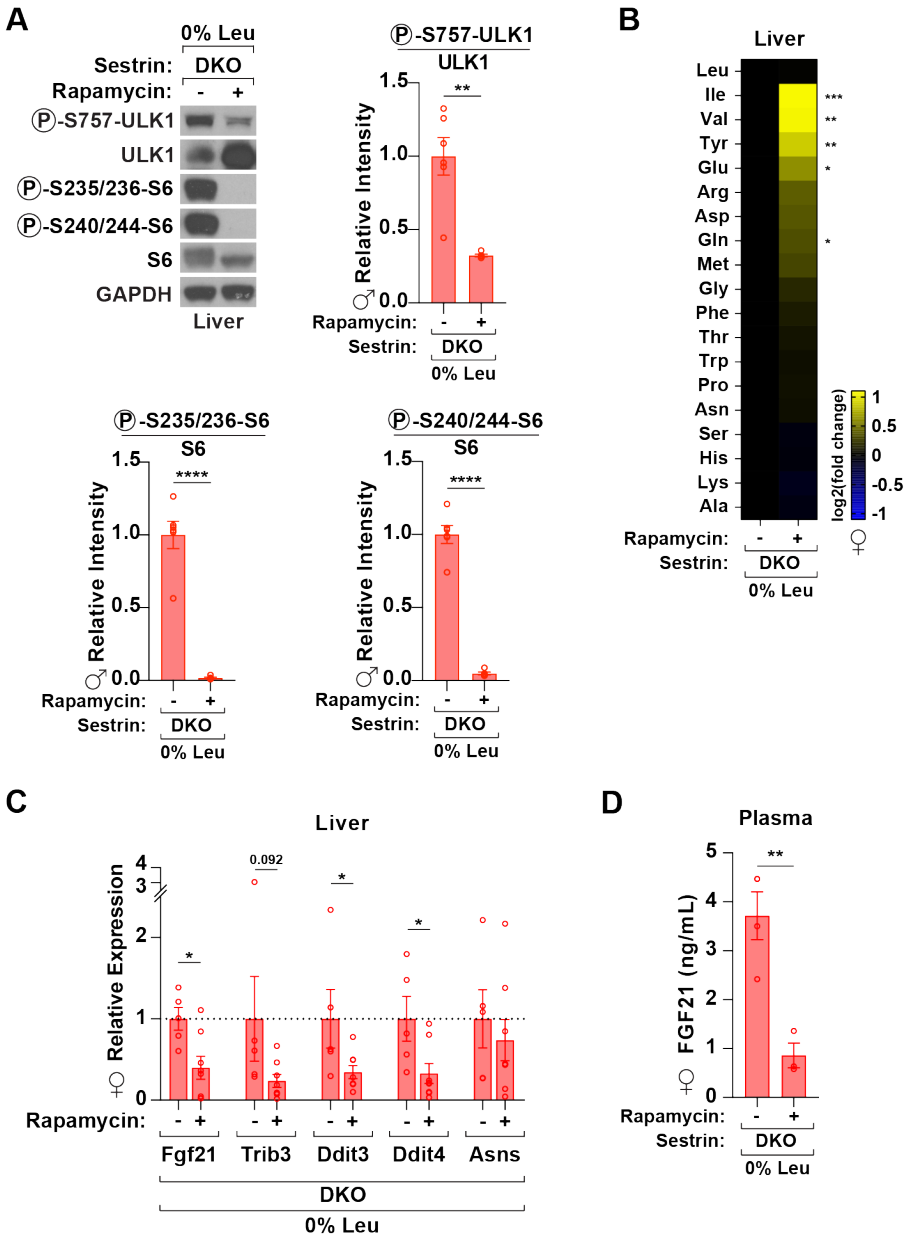

Figure S23: Pharmacological mTORC1 inhibition prevents the hepatic amino acid reduction and ATF4-FGF21 induction caused by leucine deprivation in Sestrin DKO mice. (A) Male DKO mice were fed with a leucine-free diet for 24 hours with or without injection of rapamycin. Liver lysates were analyzed by immunoblotting for the phosphorylation state and levels of the indicated proteins (n=5-6). (B) Relative abundances of amino acids in the livers of female DKO mice 24 hours after feeding with

a leucine-free diet with or without injection of rapamycin. Abundances are normalized to tissue weights and are presented as $\log_2$ fold change of mean values relative to those of the vehicle-treated group (n=6-10). (C) mRNA expression of the indicated Atf4 target genes, measured by qPCR and normalized to that of the *36B4* mRNA, in the livers of female DKO mice 24 hours after feeding with a leucine-free diet with or without injection of rapamycin (n=5-8). (D) Plasma FGF21 levels in female DKO mice 24 hours after feeding with a leucine-free diet with or without injection of rapamycin (n=3-4). Data are the mean ± s.e.m. P values were determined using two-tailed t-test. * $p < 0.05$, ** $p < 0.01$, *** $p<0.001$.

While protein synthesis can also impact levels of amino acids through their consumption and is regulated by both mTORC1 and GCN2 (Anthony et al., 2004), we found no significant impact of Sestrin expression on protein synthesis in the liver, as assessed by polysome profiling and puromycin incorporation into protein (fig. S22A-B).

In DKO mice on the leucine-free diet, inhibition of mTORC1 with rapamycin attenuated the phosphorylation of mTORC1 substrates, drop in hepatic amino acids, ATF4 target gene expression, and plasma FGF21 levels (fig. S23A-D), confirming that, as with WAT mass (fig. S10B-D), the Sestrins impact leucine-sensitive physiology through mTORC1.

Within the liver, hepatocytes are organized into a large number of hexagonally-shaped lobules. Nutrient-rich blood coming from the gastrointestinal tract enters the periphery of each lobule through branches of the portal vein and percolates through sinusoids between the hepatocytes before exiting at the central vein. Hepatocytes in

different zones of the lobule can have distinct metabolic functions and transcriptional programs (Halpern et al., 2017; Jungermann et al., 1989), so we reasoned that there might be a spatial organization to Sestrin1 and Sestrin2 expression within the liver lobule. Indeed, using single-molecule fluorescence in situ hybridization, we observed zonated expression of the Sesn1 and Sesn2 mRNAs, with many transcripts in periportal and mid-lobular hepatocytes and fewer in the pericentral hepatocytes marked by Glul expression (Fig. 5A and fig. S24A-C). This finding suggested there also might be zonal differences in the leucine sensitivity of mTORC1 signaling, which we monitored using an immunofluorescence assay for phosphorylated S6, a marker of mTORC1 activity. Strikingly, mTORC1 activity was not uniform across the liver lobule in wildtype mice fed a leucine-free diet. It was inhibited in the periportal and mid-lobular hepatocytes that express Sestrin but active in the pericentral ones that do not. In contrast, in DKO mice starved of leucine, mTORC1 activity was uniform across the lobule and indistinguishable from that in mice fed amino acid-replete food (Fig. 5B and fig. S24D).

To understand the impact of zonated mTORC1 activity, we determined the spatial pattern of Fgf21 expression in wildtype and DKO mice. Fgf21 was lowly expressed in the livers of mice fed a control diet, but was induced upon leucine deprivation in the periportal and mid-lobular hepatocytes that express Sestrin. This induction was amplified by Sestrin loss (Fig. 5C and fig. S24E), consistent with the increase in ATF4 detected by immunoblotting (Fig. 4G). Furthermore, Sesn2, which is itself an ATF4 target (Ye et al., 2015), was also induced by leucine deprivation in wildtype mice (Fig. 4G) in the same zones as Fgf21 (Fig. 5A and C). Interestingly, the pericentral hepatocytes did not activate the ISR during leucine deprivation despite

maintaining high mTORC1 activity. This suggests that they are intrinsically resistant to the negative impacts of leucine deprivation, perhaps accounting for why they are wired to have low Sestrin expression. The lack of ISR activation in these cells may itself contribute to their low expression of Sesn2, as it is an ATF4 target gene. The resistance of the pericentral hepatocytes may stem from known features of these cells, including their constitutively high levels of autophagy (Gebhardt & Hovhannisyan, 2010; Gebhardt & Coffer, 2013), expression of ER chaperones (Droin et al., 2021), and synthesis of intracellular glutamine whose efflux can drive leucine uptake (Nicklin et al., 2009). We conclude that in the liver the Sestrin-imposed and zone-specific regulation by leucine of mTORC1 signaling is necessary to attenuate the stress of dietary leucine deprivation (Figure 6).

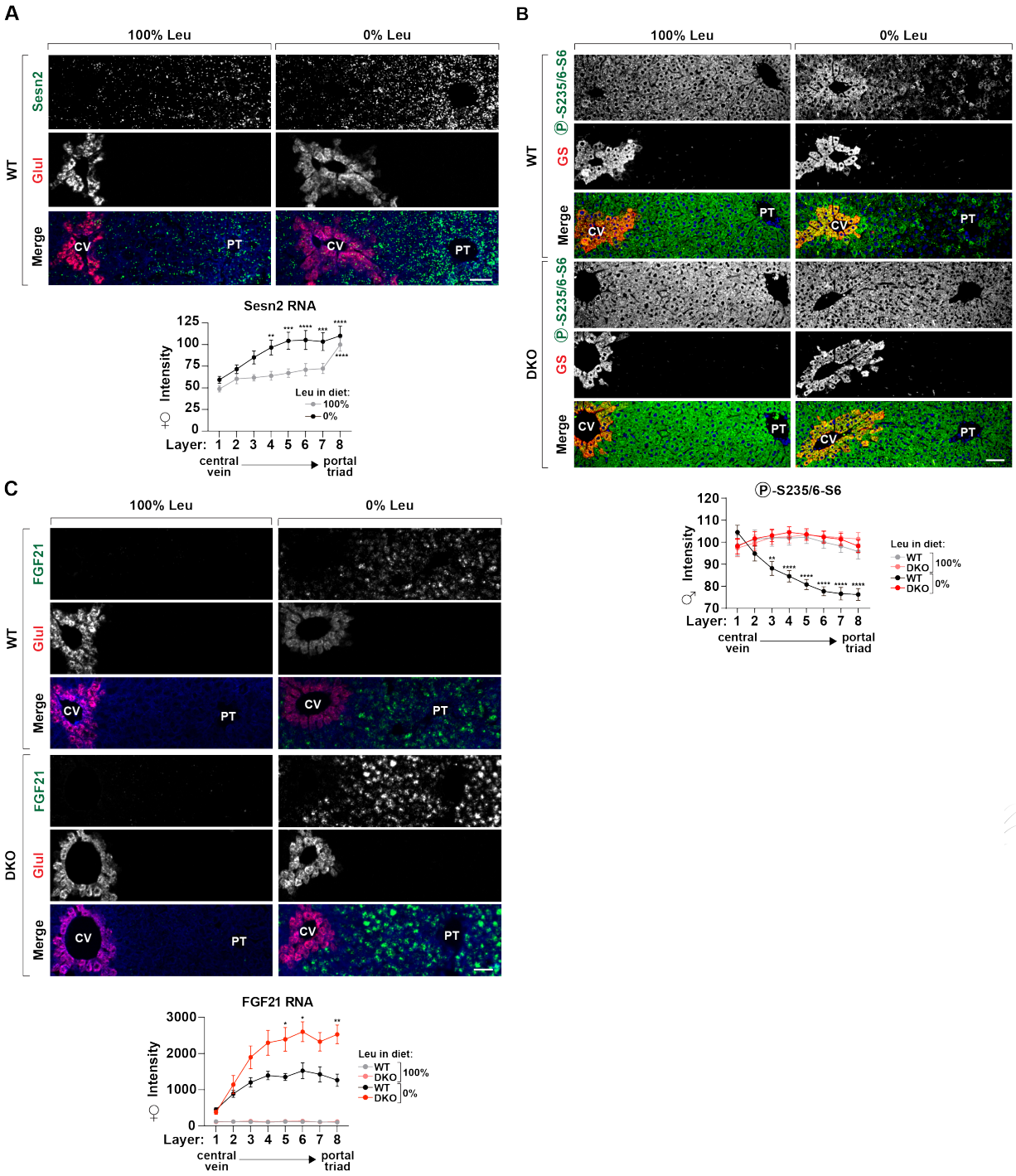

Figure 5: Zonated Sestrin expression establishes leucine-sensitive and -insensitive compartments in the liver. (A) Representative images and quantification of Sesn2 mRNA as detected by smFISH in the livers of wildtype female mice 24 hours after feeding with the indicated diets (n=16-18 lobules from n=3 mice/diet). Shown are

statistical comparisons to layer 1 for each diet. (B) Representative images and quantification of S6 phosphorylation as detected in immunofluorescence assays in liver sections from female mice of the indicated liver genotypes 3 hours after refeeding with the indicated diets (n=12-24 lobules from n=4-7 mice/genotype/diet). Statistical comparisons between genotypes on the leucine-free diet are shown. (C) Representative images and quantification of Fgf21 mRNA in liver sections of female mice of the indicated genotypes after 24 hours of feeding with the indicated diets (n=7-16 lobules from n=3 mice/genotype/diet). Statistical comparisons between genotypes on the leucine-free diet are shown. CV=central vein; PT=portal triad. Scale bars = 50 μm. Data are the mean ± s.e.m. P values were determined using two-way ANOVA with Dunnett test (A) or two-way ANOVA with Sidak test (B, C). * $p < 0.05$, ** $p < 0.01$, *** $p < 0.001$, **** $p < 0.0001$.

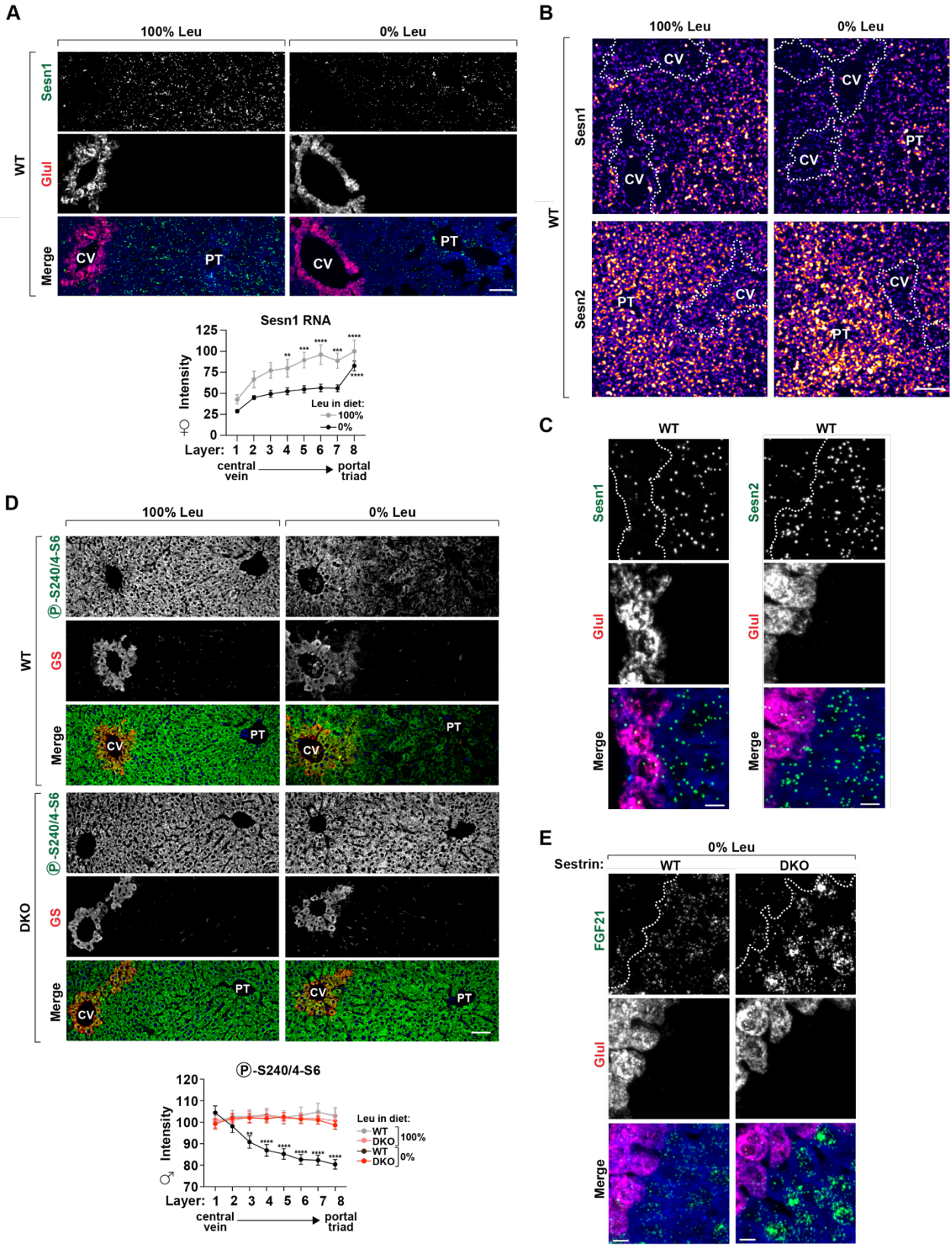
A
100% Leu
0% Leu
WT
Sesn1
Glul
Merge
CV
PT
Sesn1 RNA
Intensity
♀
Leu in diet:
100%
0%
Layer: 1 2 3 4 5 6 7 8
central vein
portal triad
B
100% Leu
0% Leu
WT
Sesn1
Sesn2
CV
PT
C
WT
WT
Sesn1
Sesn2
Glul
Merge
D
100% Leu
0% Leu
WT
DKO
Ⓟ-S240/4-S6
GS
Merge
CV
PT
Ⓟ-S240/4-S6
Intensity
♂
Leu in diet:
WT
DKO
100%
WT
DKO
0%
Layer: 1 2 3 4 5 6 7 8
central vein
portal triad
E
0% Leu
Sestrin:
WT
DKO
FGF21
Glul
Merge

Figure S24: Additional characterization of zonated leucine sensitivity in the liver lobule. (A) Representative images and quantification of *Sesn1* mRNA detected by smFISH in the liver sections from female wildtype mice following 24 hours of feeding with the indicated diets (n=12-18 lobules from n=3 mice/diet). Statistical comparisons to layer 1 for each diet are shown. (B) False-color density of *Sesn1* and *Sesn2* mRNA in liver sections of wildtype female mice following 24 hours of feeding with the indicated diets. Regions of pericentral *Glul*-expressing hepatocytes are outlined. (C) Higher magnification images of *Sesn1* and *Sesn2* mRNA detected by smFISH in pericentral hepatocytes. (D) Representative images and quantification of S6 phosphorylation as detected in immunofluorescence assays on the liver sections from female mice of the indicated liver genotypes 3 hours after refeeding with the indicated diets (n=11-34 lobules from n=3-7 mice/genotype/diet). Statistical comparisons between genotypes on the leucine-free diet are shown. (E) Higher magnification images of *Fgf21* mRNA detected by smFISH in pericentral hepatocytes. CV=central vein; PT=portal triad. Scale bars = 50 μm (A, D), 100 μm (B), or 10 μm (C, E). Data are the mean ± s.e.m. P values were determined using two-way ANOVA with Dunnett test (A) or two-way ANOVA with Sidak test (D). * $p < 0.05$, ** $p < 0.01$, *** $p < 0.001$.

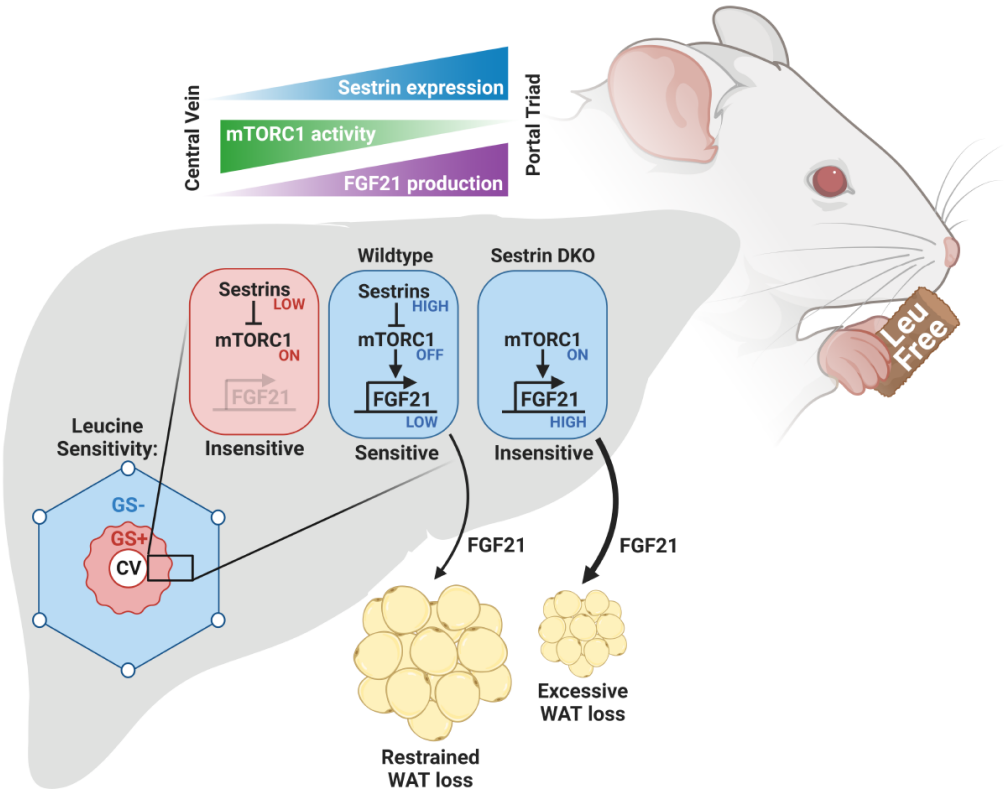

Figure 6: Spatially compartmentalized leucine sensing in the liver controls the physiological adaptation to dietary leucine deprivation. Model of zonated leucine sensing by Sestrin-mTORC1 in the liver and its role in the preservation of white adipose tissue mass in response to dietary leucine deprivation. Created using Biorender.com.

Discussion

The nature of the leucine sensing pathway upstream of mTORC1 has been controversial, and many diverse sensors and mechanisms have been proposed to play a role (Han et al., 2012; Kim et al., 2017; He et al., 2018; Duran et al., 2012; Linares et al., 2013; Lawrence et al., 2018; Son et al., 2019; Budanov & Karin, 2008), largely based on work in cultured cells. We find that Sestrin1 and Sestrin2 control mTORC1

activity in response to leucine in vivo and that this modulation is necessary for mice to adapt to limitations in dietary leucine. These data, along with previous biochemical and structural work (Wolfson et al., 2016; Saxton et al., 2016), are consistent with Sestrin1 and Sestrin2 being leucine sensors for the mTORC1 pathway. It has been proposed that the Sestrins can function through AMPK (Budanov & Karin, 2008), but we find that AMPK is not required for dietary leucine to regulate mTORC1. This does not preclude the possibility, however, that Sestrin loss may secondarily affect AMPK because mTORC1 activity is known to drive energetic stress (Aguilar et al., 2007).

We also reveal a previously unappreciated level of complexity to nutrient sensing by mTORC1 in vivo. In the liver lobules, only hepatocytes in certain zones appreciably express the Sestrins and only in these is mTORC1 signaling sensitive to dietary leucine. In considering why this might be the case, it is worth recalling that mTORC1 controls a large number of metabolic pathways and is also regulated by a diverse set of nutrients (Saxton & Sabatini, 2017; Liu & Sabatini, 2020; Condon & Sabatini, 2019; Valvezan & Manning, 2019). Such an arrangement sets up a conundrum: how can mTORC1 regulate a metabolic pathway in response to the levels of a specific nutrient—such as one consumed by the pathway—but not to others to which sensitivity would be unfavorable?

We hypothesize that, at least in the liver, the zonated expression of nutrient sensors is part of the answer, along with the well-appreciated zonation of many metabolic processes. Although at the whole-liver level we were unable to detect changes in protein synthesis (fig. S22A-B), it is noteworthy that the periportal hepatocytes that express the Sestrins also have been reported to play a predominant

role in liver protein synthesis (Gebhardt & Matz-Soja, 2014; Uchiyama and Asari, 1984), a process that can be regulated by mTORC1 and consumes leucine. Conversely, the pericentral hepatocytes that have low Sestrin expression are the main site of ketogenesis, a process that mTORC1 can inhibit (Pozefsky et al., 1976) but for which leucine sensitivity would be inappropriate given that an abundant supply of dietary glucose, regardless of leucine availability, renders ketones redundant as a fuel source. The combinatorial impact of the zonated expression of the nutrient sensors that signal to mTORC1 and of the metabolic processes controlled by it, may underlie how one pathway can appropriately regulate such a variety of metabolic processes in response to diverse nutritional states.

	Amino-acid replete (Control)		0% Leucine (Leu-free)		10% Leucine	
	gm%	**kcal%**	**gm%**	**kcal%**	**gm%**	**kcal%**
Free Amino Acids	**24.3**	**25.7**	**24.3**	**25.7**	**24.3**	**25.7**
Carbohydrate	**58.3**	**59.9**	**58.3**	**59.9**	**58.3**	**59.9**
Fat	**6.1**	**14.4**	**6.1**	**14.4**	**6.1**	**14.4**
kcal/gm		**3.79**		**3.79**		**3.79**
Ingredient (gm)						
L-Arginine	15	60	15	60	15	60
L-Histidine-HCl-H2O	9	36	9	36	9	36
L-Isoleucine	12	48	12	48	12	48
L-Leucine	18	72	0	0	1.8	7.2
L-Lysine-HCl	21	84	21	84	21	84
L-Methionine	9	36	9	36	9	36
L-Phenylalanine	12	48	12	48	12	48
L-Threonine	12	48	12	48	12	48
L-Tryptophan	3	12	3	12	3	12
L-Valine	12	48	12	48	12	48
L-Alanine	15	60	19.5	78	19.05	76.2
L-Asparagine-H2O	7.5	30	7.5	30	7.5	30
L-Aspartate	15	60	19.5	78	19.05	76.2
L-Cystine	6	24	6	24	6	24
L-Glutamic Acid	45	180	49.5	198	49.05	196.2
L-Glutamine	8	32	8	32	8	32
Glycine	15	60	19.5	78	19.05	76.2
L-Proline	8	32	8	32	8	32
L-Serine	8	32	8	32	8	32
L-Tyrosine	6	24	6	24	6	24
Total L-Amino Acids	256.5	0	256.5	0	256.5	0
Corn Starch	320	1280	320	1280	320	1280
Maltodextrin 10	110	440	110	440	110	440
Dextrose	150	600	150	600	150	600
Cellulose	75	0	75	0	75	0
Inulin	25	37.5	25	37.5	25	37.5
Soybean Oil	64	576	64	576	64	576
Mineral Mix S10001	35	0	35	0	35	0
Sodium Bicarbonate	7.5	0	7.5	0	7.5	0
Vitamin Mix V10001	10	40	10	40	10	40
Choline Bitrartrate	2	0	2	0	2	0
Red Dye, FD&C #40	0	0	0	0	0	0
Blue Dye, FD&C #1	0.05	0	0.025	0	0	0
Yellow Dye, FD&C #5	0	0	0.025	0	0.05	0
Total	**1055.05**	**4000**	**1055.05**	**4000**	**1055.05**	**4000**

Table S1: Formulations of amino acid-defined diets.

Amino Acid	Concentration (uM)
Alanine	665
Arginine	149
Asparagine	129
Aspartate	20
Cysteine	6
Glutamate	26
Glutamine	547
Glycine	126
Histidine	93
Isoleucine	136
Leucine	248
Lysine	300
Methionine	161
Phenylalanine	115
Proline	197
Serine	141
Threonine	284
Tryptophan	110
Tyrosine	126
Valine	393

Table S2: Levels of amino acids in the plasma of refed mice.

Materials and Methods

Mice and diets

All animal work was performed in accordance with the Massachusetts Institute of Technology Committee on Animal Care. Mice were under the husbandry care of Department of Comparative Medicine and housed in the Whitehead Institute for Biomedical Research animal facility at 21°C on a 12-hour light/dark cycle. Sesn1flox/flox mice and Sesn2-/- mice were generous gifts from Ming Li and described previously (Peng et al., 2014). Wildtype controls were generated by heterozygous crosses of these mice. To achieve whole-body (Sestrin DKO), adipose-specific (Sestrin AdiDKO), or liver-specific (Sestrin LiDKO) deletion of both Sesn1 and Sesn2, Sesn1flox/flox; Sesn2-/- mice were crossed with CMV-Cre mice (Jackson 006054), Adipoq-Cre mice (Jackson 028020), or Alb-Cre mice (Jackson 003574), respectively. In the whole-body Sestrin DKO mice, the CMV-Cre induced permanent recombination to generate a Sesn1-/- allele, and the CMV-Cre was subsequently removed in further crosses. Sestrin DKO mice were crossed to Fgf21-/- mice (Jackson 033846) to generate Sestrin DKO; Fgf21-/- mice.

To achieve acute liver-specific deletion of both Sesn1 and Sesn2, AAV expressing Cre driven by the liver-specific TBG promoter (AAV8-TBG-iCre, Vector Biolabs) was administered to 9-week old Sesn1flox/flox; Sesn2-/- mice mice by IP injection (2.5 x 1011 vg/mouse) 2.5 weeks prior to initiation of the dietary treatment. AAV8-TBG-LacZ (Vector Biolabs) was used as a control.

To generate mice with inducible expression of a W444L point mutant of the Sestrin2 protein (Sesn2W444L), a minigene containing 2 tandem sets of sequences

encoding exons 9-10 and the 3' UTR of Sesn2 was knocked into the endogenous Sesn2 locus. The first set encodes the wildtype Sesn2 coding sequence followed by a poly(A) signal and flanked by loxP sites. The second set encodes the W444L point mutation, such that upon Cre-mediated recombination, Sesn2 containing the mutation is expressed. ES cells ((C57BL/6J x 129S6)F1) with the knocked-in construct were generated at the Gene Targeting & Transgenic Facility at Janelia Research Campus and aggregated with CD1 embryos. Knock-in (Sesn2WT) mice were backcrossed 4 times to C57BL/6J mice. To generate a recombined mutant Sesn2W444L allele, Sesn2WT mice were crossed with CMV-Cre mice (Jackson 006054). Sesn2W444L mice and Sesn2WT mice were subsequently intercrossed. Homozygous Sesn2WT/WT and Sesn2W444L/W444L mice were used in experiments.

For generation of mice with liver-specific deletion of AMPKα1 and α2, Prkaa1flox/flox; Prkaa2flox/flox mice were generated by crossing Prkaa1flox/flox mice (Jackson 014141) and Prkaa2flox/flox mice (Jackson 014142), and were subsequently crossed to Alb-Cre mice (Jackson 003574).

Amino acid-defined diets (see Table 1 for formulations) were formulated by and purchased from Research Diets. To keep all diets isonitrogenous, diets in which an amino acid was removed were supplemented with alanine, glutamate, and aspartate, based on previous studies (Anthony et al., 2004). For at least 2 days prior to all dietary experiments, mice were acclimated to an amino acid-defined, nutritionally-complete control diet. Dietary treatments were started at the beginning of the light cycle after fasting the mice for 12 hours overnight. Mice were allowed to feed ad libitum unless otherwise noted. When possible, mice were group housed 2-3 mice per cage. Daily

body weight measurements were recorded 1-2 hours before the beginning of the dark cycle. Core body temperature was measured using a rectal thermometer at the beginning of the light cycle. For the measurement of food intake, mice were singly-housed, and their food was weighed before and after a 24-hour period (including uneaten food discarded on the cage floor). For all experiments in which the dietary treatment lasted 24 hours or longer, the mice were housed on raised wire floors, to prevent feces consumption, throughout the course of the experiment.

In all experiments, mice were studied at 8-12 weeks of age, and were age- and sex-matched within each experiment. Male or female mice were used where indicated. All blood and tissue sample collections were performed at the end of the dark cycle, during which mice do the majority of their feeding. For all experiments in which mice were fed ad libitum, the presence of ingested food in the stomach and duodenum was confirmed during tissue dissection; any mice lacking food contents or stomach distention at the time of dissection were removed from the analyses.

Rapamycin (Thermo Fisher Scientific) was dissolved in ethanol, diluted in saline with 5% PEG400 and 5% Tween80, and administered by IP injection at a dose of 8 mg/kg every 24 hours, with the final dose being 12 hours prior to tissue collection. Leupeptin (Cayman Chemical) was diluted in saline and administered by IP injection at a dose of 40 mg/kg 4 hours prior to tissue collection. Tunicamycin (Millipore Sigma) was dissolved in DMSO, diluted in saline, and administered by IP injection at a dose of 1 mg/kg 24 hours prior to tissue collection.

For intraperitoneal glucose tolerance tests, mice were fasted 6 hours and administered 2 g/kg glucose by IP injection. Tail vein blood glucose levels were

measured using a handheld glucometer (Bayer Contour). For glucose-stimulated insulin secretion assays, mice were fasted 6 hours and administered 2 g/kg glucose by IP injection. Tail vein blood was collected before and 10 minutes after the injection. For insulin stimulations, mice were fasted 6 hours and 0.75 U/kg Insulin (Sigma) was administered by IP injection 10 minutes prior to tissue collection. For assessment of protein synthesis, the SUnSET method was used (Ravi et al., 2020). Briefly, mice were administered 40 μmol/kg puromycin by IP injection 30 minutes prior to tissue collection.

Blood analyses and metabolite profiling

Blood was collected from the tail vein in small volumes (<50 μL) (for repeated sampling) or from the submandibular vein (for endpoint sampling). Blood was collected in lithium heparin-coated tubes (Sarstedt) and the plasma was extracted. Plasma FGF21 levels were measured using a mouse FGF21 ELISA kit (Abcam), and plasma insulin levels were measured using a mouse insulin ELISA kit (Crystal Chem). For experiments in which mTORC1 signaling or metabolite profiling of tissues was to be performed, blood was not collected in order to avoid acute stress-associated metabolic effects.

For polar metabolite profiling, plasma was combined 1:9 (v/v) with extraction buffer (75:25:0.2 acetonitrile:methanol:formic acid containing isotopically-labeled internal standards). Samples were then mixed by vortexing and the debris was pelleted centrifugation in a microcentrifuge (15,000 rpm for 10 min at 4°C). For extraction of polar metabolites from liver tissue, frozen tissue was homogenized in 1 mL extraction buffer (80:20 methanol:H2O containing isotopically-labeled internal standards). Samples were then mixed by vortexing, debris pelleted by centrifugation in a microcentrifuge

(15,000 rpm for 10 min at 4°C), and supernatants dried down in a Refrigerated CentriVap Benchtop Vacuum Concentrator connected to a CentriVap-105 Cold Trap (Labconco). Dried pellets were resuspended in 100 µl water and further diluted 1:10 in extraction buffer (80:20 methanol:H20 containing isotopically-labeled internal standards) to attain a linear range of signal. 2 µl of extracted sample was injected into a ZIC-pHILIC 150×2.1 mm (5 µm particle size) column (EMD Millipore). Analysis was conducted on a QExactive benchtop Orbitrap mass spectrometer equipped with an Ion Max source and a HESI II probe, which was coupled to a Dionex UltiMate 3,000 UPLC system (Thermo Fisher Scientific). External mass calibration was performed using the standard calibration mixture every 7 days. Chromatographic separation was achieved using the following conditions: buffer A was 20 mM ammonium carbonate, 0.1% ammonium hydroxide; buffer B was acetonitrile. The column oven and autosampler tray were held at 25°C and 4°C, respectively. The chromatographic gradient was run at a flow rate of 0.150 ml min−1 as follows: 0–20 min: linear gradient from 80% to 20% B; 20–20.5 min: linear gradient from 20% to 80% B; 20.5–28 min: hold at 80% B. The mass spectrometer was operated in full-scan, polarity switching mode with the spray voltage set to 3.0 kV, the heated capillary held at 275 °C, and the HESI probe held at 350 °C. The sheath gas flow was set to 40 units, the auxiliary gas flow was set to 15 units, and the sweep gas flow was set to 1 unit. The data acquisition was performed over a range of 70–1,000 m/z, with the resolution set at 70,000, the automatic gain control target at 10e6, and the maximum injection time at 20 ms. Relative quantitation of polar metabolites was performed with TraceFinder 4.1 (ThermoFisher) using a 5 p.p.m. mass tolerance and referencing an in-house library of chemical standards. For absolute

quantification of amino acids, a 1mM amino acid mixture was diluted in water to generate an amino acid standard curve (10nM-100μM) and injected alongside the samples to be analyzed. For metabolite analysis in tissues, metabolite abundance was normalized to the weight of the tissue sample extracted.

Ex vivo signaling assays

Media used for ex vivo signaling experiments was RPMI containing 11 mM glucose, 5 ng/mL insulin (Sigma Aldrich), and amino acids at concentrations measured in plasma of refed mice (listed in Table 2) at pH 7.4 to mimic physiological nutrient conditions. Amino acids were omitted from treatment media where indicated.

For the isolation of murine primary hepatocytes, the liver was perfused with disruption solution (HBSS without calcium and magnesium, 25 mM HEPES, 0.5 mM EDTA, and 0.9 mM MgCl2, pH 7.4) for 10 min followed by digestion solution (HBSS with calcium and magnesium, 25 mM HEPES, and 0.05% collagenase IV, pH 7.4) for 10 min by incising the portal vein with a 25G needle attached to a peristaltic pump. The inferior vena cava was incised immediately after perfusion began to allow fluid outflow. After perfusion was complete, the digested liver was transferred to 10 mL PBS, shaken to liberate cells, triturated with a serological pipette, passed through a 100 μm filter, and diluted with 10 mL PBS. Cells were pelleted at 30 g at 4°C for 3 min, resuspended in 12 mL PBS, and combined with 12 mL Percoll-PBS (10.8 mL Percoll, 1.2 mL 10X PBS). Cells were pelleted at 150 g at 4°C for 5 min, resuspended in PBS, counted, then pelleted at 30 g at 4°C for 3 min and resuspended in hepatocyte medium (Williams E medium without phenol red, containing 4% Cell Maintenance Cocktail B and 1.4 μM Dexamethasone (from Primary Hepatocyte Maintenance Supplements, Thermo Fisher

Scientific). Hepatocytes were plated in 6-well plates at 0.5 million cells/well and allowed to attach overnight.

Adipose explants were dissected and immediately pre-incubated in RPMI containing all amino acids for 1 hour at 37°C. This pre-incubation step was omitted for primary hepatocytes. Explants or cells were washed twice, incubated for 1 hour at 37°C in RPMI containing no amino acids, and then incubated for 1 hour at 37°C in RPMI containing the indicated amino acid conditions. For the leucine dose-response experiment with primary hepatocytes, the cells were incubated in RPMI lacking leucine for 50 min at 37°C, followed by the addition of the indicated concentrations of leucine for 10 min at 37°C.

Polysome profiling

Liver tissue was lysed in lysis buffer (10 mM Tris-HCl (pH 7.4), 5 mM MgCl2, 100 mM KCl, 1% Triton X-100, 100 µg/mL cycloheximide, EDTA-free protease inhibitor (Roche)) and cleared by centrifugation in a microcentrifuge (15,000 rpm for 10 min at 4°C). Protein concentrations were quantified for normalization using a Pierce BCA Protein Assay Kit (Thermo Fisher). 1.25 mg of protein (in a 300 µl volume) were separated onto 11 ml of a 10-45% sucrose gradient (containing 10 mM Tris-HCl (pH 7.4), 5 mM MgCl2, 100 mM KCl, 2 mM DTT, 100 µg/mL cycloheximide) by centrifugation at 36,000 rpm for 2 hours at 4°C using a SW41 rotor. The sucrose gradient was then fractionated and UV absorption at 254 nm was recorded. The lowest value of each profile was taken as the background and subtracted. Curves were then aligned based on the monosome peak of each profile. The area under the curve for the polysome and monosome peaks was measured and expressed as a ratio (PS/MS).

Immunoblotting

Tissues or cells were lysed in ice-cold RIPA buffer (150 mM sodium chloride, 1.0% Triton X-100, 0.5% sodium deoxycholate, 0.1% SDS, 50 mM Tris (pH 8.0), EDTA-free protease inhibitor (Roche), PhosSTOP phosphatase inhibitor (Roche)). Lysates were cleared by centrifugation in a microcentrifuge (15,000 rpm for 10 min at 4°C) and protein concentrations quantified for normalization using a Pierce BCA Protein Assay Kit (Thermo Fisher), or Protein Assay Dye Reagent (Bio-Rad) for adipose tissues. Lysate samples were prepared by the addition of 5× sample buffer (0.242 M Tris, 10% SDS, 25% glycerol, 0.5 M dithiothreitol (DTT) and bromophenol blue). 20-40 μg of protein (or 2 μg for S6 levels and phosphorylation and UCP1 levels) were resolved by SDS–PAGE and analyzed by immunoblotting. The following antibodies were used: phospho-T389 S6K1 (9234), S6K1 (2708), phospho-S65 4EBP1 (9451), 4EBP1 (9644), phosphor-S757 ULK1 (6888), ULK1 (8054), phospho-T308 AKT (2965), pan-AKT (4691), GAPDH (2118), Mios (13557), GCN2 (3302), AMPKα (2532), phospho-S79 ACC (3661), ACC (3662), phospho-T980 PERK (3179), PERK (3192), phospho-S51 eIF2α (9721), eIF2α (9722), LC3B (3868) from Cell Signaling Technology; phospho-T899 GCN2 (ab75836) from Abcam; ATF4 (sc-390063) from Santa Cruz Biotechnology; Puromycin (PMY-2A4) from DSHB; Sestrin1 (21668-1-AP), Sestrin2 (10795-1-AP), WDR24 (20778-1-AP) from Proteintech; Raptor from Millipore (09-217); FGF21 (AF3057) from R&D Systems; HRP-labeled anti-mouse and anti-rabbit secondary antibodies from Cell Signaling Technology; HRP-labeled anti-goat secondary antibody from Santa Cruz Biotechnology. Exposed films were scanned, band intensities were quantified using Fiji, and the background signal measured from an empty lane was then subtracted. Band intensities

were normalized to the average intensity of the WT control group of the same experimental cohort.

Co-immunoprecipitation assays

Mouse liver tissue was lysed in Triton lysis buffer (40 mM NaHEPES (pH 7.4), 5 mM MgCl2, 10 mM Na4P2O7, 10 mM Na β-glycerol phosphate, 1% Triton X-100, EDTA-free protease inhibitor (Roche), PhosSTOP phosphatase inhibitor (Roche)), cleared by centrifugation in a microcentrifuge (15,000 rpm for 10 min at 4°C), and protein quantified using a Pierce BCA Protein Assay Kit (Thermo Fisher). 2 mg of protein was incubated with 4 µg of antibody (WDR24, Proteintech 20778-1-AP) for 3 hours at 4°C, followed by incubating with 20 µl of Protein G bead slurry for an additional 1 hour at 4°C. Beads were washed once with Triton lysis buffer, followed by 3 washes with Triton lysis buffer containing 500 mM NaCl. For samples with amino acid additions, 500 µM of leucine or arginine was included in the wash buffer for all washes. Washed beads were resuspended in 100 µl of 2.5x sample buffer and boiled for 5 min.

Histology and immunofluorescence

Tissues were fixed in 10% formalin, embedded in paraffin, sectioned (5 µM-thick), and stained with hematoxylin and eosin. For immunofluorescence, antigen retrieval was performed with Borg Decloaker RTU solution (Biocare Medical) in a pressurized Decloaking Chamber (Biocare Medical) for 3 min. Sections were subsequently blocked (5% normal donkey serum, 0.3% Triton X-100 in PBS) and incubated overnight with 1% BSA, 0.3% Triton X-100, and primary antibodies at 4°C, followed by incubation at room temperature with secondary antibodies and Hoechst. Sections were mounted using Vectashield Antifade Mounting Media (Vector Labs). The

following antibodies were used: phospho-S235/236 S6 (2211), phospho-S240/244 S6 (5364) from Cell Signaling Technology; Glutamine Synthetase (sc-74430) from Santa Cruz Biotechnology; Alexa-488- and -568-conjugated secondary antibodies from Invitrogen. Images were acquired on an inverted fluorescence microscope (Zeiss) using the ZEN software package (Zeiss), and the exposure time for each channel was kept constant for all slides.

In situ hybridization

In situ hybridization was performed on frozen liver sections using RNAscope (Advanced Cell Diagnostics, Inc). The following probes were used: Mm-Sesn2 (574751), Mm-Sesn1 (811271), Mm-Fgf21 (460931), Mm-Glul-C2 (426231-C2). The RNAscope Multiplex Fluorescent Kit V2 was used. Tissue preparation and hybridization protocol were followed according to the manufacturer's instructions. Images were acquired on a spinning-disk confocal microscope (Perkin Elmer) using MetaMorph 7 software, and the exposure time for each channel was kept constant for all slides.

Image analyses

Raw image files were quantified in Fiji. For FISH confocal images, background signal from tissue autofluorescence was subtracted using a rolling ball radius set to 10. In each image analyzed, the radius of a lobule (the distance between the edge of a portal vein and the central vein) was divided into 8 bins of equal length and size, and the total signal (integrated density) in each bin was measured as signal per pixel area. Background signal per pixel area was measured within the lumen of the central vein and subtracted from the measured values. Signal intensities were normalized to the average intensity of layer 1 or layer 8 of the WT control group.

RNA-seq and Quantitative PCR

Total RNA was isolated from tissues with the miRNeasy Mini Kit (Qiagen) and cleaned using 1.5X SPRI beads. RNA seq libraries were prepared using an SPT Mosquito HV automated liquid handler using NEBNext UltraII directional RNA Library Prep for Illumina, starting with 250ng of input RNA. Quality of indexed libraries was confirmed using an Agilent Fragment Analyzer and qPCR. Samples were sequenced on a NovaSeq2000 using 50nt paired-end reads. 75x75 paired-end reads were mapped to the canonical chromosomes of the mouse genome (GRCm38/mm10) using STAR 2.7.1a (default parameters), indexed with all mouse genes from Ensembl 96. Gene counts were obtained using featureCounts (v 2.0.1, with “-p -s 2”) and the same gene annotations. Differential expression was assayed using DESeq2 (v1.26.0, with lfcShrink(type="ashr")). Gene set enrichment analysis was performed using the GSEA tool (v4.1.0) developed by the Broad Institute. Genes were ranked according to their log2 (fold change) values and analyzed using the “pre-ranked” mode of the GSEA software using the following parameters: -mode Max_probe -norm meandiv -nperm 1000 -scoring_scheme weighted -set_max 500 -set_min 15. Gene sets in the MSigDB Hallmark gene set collection (v7.5), as well as previously curated ATF4 gene signatures (Bao et al., 2016; Guo et al., 2020; Quiros et al., 2017) were used in the analysis. The accession number for the RNA sequencing data is GEO: GSE197806.

For quantitative PCR, RNA was retro-transcribed with iScript Reverse Transcription Supermix (Bio-Rad) and used at 1:100 dilution in quantitative PCR (qPCR) reactions with iTaq Universal SYBR Green Supermix (Bio-Rad). The

QuantStudio 6 Flex (Applied Biosystems) qPCR instrument was used for all reactions. The reference gene 36B4 was used for normalization. The following primers were used:

Trib3 f, CAGCAACTGTGAGAGGACGA

Trib3 r, TGGAATGGGTATCTGCCAGC

Ddit3 f, CTGGAAGCCTGGTATGAGGAT

Ddit3 r, CAGGGTCAAGAGTAGTGAAGGT

Asns f, CTGTTACAATGGTGAAATCTACAACCACAAG

Asns r, GATGAATGCAAACACCCCGTCCAGCATACAGAT

Ddit4 f, CAAGGCAAGAGCTGCCATAG

Ddit4 r, CCGGTACTTAGCGTCAGGG

Fgf21 f, TACACAGATGACGACCAAGA;

Fgf21 r, GGCTTCAGACTGGTACACAT

36B4 f, TAAAGACTGGAGACAAGGTG;

36B4 r, GTGTACTCAGTCTCCACAGA.

Statistical analyses

Genotypes on each dietary condition were compared using two-tailed t-tests for comparisons between two groups, or one-way ANOVA with post hoc tests as indicated for comparisons of three or more groups. For repeated measurements over time, comparisons between genotypes on each dietary condition were made using repeated measures two-way ANOVA with post hoc tests as indicated. P values < 0.05 were considered to indicate statistical significance.

Acknowledgments: We thank all members of the Sabatini lab, as well as Harvey Lodish and Matthew Vander Heiden, for suggestions and experimental help; Brendan Manning, Tong Zhang, Martina Wallace, Christian Metallo, Su Myung Jung, and David Guertin for discussions; and Maria Mihaylova, William Festuccia, Monther Abu-Remaileh, Nouf Laqtom, Kristina Lopez and Kristin Knouse for technical advice and assistance. We thank Ming Li for the *Sesn1*$^{flox/flox}$ and *Sesn2*$^{-/-}$ mice, and the Gene Targeting & Transgenic Facility at Janelia Research Campus for generation of the *Sesn2*^{W444L} mice. We thank the MIT BioMicroCenter for RNA library prep and sequencing. We also thank members of the Hope Babette Tang Histology Facility at the Koch Institute and Sven Holder for histology support.

Author contributions: A.L.C. and D.M.S. conceived the project. A.L.C. designed and performed all experiments with input from D.M.S. and assistance from A.M.P., T.P.N., J.M.R., A.A., and J.B.S., and A.M.P. helped with discussion and interpretation of results. T.K., B.W., S.H.C., and C.A.L. extracted metabolites, operated the LC–MS platform, and analyzed the metabolomics data. G.W.B. analyzed the RNA-seq data. W.C.C. provided technical training, established the Sestrin knockout mouse lines, and designed the genetic strategy for generating the *Sesn2*^{W444L} mice. A.H. helped with discussion and execution of liver zonation experiments. A.L.C. and D.M.S. wrote the manuscript, and all authors edited it.

Declaration of interests: D.M.S. is a founder and shareholder for Navitor Pharmaceuticals, which is targeting the mTORC1 pathway for therapeutic benefit.

References

Wallace, M., C.R. Green, L.S. Roberts, Y.M. Lee, J.L. McCarville, J. Sanchez-Gurmaches, N. Meurs, J.M. Gengatharan, J.D. Hover, S.A. Phillips, T.P. Ciaraldi, D.A. Guertin, P. Cabrales, J.S. Ayres, D.K. Nomura, R. Loomba, and C.M. Metallo. 2018. Enzyme promiscuity drives branched-chain fatty acid synthesis in adipose tissues. *Nat Chem Biol*. 14:1021-1031.

Crown, S.B., N. Marze, and M.R. Antoniewicz. 2015. Catabolism of branched chain amino acids contributes significantly to synthesis of odd-chain and even-chain fatty acids in 3T3-L1 adipocytes. *PLoS One* 10:e0145850.

Rosenthal, J., A. Angel, and J. Farkas. 1974. Metabolic fate of leucine: a significant sterol precursor in adipose tissue and muscle. *Am J Physiol*. 226:411-8.

Saxton, R.A. and D.M. Sabatini. 2017. mTOR signaling in growth, metabolism, and disease. *Cell*. 168:960-976.

Anthony, J.C., F. Yoshizawa, T.G. Anthony, T.C. Vary, L.S. Jefferson, and S.R. Kimball. 2000. Leucine stimulates translation initiation in skeletal muscle of postabsorptive rats via a rapamycin-sensitive pathway. *J Nutr*. 130:2413-9.

Duan, Y., F. Li, H. Liu, Y. Li, Y. Liu, X. Kong, Y. Zhang, D. Deng, Y. Tang, Z. Feng, G. Wu, and Y. Yin. 2015. Nutritional and regulatory roles of leucine in muscle growth and fat reduction. *Front Biosci (Landmark Ed)*. 20:796-813.

Yin, Y., K. Yao, Z. Liu, M. Gong, Z. Ruan, D. Deng, B. Tan, Z. Liu, and G. Wu. 2010. Supplementing L-leucine to a low-protein diet increases tissue protein synthesis in weanling pigs. *Amino Acids*. 39:1477-86.

Li, F., Y. Yin, B. Tan, X. Kong, and G. Wu. 2011. Leucine nutrition in animals and humans: mTOR signaling and beyond. *Amino Acids*. 41:1185-93.

Moore, W.T., S.M. Bowser, D.W. Fausnacht, L.L. Staley, K.S. Suh, and D. Liu. 2015. Beta cell function and the nutritional state: dietary factors that influence insulin secretion. *Curr Diab Rep*. 15:76.

de Oliveira, C.A., M.Q. Latorraca, M.A. de Mello, and E.M. Carneiro. 2011. Mechanisms of insulin secretion in malnutrition: modulation by amino acids in rodent models. *Amino Acids*. 40:1027-34.

Yang, J., Y. Chi, B.R. Burkhardt, Y. Guan, and B.A. Wolf. 2010. Leucine metabolism in regulation of insulin secretion from pancreatic beta cells. *Nutr Rev*. 68:270-9.

Ananieva, E.A., J.D. Powell, and S.M. Hutson. 2016. Leucine metabolism in T cell activation: mTOR signaling and beyond. *Adv Nutr*. 7:798S-805S.

Ren, W., G. Liu, J. Yin, B. Tan, G. Wu, F.W. Bazer, Y. Peng, and Y. Yin. 2017. Amino-acid transporters in T-cell activation and differentiation. *Cell Death Dis*. 8:e2655.

Torigoe, M., K. Maeshima, T. Ozaki, Y. Omura, K. Gotoh, Y. Tanaka, K. Ishii, and H. Shibata. 2019. l-Leucine influx through Slc7a5 regulates inflammatory responses of human B cells via mammalian target of rapamycin complex 1 signaling. *Mod Rheumatol*. 29:885-891.

Richardson, N.E., E.N. Konon, H.S. Schuster, A.T. Mitchell, C. Boyle, A.C. Rodgers, M. Finke, L.R. Haider, D. Yu, V. Flores, H.H. Pak, S. Ahmad, S. Ahmed, A. Radcliff, J. Wu, E.M. Williams, L. Abdi, D.S. Sherman, T. Hacker, and D.W. Lamming. 2021. Lifelong restriction of dietary branched-chain amino acids has sex-specific benefits for frailty and lifespan in mice. *Nat Aging*. 1:73-86.

D'Antona, G., M. Ragni, A. Cardile, L. Tedesco, M. Dossena, F. Bruttini, F. Caliaro, G.

Corsetti, R. Bottinelli, M.O. Carruba, A. Valerio, and E. Nisoli. 2010. Branched-chain amino acid supplementation promotes survival and supports cardiac and skeletal muscle mitochondrial biogenesis in middle-aged mice. *Cell Metab*. 12:362-372.

Solon-Biet, S.M., V.C. Cogger, T. Pulpitel, D. Wahl, X. Clark, E. Bagley, G.C. Gregoriou, A.M. Senior, Q.P. Wang, A.E. Brandon, R. Perks, J. O'Sullivan, Y.C. Koay, K. Bell-Anderson, M. Kebede, B. Yau, C. Atkinson, G. Svineng, T. Dodgson, J.A. Wali, M.D.W. Piper, P. Juricic, L. Partridge, A.J. Rose, D. Raubenheimer, G.J. Cooney, D.G. Le Couteur, and S.J. Simpson. 2019. Branched chain amino acids impact health and lifespan indirectly via amino acid balance and appetite control. *Nat Metab*. 1:532-545.

Newgard, C.B., J. An, J.R. Bain, M.J. Muehlbauer, R.D. Stevens, L.F. Lien, A.M. Haqq, S.H. Shah, M. Arlotto, C.A. Slentz, J. Rochon, D. Gallup, O. Ilkayeva, B.R. Wenner, W.S. Yancy Jr, H. Eisenson, G. Musante, R.S. Surwit, D.S. Millington, M.D. Butler, and L.P. Svetkey. 2009. A branched-chain amino acid-related metabolic signature that differentiates obese and lean humans and contributes to insulin resistance. *Cell Metab*. 9:311-26.

Lynch, C.J. and S.H. Adams. 2014. Branched-chain amino acids in metabolic signalling and insulin resistance. *Nat Rev Endocrinol*. 10:723-36.

Fontana, L., N.E. Cummings, S.I. Arriola Apelo, J.C. Neuman, I. Kasza, B.A. Schmidt, E. Cava, F. Spelta, V. Tosti, F.A. Syed, E.L. Baar, N. Veronese, S.E. Cottrell, R.J. Fenske, B. Bertozzi, H.K. Brar, T. Pietka, A.D. Bullock, R.S. Figenshau, G.L. Andriole, M.J. Merrins, C.M. Alexander, M.E. Kimple, and D.W. Lamming. 2016. Decreased consumption of branched-chain amino acids improves metabolic health. *Cell Rep*. 16:520-530.

Liu, G.Y. and D.M. Sabatini. 2020. mTOR at the nexus of nutrition, growth, ageing and disease. *Nat Rev Mol Cell Biol*. 21:183-203.

Condon, K.J. and D.M. Sabatini. 2019. Nutrient regulation of mTORC1 at a glance. *J Cell Sci*. 132:jcs222570.

Valvezan, A.J. and B.D. Manning. 2019. Molecular logic of mTORC1 signalling as a metabolic rheostat. *Nat Metab*. 1:321-333.

Han, J.M., S.J. Jeong, M.C. Park, G. Kim, N.H. Kwon, H.K. Kim, S.H. Ha, S.H. Ryu, and S. Kim. 2012. Leucyl-tRNA synthetase is an intracellular leucine sensor for the mTORC1-signaling pathway. *Cell*. 149:410-24.

Kim, J.H., C. Lee, M. Lee, H. Wang, K. Kim, S.J. Park, I. Yoon, J. Jang, H. Zhao, H.K. Kim, N.H. Kwon, S.J. Jeong, H.C. Yoo, J.H. Kim, J.S. Yang, M.Y. Lee, C.W. Lee, J. Yun, S.J. Oh, J.S. Kang, S.A. Martinis, K.Y. Hwang, M. Guo, G. Han, J.M. Han, and S. Kim. 2017. Control of leucine-dependent mTORC1 pathway through chemical intervention of leucyl-tRNA synthetase and RagD interaction. *Nat Commun*. 8:732.

He, X.D., W. Gong, J.N. Zhang, J. Nie, C.F. Yao, F.S. Guo, Y. Lin, X.H. Wu, F. Li, J. Li, W.C. Sun, E.D. Wang, Y.P. An, H.R. Tang, G.Q. Yan, P.Y. Yang, Y. Wei, Y.Z. Mao, P.C. Lin, J.Y. Zhao, Y. Xu, W. Xu, and S.M. Zhao. 2018. Sensing and transmitting intracellular amino acid signals through reversible lysine aminoacylations. *Cell Metab*. 27:151-166.e6.

Durán, R.V., W. Oppliger, A.M. Robitaille, L. Heiserich, R. Skendaj, E. Gottlieb, and M.N. Hall. 2012. Glutaminolysis activates Rag-mTORC1 signaling. *Mol Cell*. 47:349-58.

Linares, J.F., A. Duran, T. Yajima, M. Pasparakis, J. Moscat, and M.T. Diaz-Meco. 2013. K63 polyubiquitination and activation of mTOR by the p62-TRAF6 complex in nutrient-activated cells. *Mol Cell*. 51:283-96.

Lawrence, R.E., K.F. Cho, R. Rappold, A. Thrun, M. Tofaute, D.J. Kim, O. Moldavsk, J.H. Hurley, and R. Zoncu. 2018. A nutrient-induced affinity switch controls mTORC1 activation by its Rag GTPase-Ragulator lysosomal scaffold. *Nat Cell Biol*. 20:1052-1063.

Son, S.M., S.J. Park, H. Lee, F. Siddiqi, J.E. Lee, F.M. Menzies, and D.C. Rubinsztein. 2019. Leucine signals to mTORC1 via its metabolite acetyl-coenzyme A. *Cell Metab*. 29:192-201.e7.

Budanov, A.V. and M. Karin. 2008. p53 target genes sestrin1 and sestrin2 connect genotoxic stress and mTOR signaling. *Cell*. 134:451-60.

Wolfson, R.L., L. Chantranupong, R.A. Saxton, K. Shen, S.M. Scaria, J.R. Cantor, and D.M. Sabatini. 2016. Sestrin2 is a leucine sensor for the mTORC1 pathway. *Science*. 351:43-8.

Saxton, R.A., K.E. Knockenhauer, R.L. Wolfson, L. Chantranupong, M.E. Pacold, T. Wang, T.U. Schwartz, and D.M. Sabatini. 2016. Structural basis for leucine sensing by the Sestrin2-mTORC1 pathway. *Science*. 351:53-8.

Fang, Z., H.G. Kim, M. Huang, K. Chowdhury, M.O. Li, S. Liangpunsakul, and X.C. Dong. 2021. Sestrin proteins protect against lipotoxicity-induced oxidative stress in the liver via suppression of c-Jun N-terminal kinases. *Cell Mol Gastroenterol Hepatol*. 12:921-42.

Yang, B.A., J. Castor-Macias, P. Fraczek, A. Cornett, L.A. Brown, M. Kim, S.V. Brooks, I.M.A. Lombaert, J.H. Lee, and C.A. Aguilar. 2021. Sestrins regulate muscle stem cell metabolic homeostasis. *Stem Cell Reports*. 16:2078-88.

Lee, J.H., A.V. Budanov, S. Talukdar, E.J. Park, H.L. Park, H.W. Park, G. Bandyopadhyay, N. Li, M. Aghajan, I. Jang, A.M. Wolfe, G.A. Perkins, M.H. Ellisman, E. Bier, M. Scadeng, M. Foretz, B. Viollet, J. Olefsky, and M. Karin. 2012. Maintenance of metabolic homeostasis by Sestrin2 and Sestrin3. *Cell Metab*. 16:311–21.

Segalés, J., E. Perdiguero, A.L. Serrano, P. Sousa-Victor, L. Ortet, M. Jardí, A.V. Budanov, L. Garcia-Prat, M. Sandri, D.M. Thomson, M. Karin, J.H. Lee, and P. Muñoz-Cánoves. 2020. Sestrin prevents atrophy of disused and aging muscles by integrating anabolic and catabolic signals. *Nat Commun*. 11:189.

Kim M, Sujkowski A, Namkoong S, Gu B, Cobb T, Kim B, Kowalsky AH, Cho C-S, Semple I, Ro S-H, Davis C, Brooks SV, Karin M, Wessells RJ, Lee JH. 2020. Sestrins are evolutionarily conserved mediators of exercise benefits. *Nat Commun*. 11:190.

Lu, J., U. Temp, A. Muller-Hartmann, J. Esser, S. Gronke, and L. Partridge L. 2021. Sestrin is a key regulator of stem cell function and lifespan in response to dietary amino acids. *Nat Aging* 1:60–72.

Xiao, F., Z. Huang, H. Li, J. Yu, C. Wang, S. Chen, Q. Meng, Y. Cheng, X. Gao, J. Li, Y. Liu, and F. Guo. 2011. Leucine deprivation increases hepatic insulin sensitivity via GCN2/mTOR/S6K1 and AMPK pathways. *Diabetes* 60:746-56.

Wei, S., J. Zhao, S. Wang, M. Huang, Y. Wang, and Y. Chen. 2018. Intermittent

administration of a leucine-deprived diet is able to intervene in type 2 diabetes in db/db mice. *Heliyon* 4:e00830.
Xu, D., K.L. Shimkus, H.A. Lacko, L. Kutzler, L.S. Jefferson, and S.R. Kimball. 2019. Evidence for a role for Sestrin1 in mediating leucine-induced activation of mTORC1 in skeletal muscle. *Am J Physiol Endocrinol Metab*. 316:E817-E828.
Magdalon, J., P. Chimin, T. Belchior, R.X. Neves, M.A. Vieira-Lara, M.L. Andrade, T.S. Farias, A. Bolsoni-Lopes, V.A. Paschoal, A.S. Yamashita, A.J. Kowaltowski, and W.T. Festuccia. 2016. Constitutive adipocyte mTORC1 activation enhances mitochondrial activity and reduces visceral adiposity in mice. *Biochim Biophys Acta*. 1861:430-8.
Sengupta, S., T.R. Peterson, M. Laplante, S. Oh, and D.M. Sabatini. 2010. mTORC1 controls fasting-induced ketogenesis and its modulation by ageing. *Nature*. 468:1100-4.
Koketsu, Y., H. Sakoda, M. Fujishiro, A. Kushiyama, Y. Fukushima, H. Ono, M. Anai, T. Kikuchi, T. Fukuda, H. Kamata, N. Horike, Y. Uchijima, H. Kurihara, and T. Asano. 2008. Hepatic overexpression of a dominant negative form of raptor enhances Akt phosphorylation and restores insulin sensitivity in K/KAy mice. *Am J Physiol Endocrinol Metab*. 294:E719-25.
Cornu, M., W. Oppliger, V. Albert, A.M. Robitaille, F. Trapani, L. Quagliata, T. Fuhrer, U. Sauer, L. Terracciano, and M.N. Hall. 2014. Hepatic mTORC1 controls locomotor activity, body temperature, and lipid metabolism through FGF21. *Proc Natl Acad Sci U S A.* 111:11592-9.
Pozefsky, T., R.G. Tancredi, R.T. Moxley, J. Dupre, and J.D. Tobin. 1976. Effects of brief starvation on muscle amino acid metabolism in nonobese man. *J Clin Invest*. 57:444-9.
Vendelbo, M.H., A.B. Møller, B. Christensen, B. Nellemann, B.F. Clasen, K.S. Nair, J.O. Jørgensen, N. Jessen, and N. Møller. 2014. Fasting increases human skeletal muscle net phenylalanine release and this is associated with decreased mTOR signaling. *PLoS One*. 9:e102031.
Cahill. G.F. Jr. 1970. Starvation in man. *N Engl J Med.* 282:668-75.
Wolfe, R.R. 2006. The underappreciated role of muscle in health and disease. *Am J Clin Nutr*. 84:475-82.
De Sousa-Coelho, A.L., P.F. Marrero, and D. Haro. 2012. Activating transcription factor 4-dependent induction of FGF21 during amino acid deprivation. *Biochem J*. 443:165-71.
De Sousa-Coelho, A.L., J. Relat, E. Hondares, A. Pérez-Martí, F. Ribas, F. Villarroya, P.F. Marrero, and D. Haro. 2013. FGF21 mediates the lipid metabolism response to amino acid starvation. *J Lipid Res*. 54:1786-97.
Laeger, T., T.M. Henagan, D.C. Albarado, L.M. Redman, G.A. Bray, R.C. Noland, H. Münzberg, S.M. Hutson, T.W. Gettys, M.W. Schwartz, and C.D. Morrison. 2014. FGF21 is an endocrine signal of protein restriction. *J Clin Invest*. 124:3913-22.
Allard, C., F. Bonnet, B. Xu, L. Coons, D. Albarado, C. Hill, G. Fagherazzi, K.S. Korach, E.R. Levin, J. Lefante, C. Morrison, and F. Mauvais-Jarvis. 2019. Activation of hepatic estrogen receptor-α increases energy expenditure by stimulating the production of fibroblast growth factor 21 in female mice. *Mol Metab*. 22:62-70.
Lundåsen, T., M.C. Hunt, L.M. Nilsson, S. Sanyal, B. Angelin, S.E. Alexson, and M.

Rudling. 2007. PPARalpha is a key regulator of hepatic FGF21. *Biochem Biophys Res Commun*. 360:437-40.
Kim, K.H., Y.T. Jeong, H. Oh, S.H. Kim, J.M. Cho, Y.N. Kim, S.S. Kim, D.H. Kim, K.Y. Hur, H.K. Kim, T. Ko, J. Han, H.L. Kim, J. Kim, S.H. Back, M. Komatsu, H. Chen, D.C. Chan, M. Konishi, N. Itoh, C.S. Choi, and M.S. Lee. 2013. Autophagy deficiency leads to protection from obesity and insulin resistance by inducing Fgf21 as a mitokine. *Nat Med*. 19:83-92.
Maruyama, R., M. Shimizu, J. Li, J. Inoue, and R. Sato. 2016. Fibroblast growth factor 21 induction by activating transcription factor 4 is regulated through three amino acid response elements in its promoter region. *Biosci Biotechnol Biochem*. 80:929-34.
Harding, H.P., I. Novoa, Y. Zhang, H. Zeng, R. Wek, M. Schapira, and D. Ron. 2000. Regulated translation initiation controls stress-induced gene expression in mammalian cells. *Mol Cell*. 6:1099-108.
Torrence, M.E., M.R. MacArthur, A.M. Hosios, A.J. Valvezan, J.M. Asara, J.R. Mitchell, and B.D. Manning. 2021. The mTORC1-mediated activation of ATF4 promotes protein and glutathione synthesis downstream of growth signals. *Elife*. 10:e63326.
Ben-Sahra, I., G. Hoxhaj, S.J.H. Ricoult, J.M. Asara, and B.D. Manning. 2016. mTORC1 induces purine synthesis through control of the mitochondrial tetrahydrofolate cycle. *Science*. 351:728-733.
Lange, P.S., J.C. Chavez, J.T. Pinto, G. Coppola, C.W. Sun, T.M. Townes, D.H. Geschwind, and R.R. Ratan. 2008. ATF4 is an oxidative stress – inducible, prodeath transcription factor in neurons in vitro and in vivo. *J Exp Med*. 205:1227-42.
Miyamoto, N., H. Izumi, R. Miyamoto, H. Bin, H. Kondo, A. Tawara, Y. Sasaguri, and K. Kohno. 2011. Transcriptional regulation of Activating Transcription Factor 4 under oxidative stress in retinal pigment epithelial ARPE-19/HPV-16 cells. *Invest Ophthalmol Vis Sci*. 52:1226-34.
Madrigal-Matute, J. and A.M. Cuervo. 2016. Regulation of liver metabolism by autophagy. *Gastroenterology*. 150:328-39.
Ezaki, J., N. Matsumoto, M. Takeda-Ezaki, M. Komatsu, K. Takahashi, Y. Hiraoka, H. Taka, T. Fujimura, K. Takehana, M. Yoshida, J. Iwata, I. Tanida, N. Furuya, D.M. Zheng, N. Tada, K. Tanaka, E. Kominami, and T. Ueno. 2011. Liver autophagy contributes to the maintenance of blood glucose and amino acid levels. *Autophagy*. 7:727-36.
Moulis, M. and C. Vindis. 2017. Methods for measuring autophagy in mice. *Cells* 6:14.
Haspel, J., R.S. Shaik, E. Ifedigbo, K. Nakahira, T. Dolinay, J.A. Englert, and A.M.K. Choi AMK. 2011. Characterization of macroautophagic flux in vivo using a leupeptin-based assay. *Autophagy* 7:629-42.
Anthony, T.G., B.J. McDaniel, R.L. Byerley, B.C. McGrath, D.R. Cavener, M.A. McNurlan, and R.C. Wek. 2004. Preservation of liver protein synthesis during dietary leucine deprivation occurs at the expense of skeletal muscle mass in mice deleted for eIF2 kinase GCN2. *J Biol Chem*. 279:36553-61.
Halpern, K.B., R. Shenhav, O. Matcovitch-Natan, B. Toth, D. Lemze, M. Golan, E.E. Massasa, S. Baydatch, S. Landen, A.E. Moor, A. Brandis, A. Giladi, A.S. Avihail, E. David, I. Amit, and S. Itzkovitz. 2017. Single-cell spatial reconstruction reveals global division of labour in the mammalian liver. *Nature*. 542:352-356.
Jungermann, K. and N. Katz. 1989. Functional specialization of different hepatocyte

populations. *Physiol Rev*. 69:708-64.
Ye, J., W. Palm, M. Peng, B. King, T. Lindsten, M.O. Li, C. Koumenis, and C.B. Thompson. 2015. GCN2 sustains mTORC1 suppression upon amino acid deprivation by inducing Sestrin2. *Genes Dev*. 29:2331-6.
Gebhardt, R. and A. Hovhannisyan. 2010. Organ patterning in the adult stage: the role of Wnt/beta-catenin signaling in liver zonation and beyond. *Dev Dyn*. 239:45-55.
Gebhardt, R., and P.J. Coffer. 2013. Hepatic autophagy is differentially regulated in periportal and pericentral zones - a general mechanism relevant for other tissues? *Cell Commun Signal*. 11:21.
Droin, C., J.E. Kholtei, K.B. Halpern, C. Hurni, M. Rozenberg, S. Muvkadi, S. Itzkovitz, and F. Naef. 2021. Space-time logic of liver gene expression at sub-lobular scale. *Nat Metab*. 3:43-58.
Nicklin, P., P. Bergman, B. Zhang, E. Triantafellow, H. Wang, B. Nyfeler, H. Yang, M. Hild, C. Kung, C. Wilson, V.E. Myer, J.P. MacKeigan, J.A. Porter, Y.K. Wang, L.C. Cantley, P.M. Finan, and L.O. Murphy. 2009. Bidirectional transport of amino acids regulates mTOR and autophagy. *Cell*. 136:521-34.
Aguilar, V., S. Alliouachene, A. Sotiropoulos, A. Sobering, Y. Athea, F. Djouadi, S. Miraux, E. Thiaudière, M. Foretz, B. Viollet, P. Diolez, J. Bastin, P. Benit, P. Rustin, D. Carling, M. Sandri, R. Ventura-Clapier, and M. Pende. 2007. S6 kinase deletion suppresses muscle growth adaptations to nutrient availability by activating AMP kinase. *Cell Metab*. 5:476-87.
Gebhardt, R. and M. Matz-Soja. 2014. Liver zonation: Novel aspects of its regulation and its impact on homeostasis. *World J Gastroenterol*. 20:8491-504.
Uchiyama, Y. and A. Asari. 1984. A morphometric study of the variations in subcellular structures of rat hepatocytes during 24 hours. *Cell Tissue Res*. 236:305-15.
Peng, M., N. Yin, and M.O. Li. 2014. Sestrins function as guanine nucleotide dissociation inhibitors for Rag GTPases to control mTORC1 signaling. *Cell*. 159:122-133.
Ravi, V., A. Jain, S. Mishra, and N.R. Sundaresan. 2020. Measuring protein synthesis in cultured cells and mouse tissues using the non-radioactive SUnSET assay. *Curr Protoc Mol Biol*. 133:e127.
Bao, X.R., S.E. Ong, O. Goldberger, J. Peng, R. Sharma, D.A. Thompson, S.B. Vafai, A.G. Cox, E. Marutani, F. Ichinose, W. Goessling, A. Regev, S.A. Carr, C.B. Clish, and V.K. Mootha. 2016. Mitochondrial dysfunction remodels onecarbon metabolism in human cells. *eLife* 5:e10575.
Guo, X., G. Aviles, Y. Liu, R. Tian, B.A. Unger, Y.H.T. Lin, A.P. Wiita, K. Xu, M.A. Correia, and M. Kampmann. 2020. Mitochondrial stress is relayed to the cytosol by an OMA1-DELE1-HRI pathway. *Nature* 579:427–32.
Quirós, P.M., M.A. Prado, N. Zamboni, D. D'Amico, R.W. Williams, D. Finley, S.P. Gygi, and J. Johan Auwerx. 2017. Multi-omics analysis identifies ATF4 as a key regulator of the mitochondrial stress response in mammals. *J Cell Biol* 216:2027-45.

Chapter 3

Reprinted from *Cell Metabolism*

A Nutrient-Sensing Transition at Birth Triggers Glucose-Responsive Insulin Secretion

Aharon Helman,[1,7,8,*] Andrew L. Cangelosi,[2,3,4,5,6,7] Jeffrey C. Davis,[1] Quan Pham,[1] Arielle Rothman,[1] Aubrey L. Faust,[1] Juerg R. Straubhaar,[1] David M. Sabatini,[2,3,4,5,6,*] and Douglas A. Melton[1,4,9,*]

[1]Department of Stem Cell and Regenerative Biology, Harvard University, Cambridge, MA 02138, USA
[2]Whitehead Institute for Biomedical Research, Cambridge, MA 02142, USA
[3]Department of Biology, Massachusetts Institute of Technology, Cambridge, MA 02142, USA
[4]Howard Hughes Medical Institute, Cambridge, MA 02139, USA
[5]Koch Institute for Integrative Cancer Research, Cambridge, MA 02139, USA
[6]Broad Institute of MIT and Harvard, Cambridge, MA 02142, USA
[7]These authors contributed equally
[8]Present address: Institute of Biochemistry, Food Science and Nutrition, The Hebrew University of Jerusalem, Rehovot 76100, Israel
[9]Lead Contact
*Correspondence: ronnyhelman@gmail.com (A.H.), sabatini@wi.mit.edu (D.M.S.), dmelton@harvard.edu (D.A.M.)

Experiments in Fig. 1a-h were performed by A.L.C. and A.H.
Experiment in Fig. S1a was performed by A.L.C. and A.H.
Experiment in Fig. S1b was performed by A.H. and Q.P.
Experiments in Fig. 2a-d were performed by A.H. and Q.P.
Analysis in Fig. 2a-b was performed by A.L.F. and J.R.S.
Experiments in Fig. 2e-g were performed by A.L.C. and A.H.
Experiments in Fig. S2a-d were performed by A.H. and Q.P.
Experiment in Fig. S2e was performed by A.L.C. and A.H.
Experiments in Fig. 3a-e were performed by A.L.C. and A.H.
Experiments in Fig. S3a-e were performed by A.L.C. and A.H.
Experiments in Fig. 4a-f were performed by A.L.C. and A.H.
Experiments in Fig. S4a-c were performed by A.L.C. and A.H.
Experiment in Fig. S4d was performed by A.L.C.
Experiments in Fig. 5a-e were performed by A.L.C. and A.H.
Experiment in Fig. 5f was performed by J.C.D.
Analysis in Fig. 5f was performed by A.R.
Experiments in Fig. 5g-j were performed by A.L.C. and A.H.
Experiment in Fig. 5k was performed by A.H. and Q.P.
Analysis in Fig. 5k was performed by A.L.F. and J.R.S.

Experiment in Fig. S5a was performed by A.H. and Q.P.
Experiment in Fig. S5b was performed by J.C.D.
Analysis in Fig. S5b was performed by A.R.
Experiment in Fig. S5c was performed by A.H. and Q.P.
Experiments in Fig. S5d-g were performed by A.L.C. and A.H.
Experiment in Fig. S5h was performed by A.H. and Q.P.
Analysis in Fig. S5h was performed by A.R.

Abstract

A drastic transition at birth, from constant maternal nutrient supply in utero to intermittent postnatal feeding, requires changes in the metabolic system of the neonate. Despite their central role in metabolic homeostasis, little is known about how pancreatic β cells adjust to the new nutritional challenge. Here, we find that after birth β cell function shifts from amino acid- to glucose-stimulated insulin secretion in correlation with the change in the nutritional environment. This adaptation is mediated by a transition in nutrient sensitivity of the mTORC1 pathway, which leads to intermittent mTORC1 activity. Disrupting nutrient sensitivity of mTORC1 in mature β cells reverts insulin secretion to a functionally immature state. Finally, manipulating nutrient sensitivity of mTORC1 in stem cell-derived β cells in vitro strongly enhances their glucose-responsive insulin secretion. These results reveal a mechanism by which nutrients regulate β cell function, thereby enabling a metabolic adaptation for the newborn.

Introduction

At birth, mammals are faced with a challenge as they break from the supportive maternal environment into the outside world, a transition requiring an independent physiology. The respiratory, circulatory, digestive and endocrine systems all undergo adaptations during this early neonatal period, which is termed functional maturation (Morton and Brodsky, 2016; Ward Platt and Deshpande, 2005). Because nutrient consumption changes from placental nutrition *in utero* to meal feeding after birth, the metabolic adaptation of the neonate to intermittent feeding and glucose fluctuations is critical. Pancreatic β cell maturation involves developing a higher threshold for glucose-stimulated insulin secretion (GSIS), as evidenced by inhibition of insulin secretion at low glucose and enhanced insulin secretion in response to high glucose. This physiological adaptation is essential to maintain nearly constant glucose levels, preventing hypoglycemia (Blum et al., 2012; Rozzo et al., 2009).

The initial functional maturation period in which responsiveness to glucose is acquired occurs within the first week after birth. β cells continue to develop, however, and improve in secretory function during, and even months, after weaning (Bliss and Sharp, 1992, Avrahami et al., 2015; Stolovich-Rain et al., 2015; Helman et al., 2016, Arda et al.; 2016, Bader et al., 2016). MAFA and Urocortin3 (UCN3) serve as established markers of β cell maturation since their expression increases over the maturation period in mouse and human β cells (Aguayo-Mazzucato et al.; 2011, Blum et al., 2012; van der Meulen and Huising, 2014). Other genes, related to glucose sensing and insulin secretion, including NEUROD1, NKX6–1 and Glucokinase (GCK) improve glucose sensitivity in immature β cells (Matsuoka et al., 2007; Zhang et al., 2005; Wang

et al., 2007; Artner et al., 2010; Aguayo-Mazzucato et al., 2011). The expression of specific genes termed disallowed genes (Martinez-Sanchez et al., 2015; Lemaire et al., 2016) become repressed in the postnatal β cells as part of the metabolic switch associated with functional maturation (Thorrez et al., 2011; Dhawan et al., 2015; Yoshihara et al., 2016). However, changes in expression of maturation markers and disallowed genes occur during the second and third weeks of life and it is not known what drives the initial acquisition of glucose responsiveness during the first week after birth (Conrad et al., 2014; Liu and Hebrok, 2017).

Understanding functional maturation is important for the application of stem cell-derived tissues in regenerative medicine (Robinton and Daley, 2012). In recent years, a more advanced understanding of the intrinsic transcriptional programs in vivo led to a rapid progress in the generation of many cell types, including β cells, from human pluripotent stem cells (Hrvatin et al., 2014; Sneddon et al., 2018). Nevertheless, due to a lack of knowledge regarding initiation of functional maturation, differentiated tissues derived from stem cells often resemble fetal tissues and lack full physiological function (Henquin and Nenquin, 2018; Hrvatin et al., 2014; Jiang et al., 2018; Lundy et al., 2013; Arlotta and Pasca, 2019). Developing permissive conditions for the maturation of stem cell-derived tissues in vitro, without genetic modifications, will enhance their use in drug discovery and cell transplantation.

Functional maturation has generally been viewed as an intrinsic part of a transcriptional differentiation program rather than a process that can be regulated by extrinsic factors in the environment. Yet it is known that cells sense extrinsic signals and coordinate cellular adaptations accordingly. For example, cells modulate their

metabolism and growth in response to nutrients and growth factors via regulation of the mechanistic target of rapamycin complex 1 (mTORC1). mTORC1 kinase activity controls cellular growth and metabolism by activating anabolic processes and repressing catabolic ones (Sancak et al., 2010; Sancak et al., 2008; Saxton and Sabatini, 2017). Several cytosolic proteins have been identified that signal the availability of nutrients and growth factors to control mTORC1 activity (Saxton and Sabatini, 2017).

Several recent findings have uncovered the importance of mTORC1 as a significant regulator of β cell maturation and function. β cell-specific activation of mTORC1 in genetic mouse models found that hyperactivation of mTORC1 signaling resulted in increased β cell function and improved glucose tolerance (Blandino-Rosano et al., 2017; Hamada et al., 2009, Mori et al., 2009; Rachdi et al., 2008; Shigeyama et al., 2008). Consistently, β cell-specific ablation of mTORC1 resulted in lower insulin secretion caused by mitochondrial dysfunction and oxidative stress, indicating that mTORC1 activity is essential for β cell function and maturation (Sinagoga et al., 2017; Chau et al., 2017; Ardestani et al., 2018; Maedler and Ardestani, 2017; Ni et al., 2017; Blandino-Rosano et al., 2017; Alejandro et al., 2017). In contrast, other findings show that chronically increased mTORC1 activity can induce β cell failure (Mori et al., 2009; Sun et al., 2010; Swisa et al., 2015; Elghazi et al., 2010; Bartolome and Guillen, 2014; Koyanagi et al., 2011; Jaafar et al., 2019). Although the genetic components of the mTORC1 pathway are clearly important for proper β cell mass and function, these studies raise questions about how the pathway is post-transcriptionally regulated and whether mTORC1 activation positively or negatively contributes to β cell maturation.

The present study investigates the possibility that sensing environmental nutrients by mTORC1 contributes to cell and tissue maturation. We describe a perinatal change in the regulation of mTORC1 signaling by nutrients that modifies the dynamics of mTORC1 activity from constitutive to intermittent after birth. The combination of mTORC1 inhibition and activation after birth enables the functional shift from amino acid-responsive to glucose-responsive insulin secretion. These findings demonstrate a role for nutrient sensing by mTORC1 in the initiation of functional maturation of pancreatic β cells.

Results

Changes in the nutritional environment alter insulin secretion in response to nutrients

Insulin-expressing β cells appear about embryonic day 13.5 (E13.5) in mice and week 8 – 9 post-conception in humans (Koyanagi et al., 2011; Slack, 1995), but glucose-stimulated insulin secretion (GSIS) begins only days after birth (Blum et al., 2012; Rozzo et al., 2009). Since a major change from embryonic to postnatal physiology is nutrient consumption, we explored whether an altered nutrient supply plays a role in the transition from immature to mature insulin secretion by β cells (Figure 1A). We compared the metabolite profiles of fetal and neonatal plasma, collected from mice throughout the first week after birth, and found changes imposed by the onset of intermittent feeding. These changes include an increase in fasting-associated metabolites, e.g. ketone bodies, in the neonates at birth and a different composition of amino acids and glucose in the plasma of embryonic, neonatal and adult mice. Generally, levels of amino acids and amino acid-derived metabolites in the plasma of

immature mice were higher and glucose was much lower compared to plasma of the adult mice (Figures 1B and 1C and Table S1); see also (Hay, 2006; Young and Prenton, 1969; Zeng et al., 2017). This shift in plasma nutrients abundances occurs gradually after birth, as shown in Figure 1C.

Since the embryo is exposed to an amino acid-rich environment in utero, we tested the effects of physiological levels of amino acids (Cantor et al., 2017) on insulin secretion by fetal islets compared to mature islets. Surprisingly, amino acids alone do not induce a response in mature islets (Figure 1D and 1F), but stimulate insulin secretion in embryonic islets from mouse and human (Figure 1E and 1G), independently of glucose (Kervran and Randon, 1980). High glucose, in contrast, stimulates strong insulin secretion only in mature islets and has no effect on mouse and human fetal islets (Figure 1D-G). Together, these results identify a shift from amino acid-responsive insulin secretion in immature β cells to glucose-responsive secretion in mature β cells. This shift occurs gradually, as neonatal islets of postnatal day 6 mice secrete insulin in response to amino acids or glucose alone, demonstrating a transitional state from amino acid- to glucose-responsiveness (Figure 1H). To test whether the nutritional environment contributes to this change in nutrient-responsiveness, we tested the prolonged effects of nutrient levels on insulin secretion dynamics in immature β cells. Human fetal β cells grown in a mature-like environment (low amino acid concentrations), for four days, can be shifted in vitro to glucose-responsive insulin-secreting cells, whereas these same β cells grown in an immature-like environment (high amino acid concentrations) continue to secrete insulin in response to amino acids but not to glucose (Figure 1I).

To understand if the nutrient environment continues to play a role in the function of mature β cells, we tested the ability of mature human β cells to remain glucose-responsive following extended incubation in vitro. Human islets from adult donors, incubated for four days in low amino acid concentration, demonstrated a higher response to glucose than islets grown in high levels of amino acids (Supplementary Figure 1). Therefore, in addition to having a role in the onset of glucose-responsiveness in immature β cells, amino acid levels in the environment also contribute to maintaining function in mature β cells.

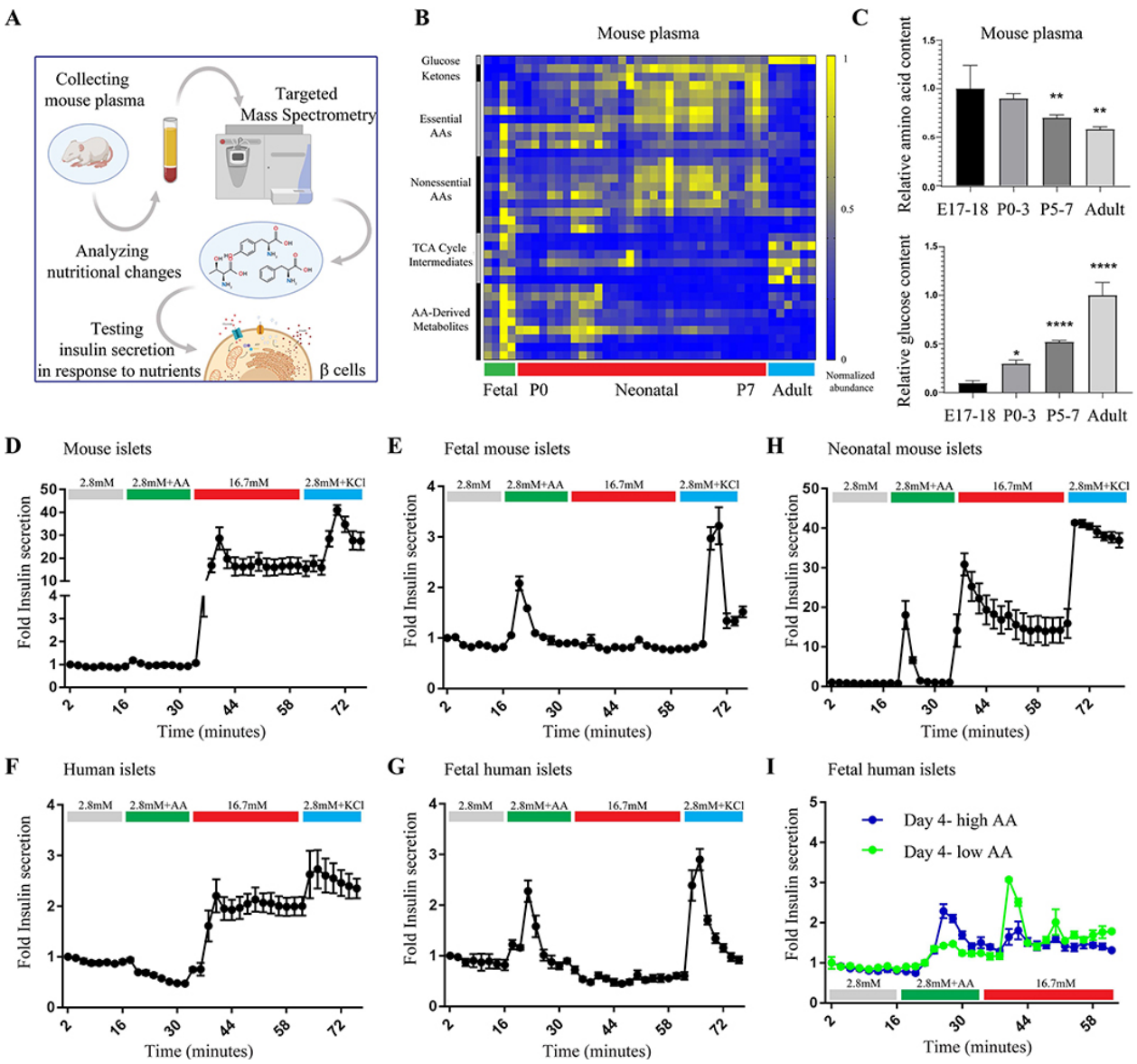

Fig. 1: Dynamic insulin secretion in response to nutrients in mature and immature islet cells. (A) Schematic representation of experimental design. (B) Representative heat map of metabolite abundance in serum of embryos, neonates and adult mice. Experiment was repeated twice using embryonic samples (n=4), neonates (n=32) and adults (n=6). (C) A relative ratio of amino acids and their metabolites (left graph) and glucose (right graph) in the serum of mice of indicated age. Data points represent mean ± SEM. P-values, * P<0.05, ** P<0.01, *** P<0.001, **** P<0.0001, unpaired Student's t

test. (D-G) Fold insulin levels secreted by mature mouse (n=6) and human islets (D and F, respectively) and fetal mouse (E18, n=6) and human islets (E and G, respectively) in a dynamic perfusion assay in low glucose (2.8 mM), low glucose and physiological levels of amino acids, high glucose (16.7 mM) and KCl (30mM). The fetal and adult human data is representative from single donors using 6 technical replicates and repeated in three independent experiments. Data points represent mean ± SEM. (H) Fold insulin levels secreted by islets from neonatal mice (P5, n=6) in a dynamic perfusion assay. Secreted insulin levels were normalized to basal insulin secretion of each sample. (I) Fold insulin levels secreted by fetal human islets that were cultured in vitro in a fetal-like medium (blue, 5.5mM glucose and high amino acid levels) and mature-like medium (green, 5.5mM glucose and low amino acid levels). The result was repeated in three independent experiments.

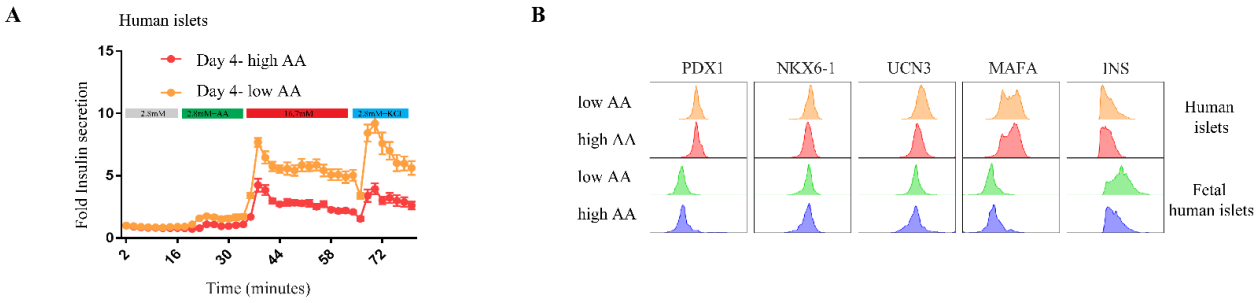

Fig. S1: Related to Fig. 1. (A) Fold insulin levels secreted by mature human islets that were cultured in vitro in a fetal-like medium (red, 5.5mM glucose and high amino acid levels) and mature-like medium (orange, 5.5mM glucose and low amino acid levels). The result was repeated in three independent experiments. (B) Representative FACS staining histograms for PDX1, NKX6-1, UCN3, MAFA and INS of c-peptide+ cells from

fetal (top) and mature (bottom) human islets that were cultured in vitro in a fetal-like medium and mature-like medium.

Onset of glucose-responsiveness is independent of expression of canonical β cell markers

To identify signaling pathways that are correlated with the transition in β cell response to nutrients, we conducted a single cell RNA sequencing on fetal human islets grown for four days in a mature-like environment (low amino acid concentrations) and in an immature-like environment (high amino acid concentrations). Transcription of genes related to β cell identity and maturation such as Chromogranin (CHGA), Insulin and MAFA, did not change significantly during the four-day incubation in the two conditions (Figure 2A and 2B).

FACS staining verified that the protein expression of PDX1, NKX6–1, UCN3 and MAFA in β cells were not different between the two nutritional conditions, indicating that they are not responsible for the gain of glucose responsiveness. (Supplementary Figure 1).

Consistent with this in vitro study, we find that staining for MAFA, UCN3 and NKX6–1 in mice embryos (E18), neonates (P6) and adults (P60), shows the expression of these genes does not change significantly in the first days after birth at the time of gaining glucose responsiveness (Figure 2C and Supplementary Figure 2). MAFA, UCN3 and NKX6–1 are also expressed in human embryonic β cells (by gestational day 120) (Figure 2D and Supplementary Figure 2).

These results identify a novel extracellular determinant of β cell maturation, by which changes in the nutritional environment before and after birth play a role, independently of changes in expression of canonical β cell identity markers, in a transition from constitutive, amino acid-stimulated insulin secretion in utero to a dynamic, glucose-responsive, insulin secretion after birth.

Activity of the mTORC1 pathway in immature β cells differs from mature β cells

We hypothesized that the activity of a metabolic pathway such as the mTOR pathway could mediate the functional transition from amino acid- to glucose-mediated insulin secretion in fetal and mature β cells, respectively. To measure mTORC1 signaling activity in immature and mature β cells, pancreatic tissues were immunostained for phosphorylation of ribosomal protein S6 (p-S6), a downstream target of the mTORC1 kinase. As indicated by p-S6 immunoreactivity, the mTORC1 pathway is strongly activated in β cells of embryonic (E18) mice in utero, whereas the β cells in their fasted pregnant mothers concurrently had low mTORC1 activity (Figure 2E). Active mTORC1 signaling in fetal β cells is also evident in human fetal pancreatic tissue compared to adult human β cells (Figure 2F).

Staining pancreatic sections showed that p-S6 is detected under basal conditions (after separation from their mothers) in β cells of neonatal pups, between P1 and P9, as reported previously (Ni et al., 2017), but not robust as in fetal β cells from E18 embryos (Supplemental Figure 2). Since the mTORC1 pathway is strongly activated in fetal β cells, postnatal mTORC1 activation by itself does not explain how β cells acquire glucose-induced insulin secretion. Furthermore, detection of p-S6 that coincides with the transition to glucose-stimulated insulin secretion suggests that mTORC1 inhibition is

not directly associated with glucose responsiveness in β cells (Jaafar et al., 2019; Ni et al., 2017; Sinagoga et al., 2017). Thus, the regulation of mTORC1 activity before and after birth, and the control of β cell maturation by mTORC1, are more dynamic and complex than suggested previously.

In support of increased regulation of mTORC1 activity, gene expression analysis on sorted β cells from fetal, neonatal and adult murine β cells revealed that the expression of genes encoding negative regulators of mTORC1, including Tuberous sclerosis (TSC), Sestrin1 (SESN1) and Sestrin2 (SESN2), and the catalytic subunit of AMP-activated protein kinase (AMPK), is increased during the transition to mature β cells (Figure 2G), which corresponds to potentiated inhibitory regulation of mTORC1 activity during β cell functional maturation. These results suggest that the regulation on mTORC1 activity could play a role in the transition from amino acid- to glucose-stimulated insulin secretion transition of β cells, in adaptation to the changes in the nutritional environment after birth.

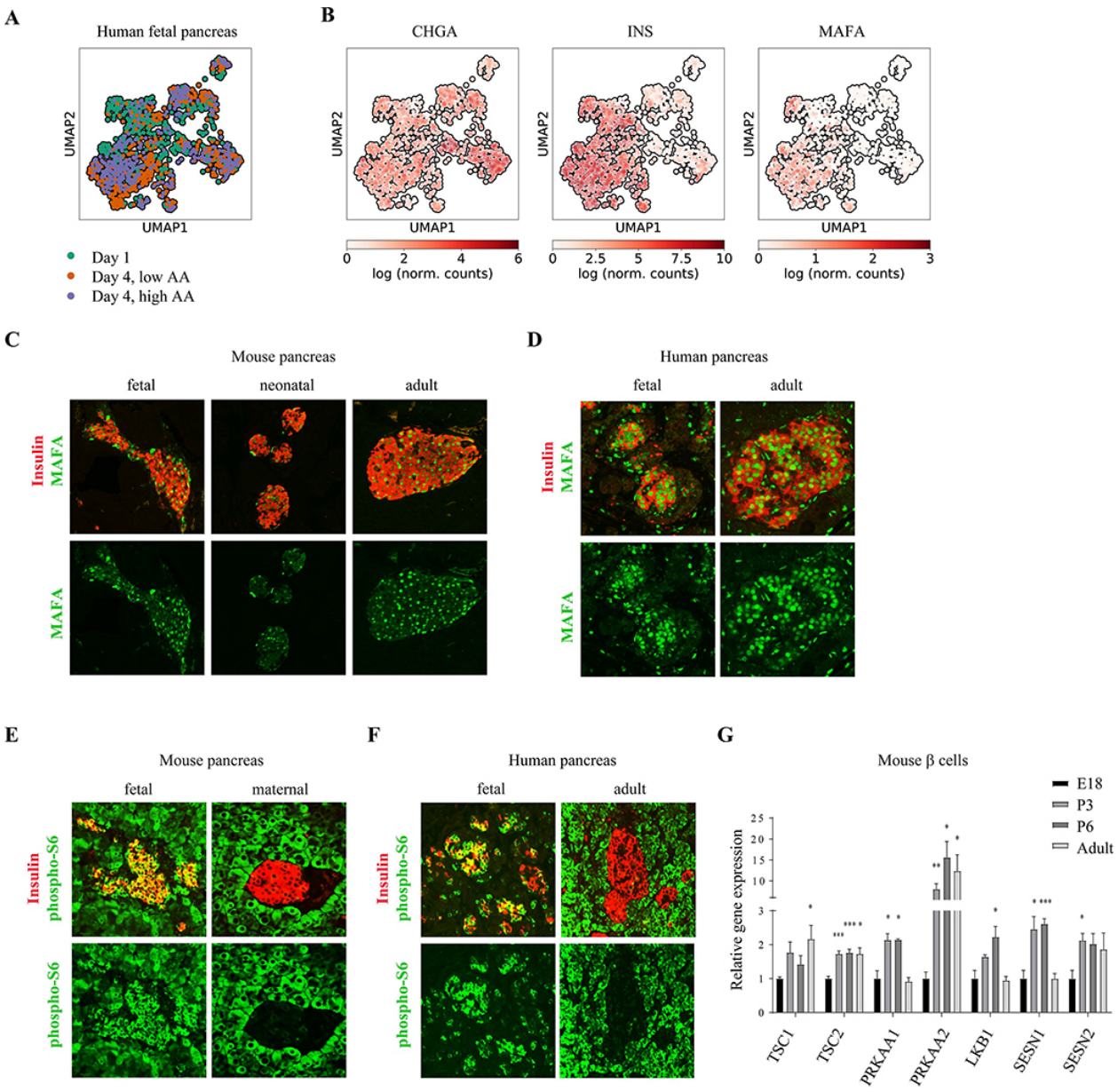

Fig. 2: Differential mTORC1 activity in immature and mature β cells. (A) UMAP visualization of the single fetal human β cells analyzed. Colors represent time and condition of collected cells that were used for differential expression analysis. (B) UMAP maps overlaid with the relative expression level of the indicated gene in each cell. (C) Representative immunostainings of MAFA (green) and insulin (labeling β cells, red) in pancreatic tissues from fetal (E18) neonatal (P6) and adult (P60) mice with indicated

antibodies. Note that MAFA levels do not change significantly 6 days after birth (D) Representative immunostainings of pancreatic tissues from fetal (D120) and adult human subjects with indicated antibodies. (E) Representative immunostainings of p-S6 (green) and insulin (labeling β cells, red), in pancreatic islet of fasted pregnant female mouse (right) and its E18 embryo (left). Note the strong mTORC1 activity in fetal compared to maternal β cells. Experiment was repeated four times, using pancreases of embryos from one pregnant female each time. (F) Representative immunostainings of p-S6 (green) and insulin (labeling β cells, blue), in adult (left) and fetal (right) human pancreatic islets. For each group n=4. (G) A relative gene expression ratio of indicated mTORC1 regulators in sorted GFP-expressing β cells from E18 embryos (n=3, black bars), P6 neonates (n=3), and adult (n=5, grey bars) mice. Data points represent mean ± SEM. P-values, * $P<0.05$, ** $P<0.01$, *** $P<0.001$, unpaired Student's t test.

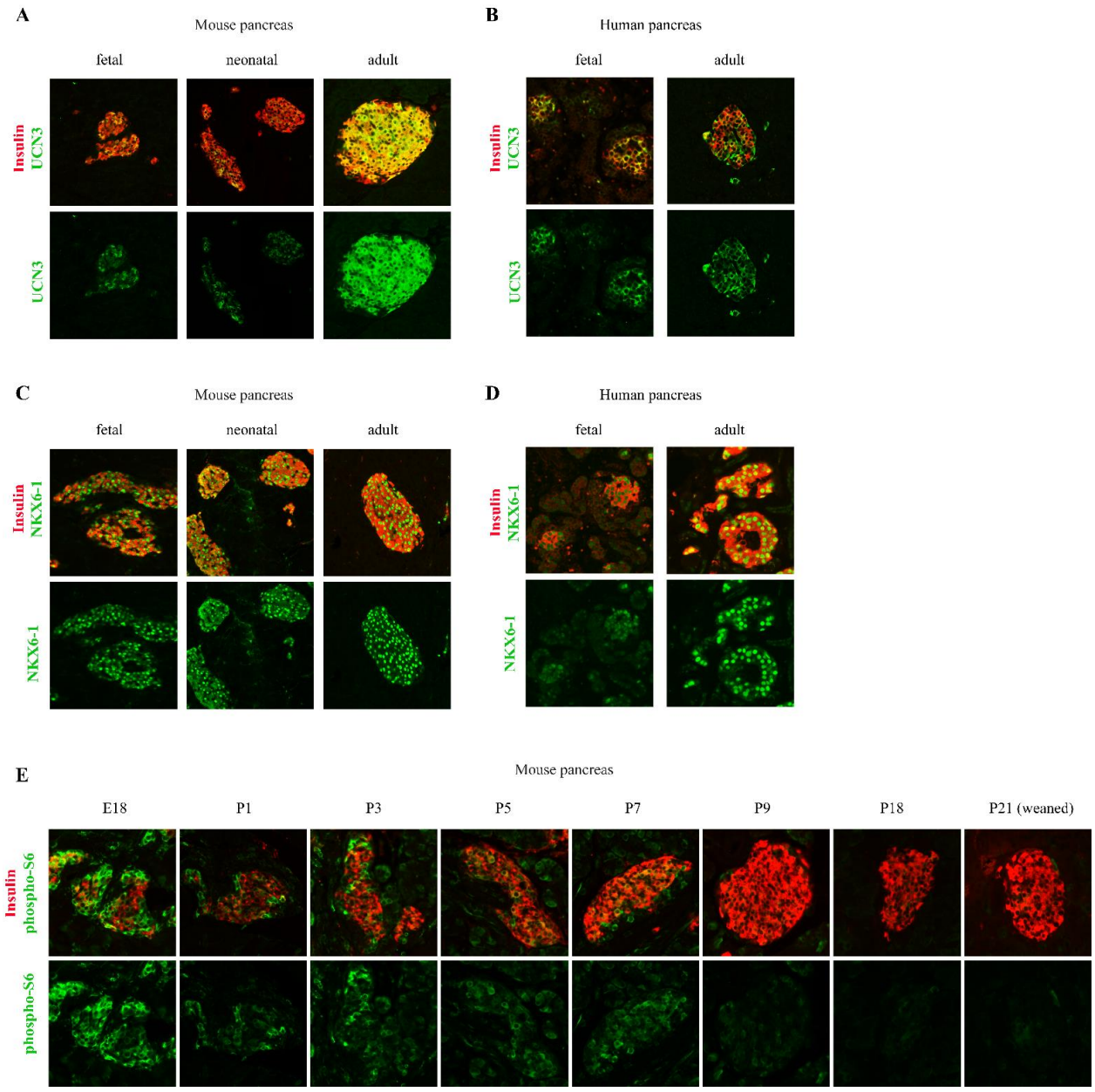

Fig. S2: Related to Fig. 2. (A) Representative immunostainings of UCN3 (green) and insulin (labeling β cells, red), in pancreatic islet of E18 mouse embryo (left, n=3) P6 neonate (middle, n=3) and adult (P60, right, n=3) mice. (B) Representative immunostainings of UCN3 (green) and insulin (labeling β cells, red), in pancreatic islet of human embryo (Day 120, left) and adult (right) subjects. (C) Representative

immunostainings of NKX6-1 (green) and insulin (red), in pancreatic islet of E18 mouse embryo (left) P6 neonate (middle) and adult (P60, right) mice. (D) Representative immunostainings of NKX6-1 (green) and insulin (red), in pancreatic islet of human embryo (Day 120, left) and adult (right) subjects. Staining of human samples was repeated in 4 samples of fetal (gestational days 90-130) and 3 samples of adult pancreas. (E) Representative pancreatic sections from mice at indicated days after birth, immunostained for p-S6 (green) and insulin (red) (n=3 for each stage).

mTORC1 activity in mature β cells is dynamic and regulated by nutrients

The mTORC1 pathway is well-established to be highly responsive to the availability of nutrients, including amino acids and glucose (Saxton and Sabatini, 2017). As changes in nutrient conditions affect β cell function, we reasoned that nutrient-sensitive cellular responses may control the transition from amino acid- to glucose-dependent insulin secretion after birth. To determine how mTORC1 signaling in β cells is affected by nutrient conditions, we investigated the nutrient sensitivity and dynamics of mTORC1 in isolated islets. We developed a FACS-based assay to quantify mTORC1 activation specifically in β cells within the islet (Figure 3A and Supplementary Figure 3). We found differential effects by nutrients on mTORC1 activation in mature human β cells, as measured by the intensity of p-S6 staining. Amino acids alone are not sufficient to activate mTORC1, inducing only slightly more S6 phosphorylation in the β cell population than the basal mTORC1 activity in mature β cells. Glucose alone induces activation of mTORC1 in a higher percentage of β cells, whereas addition of both glucose and amino acids generates a robust activation (~80% of β cells) (Figure 3B).

These results demonstrate a greater dependence on glucose for mTORC1 activation in mature human β cells and a requirement of both amino acids and glucose for full mTORC1 activity. We also tested the responsiveness of mTORC1 to nutrients in mature mouse islets and found that glucose and amino acids are both required to fully induce mTORC1 activity, comparable to that seen in human β cells (Figure 3B and 3C). However, glucose alone is not sufficient to activate the pathway in murine β cells (Figure 3B and 3C), suggesting a stronger regulation by amino acid-dependent repression and thus greater dependence on amino acids for mTORC1 activation.

The activity of AMPK in mature human and mouse β cells, as measured by p-AMPK antibody, is also dynamic and shows the opposite activity and response to nutrients compared to mTORC1, in agreement with its role in repressing mTORC1 activity; fully activated in the absence of glucose and inhibited in the presence of glucose (Supplementary Figure 3).

mTORC1 activity in β cells is increased by amplifiers of insulin secretion, including Exendin-4 (Ex-4), a Glucagon-like peptide 1 (Glp1) analogue, and Forskolin (Fsk), a PKA activator, that trigger an increase in cAMP and PKA activation (Tengholm and Gylfe, 2017). This further demonstrates a positive correlation between insulin secretion and mTORC1 activation (Figure 3C and Supplementary Figure 3). Pharmacologically suppressing insulin secretion with diazoxide (Dz), an activator of ATP-sensitive potassium channels that mediates a decrease in calcium influx, dramatically reduces mTORC1 activity in β cells, even in the presence of glucose and amino acids together, and this is rescued by the addition of Fsk or Ex-4 (Figure 3C and Supplementary Figure 3). One possible explanation for this correlation between

mTORC1 activity and insulin secretion is activation of mTORC1 by autocrine insulin signaling. However, blocking insulin receptor signaling did not impair mTORC1 activation in the presence of glucose (Figure 3C and Supplementary Figure 3), indicating that the response of mTORC1 to nutrients is not mediated by the autocrine action of secreted insulin. Further, in the absence of glucose, neither stimulation with insulin nor with insulin and amino acids together is able to activate mTORC1 in β cells. These results suggest intracellular crosstalk between insulin secretory function and mTORC1 activity, whereby calcium flux downstream of the ATP-sensitive potassium channels, that regulates insulin granules trafficking and exocytosis, is required for mTORC1 activation in mature β cells.

Among amino acids, leucine is a potent mTORC1 activator and is a known amplifier of insulin secretion. We find that leucine strongly potentiates the activation of the mTORC1 pathway in the presence of glucose. In fact, while different concentrations of glucose (from 8–20mM) dose-dependently enhance mTORC1 activity in β cells, including a physiological concentration of leucine (0.3mM) results in full mTORC1 activation even at intermediate glucose concentrations (8–11mM) (Supplementary Figure 3). Leucine levels therefore play a role in establishing the range of glucose concentrations capable of regulating mTORC1 activity in β cells.

These results raise the possibility that mTORC1 signaling in mature β cells in vivo is generally inhibited becoming activated only transiently, following feeding when levels of both glucose and amino acids are high. Consistent with this model, immunostaining for p-S6 in murine pancreatic tissue shows that mTORC1 is strongly stimulated by feeding and inhibited by fasting in mature β cells (Figure 3D and 3E). To

understand the nutrient changes responsible for feeding-induced mTORC1 activation in β cells, we administered glucose and/or leucine to fasted mice. Administration of leucine alone is not sufficient to activate the pathway, whereas glucose partially activates mTORC1 in the β cells. Injection of glucose and leucine together activates mTORC1 in most β cells to similar levels as feeding (Figure 3D and 3E), consistent with the responses of isolated murine islets to nutrient treatments in vitro. Altogether, these results indicate that mTORC1 in mature β cells is strongly regulated by nutrients and activated during periods of high glucose and amino acid levels upon feeding.

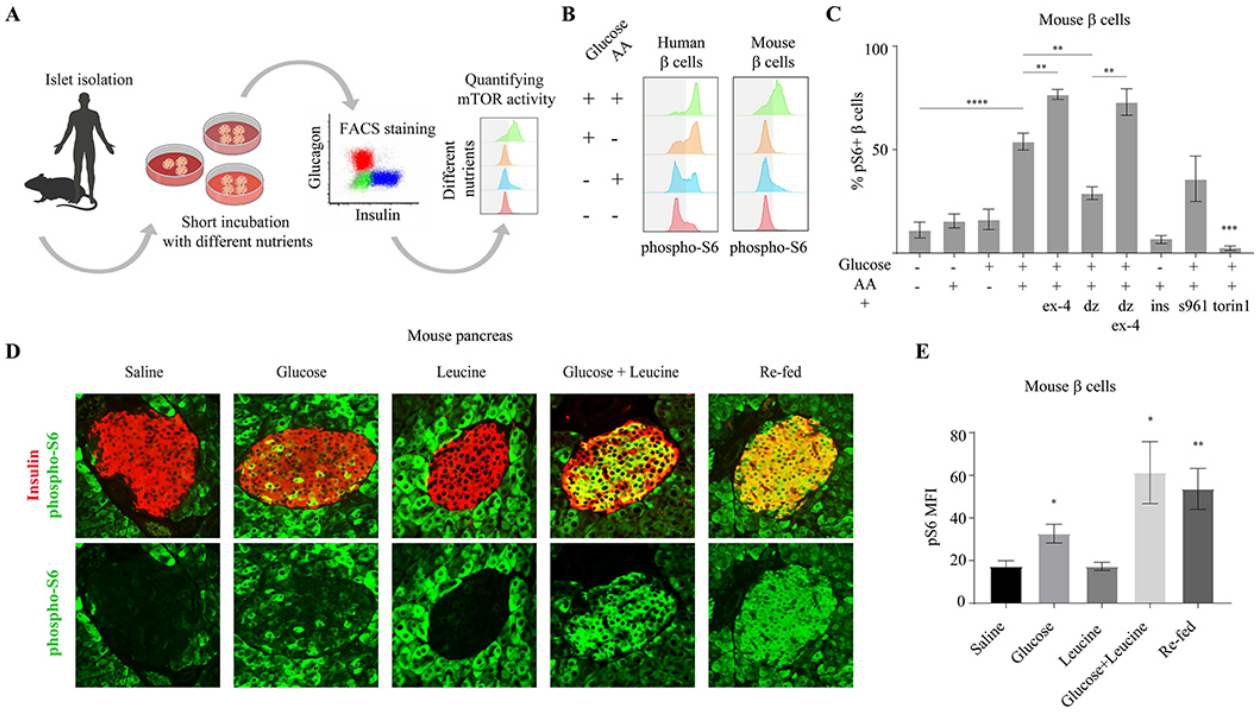

Fig. 3: mTORC1 activity in mature β cells is dynamic and regulated by nutrients.

(A) Schematic representation of experimental method to quantify mTORC1 activity in β cells. (B) Representative p-S6 staining histograms of insulin+ cells from adult human (left) and mouse (right) islets, detected by FACS analysis compared to secondary

antibodies only control. (C) Percentages of p-S6 positive β cells in mouse islets, after 30 minutes incubation in the indicated conditions, detected by FACS compared to secondary antibodies only control. n=10, 7, 6, 10, 4, 4, 3, 3, 3, 3 biological replicates; left to right. Data points represent mean ± SEM. P values, * P<0.05, ** P<0.01, *** P<0.001, **** P<0.0001, unpaired Student's t test. S961- insulin receptor antagonist, torin1- mTOR inhibitor. (D) Representative immunostainings of p-S6 (green) and insulin (labeling β cells, blue), in pancreatic islets of fasted mice injected with the indicated nutrients or re-fed. (E) Mean fluorescent intensity (MFI) of p-S6 staining in islets of mice injected with indicated nutrients or re-fed, n=4 for each condition. Data points represent mean ± SEM. P-values, * P<0.05, ** P<0.01, unpaired Student's t test.

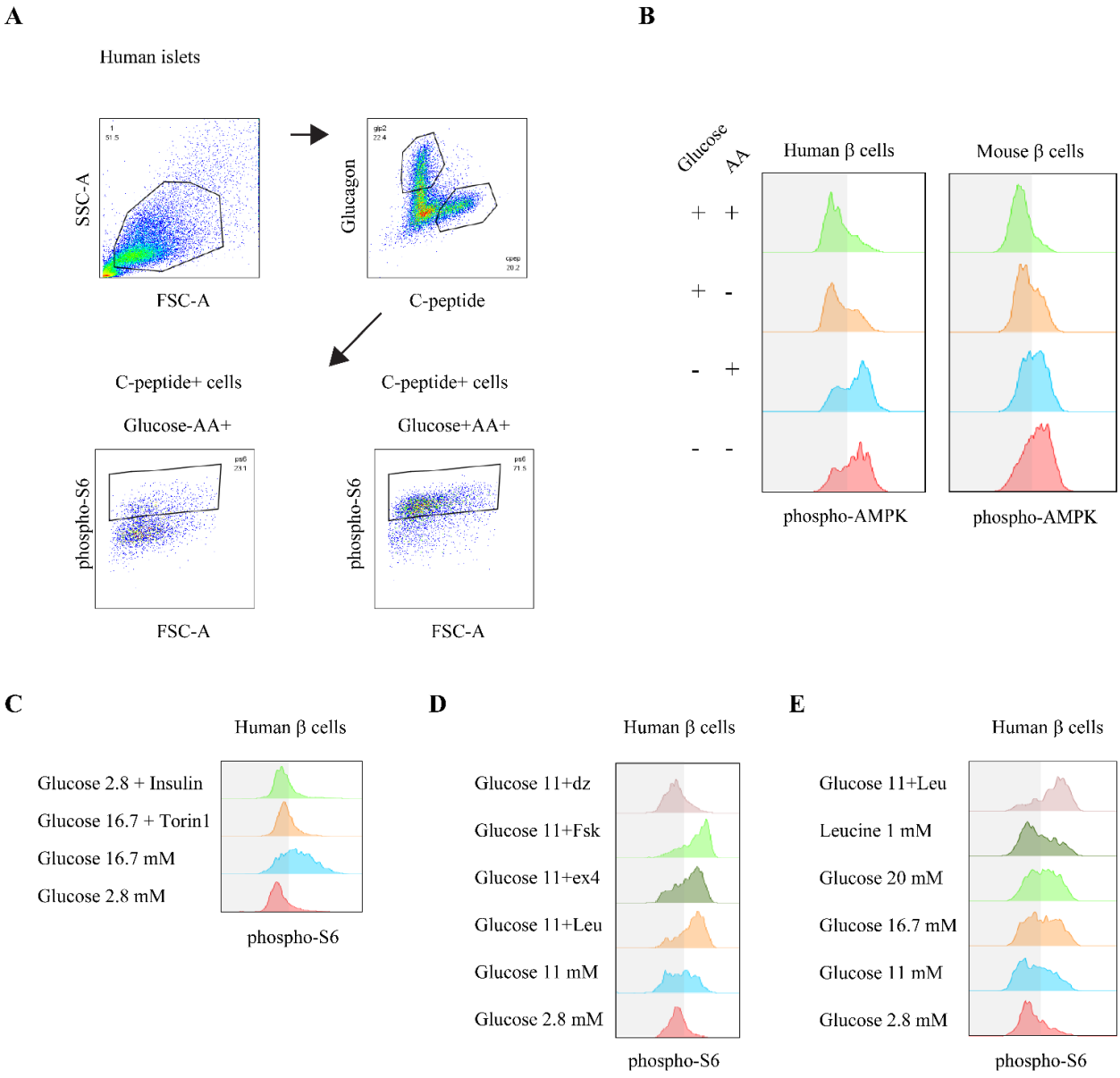

Fig. S3: Related to Fig. 3. (A) FACS analysis strategy to detect mTORC1 activation in endocrine cells. Clusters are dispersed, fixed and stained for C-peptide (for human islets), Insulin (for mouse islets), Glucagon and p-S6, and the intensity of p-S6 and the percentages of p-S6+ cells in C-peptide+ and Glucagon+ cells in the different conditions is calculated. (B) Representative p-AMPK staining histograms of insulin+ cells from adult human (left) and mouse (right) islets, detected by FACS analysis compared to

secondary antibodies only control. (C) Representative p-S6 staining histograms of c-peptide+ cells (human β cells) following 30 minutes incubation of human islets in RPMI with indicated nutrients. Note that phosphorylation of rpS6 in response to glucose stimulation is inhibited by Torin1 and is not mimicked by addition of insulin. (D) Representative p-S6 staining histograms of c-peptide+ cells (human β cells) following 30 minutes incubation of human islets in RPMI with glucose in the indicated concentrations and with the indicated compounds. Note that amplifiers of insulin secretion (forskolin, fsk and exendin4, ex4) strongly activate mTORC1 in β cells while blocking insulin secretion (with diazoxide, dz) inhibits mTORC1 activation. (E) Representative p-S6 staining histograms of c-peptide+ cells (human β cells) following 30 minutes incubation of human islets in RPMI with glucose in the indicated concentrations and with leucine. Note that addition of leucine amplifies the response to glucose in β cells.

The nutrient requirements for mTORC1 activation change as β cells undergo maturation

The observations that fetal β cells maintain high mTORC1 activity under low glucose conditions in utero, while mature β cells require high glucose for mTORC1 activation in adult animals, suggest that mTORC1 nutrient sensitivity changes during β cell maturation. To assess the nutrient sensitivity of mTORC1 in fetal β cells, we treated isolated embryonic islets with combinations of glucose and amino acids ex vivo. As indicated by p-S6 intensity, mTORC1 activity in human and murine embryonic β cells is entirely independent of glucose stimulation and requires only amino acids for full

activation (Figure 4A and 4B). Similarly, we found that mTORC1 signaling in murine neonatal β cells undergo a shift in nutrient responsiveness that occurs throughout the first postnatal week. As neonates age from postnatal day 1 to day 7, their β cells develop a progressively increased requirement for glucose to activate mTORC1, evidenced by the gradually suppressed induction of mTORC1 activity by amino acids in the absence of glucose (Figure 4B and 4C).

To test the regulation of mTORC1 by glucose in neonatal β cells in vivo, glucose was injected into neonates and their pancreata were dissected and assessed for mTORC1 activity. In the first day after birth, injection of glucose is unable to activate mTORC1 in β cells. By postnatal day 5, glucose injection is sufficient to strongly activate mTORC1 in β cells, which do not activate the pathway in response to leucine, in accordance with the shift in glucose sensitivity observed ex vivo (Supplementary Figure 4).

Inhibition of mTORC1 during nutrient limitation is required for glucose-stimulated insulin secretion

We next sought to understand the role of dynamic, nutrient-responsive mTORC1 activity in controlling insulin secretion by mature β cells. To that end, we selectively ablated negative regulators of the mTORC1 pathway, including TSC (via TSC1 deletion) and AMPK (via co-deletion of PRKAA1 and PRKAA2), in β cells of adult mice by expressing tamoxifen-inducible Cre driven under control of the insulin promoter (Ins-CreER). β cells lacking TSC responded to all combinations of glucose and amino acids with stronger activation of mTORC1 than the wildtype control cells (Ins-CreER mice injected with tamoxifen) (Figure 4D), suggesting that in TSC-ablated β cells, the mTORC1 pathway can maintain activity in conditions in which availability of glucose or

amino acids is limited. An important role of AMPK in postnatal β cell function has been recently reported (Jaafar et al., 2019); however, AMPK deletion in mature β cells imparted a weaker effect on mTORC1 activation in response to physiological levels of either glucose or amino acids (Figure 4D). Therefore, the perinatal shift in nutrient regulation of mTORC1 and resulting effects of altered mTORC1 signaling dynamics on insulin secretion, are likely due to changes which are not dependent on AMPK activity.

In dynamic insulin secretion assays, β cells lacking TSC demonstrated elevated insulin secretion in response to amino acids, a feature of fetal islets (Figure 4E and 4F). These results suggest that inhibition of mTORC1 activity in conditions of limited nutrients is required to gain and retain proper glucose-stimulated insulin secretion.

In agreement with these findings, it has been reported previously that mouse models of TSC or AMPK deletion in β cells have increased insulin secretion in a fasted state (in which amino acids are abundant, as opposed to glucose) (Beall et al., 2010; Mori et al., 2009; Jaafar et al., 2019). Importantly, mice with short-term deletion of TSC in β cells have altered glucose clearance, as assessed by glucose tolerance test, which can be attributed to altered regulation of mTORC1 activity and insulin secretion in these cells (Supplementary Figure 4). Appropriate regulation of mTORC1 is therefore crucial for the establishment of glucose-dependent insulin secretion after birth and its maintenance in the adult animal.

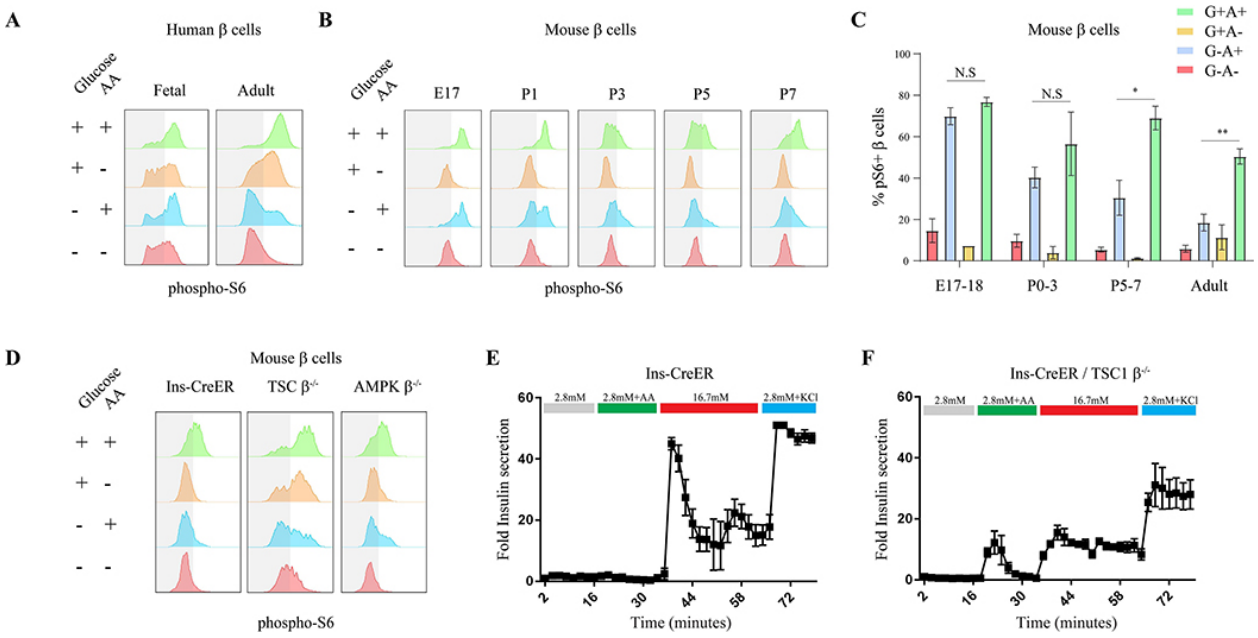

Fig. 4: A neonatal shift in mTORC1 nutrient sensitivity controls β cell function. (A) Representative p-S6 FACS staining histograms of c-peptide+ cells from fetal (left column) and adult (right column) human subjects, following 30 minutes incubation of human islets in RPMI with indicated nutrients. Experiment was repeated three times on three different samples of fetal human pancreas from embryonic days 90, 92 and 120. (B) Representative p-S6 staining histograms of insulin+ cells from mice of indicated age following 30 minutes incubation of islets in RPMI with indicated nutrients. Note that at P7 mTORC1 dynamics is equivalent to mature β cells. (C) Percentages of p-S6 positive β cells from mice of indicated age in response to indicated nutrients, detected by FACS analysis compared to secondary antibodies only control. Data points represent mean ± SEM. P-values, * P<0.05, ** P<0.01, *** P<0.001, unpaired Student's t test. n=3, 3, 3, 4 biological replicates; left to right. Control of mTORC1 dynamics affects insulin secretion in mature β cells. (D) Representative p-S6 staining histograms of insulin+ cells of Ins-CreER (left column) AMPK and TSC deficient (β cell-specific) mice following 30 minutes

incubation of mouse islets in RPMI with indicated nutrients. (E-F) Fold insulin levels secreted by isolated islets from Ins-CreER (E, n=4) and TSC knockout (F, n=4) β cells, in a dynamic GSIS assay in low (2.8 mM, grey line), amino acids (green), high (16.7 mM, red) glucose concentrations and KCl (30 mM, blue). Note the increased insulin secretion in response to amino acids in β cells with perturbed mTORC1 activity.

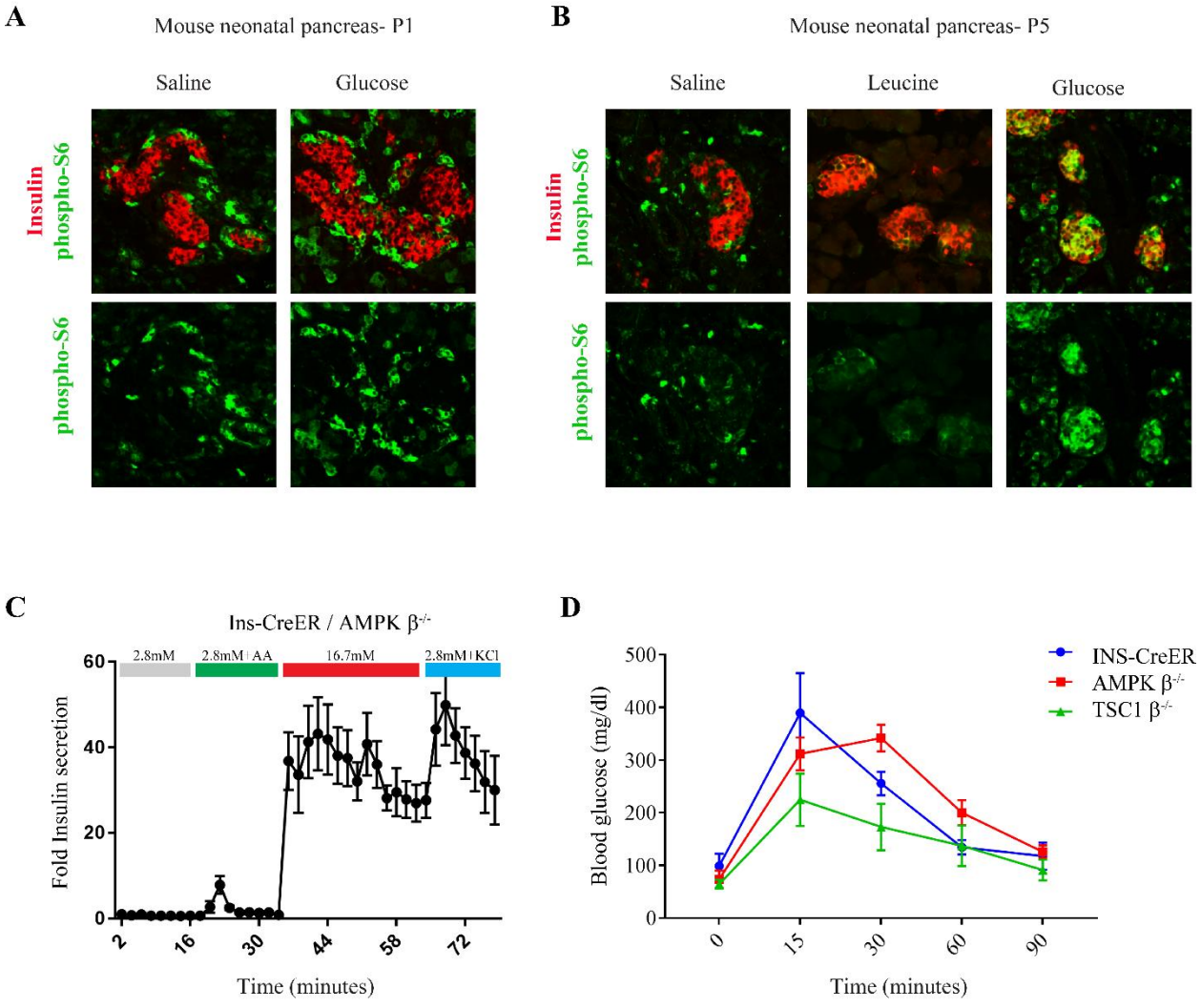

Fig. S4: Related to Fig. 4. (A) Representative immunostainings of p-S6 (green), and insulin (labeling β cells, red), in pancreatic islets of fasted P1 neonatal mice, injected

with saline (n=3) or glucose (n=3) as indicated. (B) Representative immunostainings of p-S6 (green), and insulin (labeling β cells, red), in pancreatic islets of fasted P5 neonatal mice, injected with saline (n=3), leucine (n=3) or glucose (n=3) as indicated. Note that mTORC1 response to glucose is acquired by postnatal day 5. (C) Fold insulin levels secreted by isolated islets from AMPK knockout β cells (n=4), in a dynamic GSIS assay in low (2.8 mM, grey line), amino acids (green), high (16.7 mM, red) glucose concentrations and KCl (30 mM, blue). (D) Glucose tolerance test on Ins-CreER (blue, n=4), TSC (green, n=4) and AMPK (red, n=4) β cell-specific deficient mice.

Nutrient-regulated mTORC1 activity controls SC-β cell functionality

The drastic change in nutrient availability at birth is followed by a β cell-specific switch in mTORC1 sensitivity to nutrients, and a switch from amino acid-induced to glucose-induced insulin secretion. These findings raise the question of whether changes in mTORC1 nutrient sensitivity contribute to the acquisition of glucose-responsive insulin secretion in β cells.

In vitro differentiation protocols generate functional insulin-secreting β cells derived from human induced pluripotent stem cells (SC-β cells) that respond to glucose to varying degrees (Pagliuca et al., 2014; Russ et al., 2015; Nair et al., 2019; Rezania et al., 2014). We sought to compare the responsiveness to physiological levels of glucose and amino acids in SC-β cells generated using our previously published protocol (Pagliuca et al., 2014). Interestingly, we found that amino acid stimulation of SC-β cells induces a more robust insulin secretion which is glucose-independent (Figure 5A), indicating that SC-β cells maintain features of fetal β cells. Importantly, SC-β cells

generated by this protocol express close to mature levels of β cell identity and function markers, including PDX1 and NKX6–1 (Supplementary Figure 5), but lack high expression of the maturation markers MAFA and UCN3.

Given that SC-β cells are functionally reminiscent of immature β cells, we next asked if SC-β cells likewise display fetal-like nutrient sensitivity of the mTORC1 pathway. mTORC1 signaling in SC- β cells is strongly activated in response to amino acids, but is unaffected by the presence of glucose, which was confirmed by FACS (Figure 5B and 5C) and immunostaining (Figure 5D). This suggests that nutrient regulation of mTORC1 signaling in SC-β cells is dominated by amino acids and independent of glucose, strikingly similar to fetal β cells.

Considering the fetal-like properties of mTORC1 regulation in SC-β cells, we sought to understand how a mature in vivo environment impacts the nutrient sensitivity and dynamics of mTORC1 in these cells. To test this, we transplanted SC-β cells into the kidney capsule of adult mice. Following transplantation, SC-β cells undergo a maturation process that results in increased expression of genes that are associated with β cell maturation and enhanced glucose-responsive insulin secretion (Supplementary Figure 5). Further, we found that this transplantation-induced maturation in SC- β cells corresponds to a significant shift in mTORC1 nutrient sensitivity towards that of mature adult β cells which occurs twelve to eighteen days after transplantation. As in mature β cells, the mTORC1 pathway remains inactive in the transplanted SC-β cells during fasting and not activated by injection of leucine into the recipient mouse, while feeding or injection of glucose strongly activates mTORC1 (Figure 5E). These results demonstrate that changing the environment of the cells can

shift the nutrient sensitivity of mTORC1 towards a mature glucose-sensitive state. Further, the transplantation-induced glucose dependence of mTORC1 activity implies a corresponding acquisition of transient mTORC1 signaling dynamics in transplanted SC-β cells that is dictated by fluctuating glucose levels in vivo. Interestingly, the changes in regulation of mTORC1 precede the changes observed in glucose-responsive insulin secretion and in the expression of MAFA and coincides with UCN3 expression (Supplementary Figure 5). This suggests that transplantation alters mTORC1 nutrient sensitivity independently of changes in MAFA expression and may play an early role in functional maturation.

To identify molecular drivers for the transplantation-induced change in mTORC1 regulation by nutrients, we compared gene expression profiles of sorted SC-β cells, collected before and after transplantation. Expression of known maturation markers, including SIX2, IAPP, MAFA, FOXA1, FOXA2 and the senescence marker CDKN2A were elevated after transplantation (Gao et al., 2010; Sun et al., 2010; Aguayo-Mazzucato et al., 2011; Artner et al., 2010; Helman et al., 2016; Nishimura et al., 2015). Further, genes that have been reported as “disallowed” in β cells such as CPT1 and LDHA (Pullen and Rutter, 2013) were downregulated following transplantation (Supplementary Figure 5). Notably, we find that the expression of genes encoding inhibitory regulators of the mTORC1 pathway was induced after transplantation, including the leucine sensors SESN1 and SESN2, as well as the arginine sensor component CASTOR2 and the AMPK activator LKB1 (Figure 5F). These results indicate that transplantation increases the nutrient requirements for mTORC1 activation in SC-β cells by increasing the expression of inhibitory nutrient-sensitive mTORC1 regulators.

As mTORC1 signaling in SC-β cells is highly sensitive to amino acids, we hypothesized that recapitulating the postnatal change in nutrients and mTORC1 activity in vitro, by reducing amino acid levels in the culture media, might improve insulin secretion in response to glucose. Fully differentiated SC-β cells were cultured for two weeks in media with varying amino acid concentrations. SC-β cells grown in media with a low concentration of amino acids (25% of standard media concentrations) had suppressed mTORC1 activity as measured by FACS staining for p-S6 (Supplementary Figure 5). While SC-β cells cultured in amino acid-rich media were not dependent on glucose for full mTORC1 activity (Figure 5D and and5H),5H), cells cultured in low amino acid levels suppressed mTORC1 signaling in the absence of glucose (Figures 5G and 5H), indicating that reduced amino acid conditions can induce SC-β cells to acquire a mature-like sensitivity of mTORC1 to glucose levels.

To understand the functional impact of amino acid levels on SC-β cells, we asked if the changes in mTORC1 glucose sensitivity and activity induced by low amino acid conditions affect insulin secretion. Glucose-induced insulin secretion of SC-islets was tested following culture in different concentrations of amino acids. SC-β cells cultured in an amino acid-rich environment displayed poor insulin secretion in response to high glucose. However, reducing amino acid levels to 50% or 25% of the amino acid-rich media increased glucose-stimulated insulin secretion of the cells by 1.6 and 2-fold, respectively (Figure 5I and Supplementary Figure 5). Remarkably, culturing SC-β cells with 25% of media amino acid levels increases the average cellular insulin content (Supplementary Figure 5), which was also observed in human fetal islets (Supplementary Figure 1), as detected by FACS staining, perhaps due to the reduced

amino acid-induced insulin secretion and conservation of intracellular insulin. The change in glucose responsiveness of SC-β cells was accompanied by a significant increase in the expression levels of the glucose transporter SLC2A1 and a reduction in the Glucose-6-phosphatase G6PC2, indicating a shift towards more efficient glucose transport (Supplementary Figure 5). Importantly, similar enhancement of glucose-stimulated insulin secretion was induced by treating cells that were grown in an amino-acid rich media with Torin1 for 48 hours, providing evidence that amino acid reduction improves glucose responsiveness via inhibition of mTORC1 activity (Figure 5J). Correlation analysis shows that the gene expression profile of SC-β cells cultured in low amino acid levels was more similar to transplanted SC-β cells than SC-β cells cultured in high amino acid levels (Figure 5K). Together, these results demonstrate that environmental nutrients regulate mTORC1 in SC-β cells, and that mimicking the postnatal nutrient changes that occur in vivo influences SC-β cell function in a manner that recapitulates the postnatal progression of β cell maturation (Figure 6).

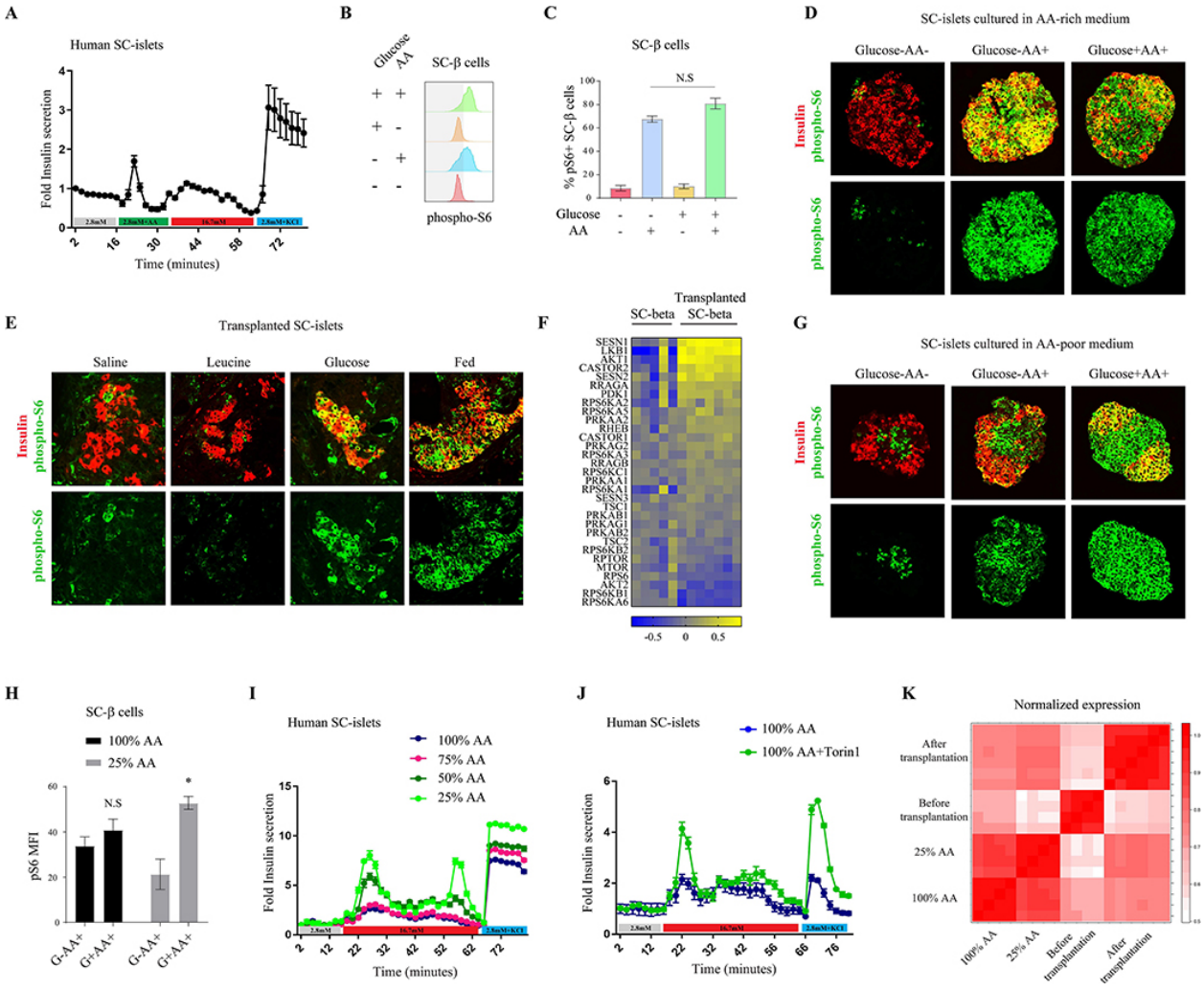

Fig. 5: A shift in mTORC1 nutrient sensitivity dictates SC-β cell function. (A) Fold insulin levels secreted by isolated islets from SC-β cells (n=6), in a dynamic GSIS assay in low (2.8 mM, grey line), amino acids (green), high (16.7 mM, red) glucose concentrations and KCl (30 mM, blue). Note the insulin secretion in response to amino acids in SC-β cells. (B) Representative p-S6 staining histograms of c-peptide+ cells (SC-β cells) and (C) Percentages of p-S6 positive SC-β cells detected by FACS analysis following 30 minutes incubation of SC-clusters in RPMI with indicated nutrients. Note the strong mTORC1 response of SC-β cells to amino acids only. n=9 biological replicates. (D) Representative immunostainings of p-S6 (green), and c-peptide (labeling

SC-β cells, red), in clusters of in-vitro differentiated stem cells grown in an amino acid-rich media and incubated for 30 minutes with indicated nutrients. (E) Representative immunostainings of p-S6 (green) and c-peptide (labeling SC-β cells, blue), in kidney capsule-transplants of SC-β cells. Transplanted mice were fasted overnight and injected with the indicated nutrients or re-fed. Note the weak response of mTORC1 to leucine and the acquired glucose responsiveness 12 days after transplantation. Experiment was conducted with similar results 12 days, 18 days and 4 weeks after transplantation (n=6). (F) Gene expression heat map of known regulators of mTORC1 signaling in SC-β cells four weeks after transplantation under the kidney capsule of mice, normalized to expression levels of the genes in SC-β cells before transplantation. SC-β cells were sorted from five independent differentiation flasks and seven transplanted mice. (G) Representative immunostainings of p-S6 (green), and c-peptide (labeling SC-β cells, red), in clusters of in-vitro differentiated stem cells grown in an amino acid-poor media and incubated for 30 minutes with indicated nutrients. (H) Mean fluorescent intensity (MFI) of p-S6 staining in SC-β cells from indicated conditions, n=4 for each condition. Data points represent mean ± SEM. P-values, * $P<0.05$, unpaired Student's t test. (I) Insulin levels secreted by SC-β cells from indicated growing condition in a dynamic perfusion assay in low (2.8 mM, grey line), high (16.7 mM, red) glucose concentrations and KCl (30mM, blue line). Secreted insulin levels were normalized to basal insulin secretion of each sample. The experiments with all conditions were done on six independent differentiation flasks. (J) Insulin levels secreted by SC-β cells from amino acid-rich media (100% AA), with (green) or without (blue) Torin1, in a dynamic perfusion assay in low (2.8 mM, grey line) and high (16.7 mM, red line) glucose concentrations

and KCl (30mM, blue line). Secreted insulin levels were normalized to basal insulin secretion of each sample. Experiment was done on three independent differentiation flasks. (K) Correlation heat map presenting data from two different experiments; SC-β cells before and after transplantation and SC-β cells cultured in different concentrations of AA (100% and 25% of total amino acids in the rich-media).

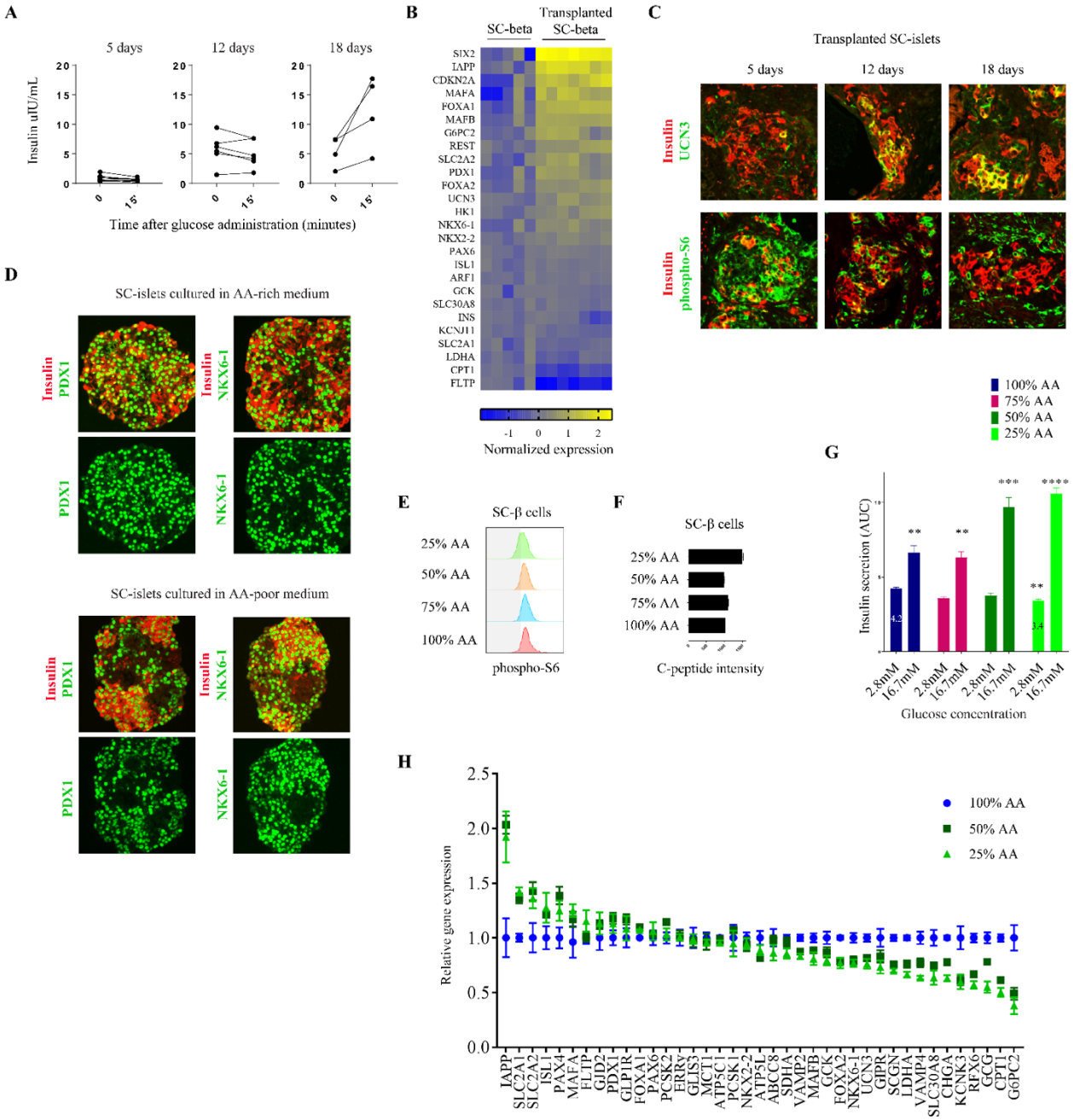

Fig. S5: Related to Fig. 5. (A) ELISA measurements of human insulin from the serum of mice transplanted with SC-β cells. Measurements were taken before (time 0) and 15 min after a glucose injection of mice at the indicated days post-transplantation. (B) Gene expression heat map of known regulators of β cell maturation and function four weeks after transplantation under the kidney capsule of mice, normalized to expression

levels of the genes in SC-β cells before transplantation. SC-β cells were sorted from five independent differentiation flasks and seven transplanted mice. (C) Representative immunostainings of UCN3 (top panels, green), p-S6 (bottom panels, green) and c-peptide (labeling SC-β cells, red), in SC-β cells transplanted under the kidney capsule for indicated days. Transplanted mice were fasted overnight before transplant collection. Note the inhibition of mTORC1 signaling 12 days after transplantation. (D) Representative immunostainings of PDX1 or NKX6-1 (green) and c-peptide (labeling SC-β cells, red), in clusters of in-vitro differentiated stem cells grown in an amino acid-rich media (left panels) or acid-poor media (right panels). (E) Representative p-S6 staining histograms of c-peptide+ cells (SC-β cells) and percentages of p-S6 positive and negative SC-β cells grown in media with indicated amino acid levels compared to the amino acid-rich media (100% AA). (F) Staining intensity of c-peptide in SC-β cells grown in media with indicated amino acid levels (n=6 for each condition), compared to amino acid-rich culture media (100% AA). (G) Basal and stimulated insulin secretion levels as measured by the area under the curve (AUC) of the dynamic insulin secretion in 4I, for the indicated conditions. Data points represent mean ± SEM. P-values, * P<0.05, ** P<0.01, *** P<0.001, **** P<0.0001, unpaired Student's t-test. (H) A relative RNA expression ratio of indicated β cell function regulators in sorted TSQ-expressing cells from the indicated conditions (n=4 for each condition).

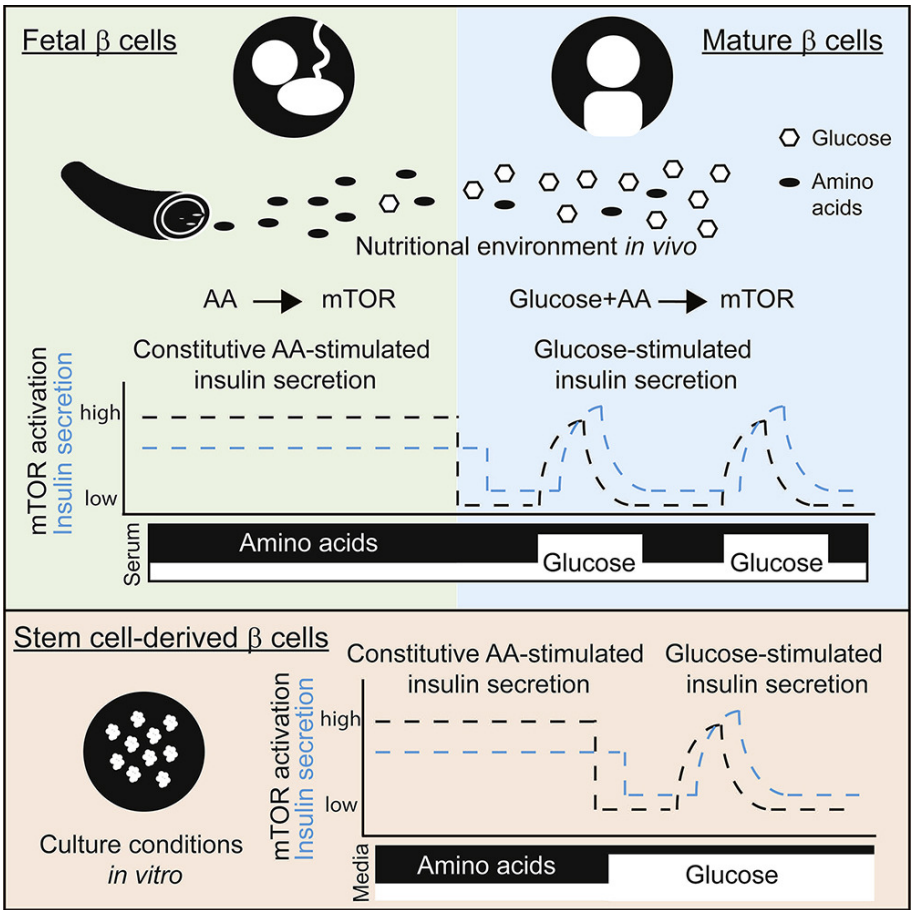

Fig. 6: Changes in environmental nutrients and mTORC1 nutrient sensitivity control glucose-responsiveness of β cells. Model of how environmental nutrients and mTORC1 nutrient sensitivity regulate the functional maturation of β cells before and after birth, and of stem cell-derived β cells.

Discussion

Rapid growth of the embryo in utero occurs under steady maternal supply of nutrients and requires stable secretion of insulin by the fetal β cells (Xu et al., 2004). In effect, fetal insulin acts as a generic growth factor as the embryo is built by cell division and growth. At birth, a drastic change to intermittent postnatal feeding requires increased insulin secretion by β cells to maximize nutrient absorption during feeding, as

well as suppressed release during fasting to avoid hypoglycemia. Therefore, the functional shift of β cells from constitutive to glucose-regulated insulin secretion after birth is vital for the survival of the neonate. Our findings show that glucose responsiveness, which is of the sine qua non of β cell maturation, is post-transcriptionally regulated by nutrients and mTORC1 signaling within few days after birth.

We demonstrate that the mechanisms controlling mTORC1 activity in β cells are plastic, changing substantially from the fetal to adult stage. The constitutive activation of mTORC1 in utero induces insulin secretion in an amino acid-dependent manner. Since the fetal serum is rich in amino acids, fetal β cells secrete insulin constantly. Our data strongly suggest that the change in the nutritional environment at birth shifts the nutrient sensitivity of mTORC1 signaling in β cells and mediates the change from constitutive to dynamic mTORC1 activity, resulting in a transition from amino acid to glucose-dependent insulin secretion.

The amino acid dependency of fetal insulin secretion indicates a potential role of fetal insulin in the negative effects of maternal malnutrition during gestation. Maternal dietary protein restriction has been demonstrated to impair fetal growth (Gonzalez et al., 2016; Herring et al., 2018). It is also recognized that insulin secretion by the fetus is essential for proper fetal growth (Fowden, 1992). Our findings therefore suggest that impaired fetal growth under maternal protein restriction may be attributed, at least in part, to reduced amino acid-sensitive insulin secretion by the fetus.

Complex machinery in mature β cells keeps mTORC1 inactive in conditions unsuitable for growth. This regulatory network includes inhibitors such as TSC, AMPK

and SESN whose inhibition is released by growth factors, energy levels and amino acids, respectively (Saxton and Sabatini, 2017). In the embryonic in utero environment, an abundance of nutrients, especially amino acids, constitutively releases these inhibitions and enables continuous mTORC1 activity. In the adult the availability of nutrients is periodic, leading to dynamic mTORC1 activity. Nevertheless, we observe that the serum of the fetus contains very low levels of glucose, which raises the question of how mTORC1 is activated under these conditions. Our data suggest that the answer lies in the sensitivity of the mTORC1 pathway to nutrients. In immature β cells, amino acids are sufficient for mTORC1 activation, perhaps due to reduced activity of inhibitory sensors such as TSC and AMPK, enabling full activity in the presence of amino acids only.

Consistent with nutrient sensing by the mTORC1 pathway playing a role in β cell functional maturation after birth, we propose that nutrient sensing likewise plays a critical role in the functional maturation of stem cell-derived tissues. As we demonstrate, this can be exploited by altering nutrient conditions to improve functional maturation in vitro. Our data indicate that recreating the adult in vivo environment permits further functional maturation and this may be true for other stem-cell derived tissues. Recent developments in culture media which reflect physiologic conditions may therefore be a promising approach to improve functional maturation of stem cell-derived tissues.

In conclusion, we show here that a shift in the sensitivity of mTORC1 to nutrients, which coincides with drastic nutritional changes at birth, alters mTORC1 signaling dynamics and leads to a change in β cell function, from amino acid to glucose-dependent insulin secreting cells. This metabolic regulation of β cell maturation,

triggered by extrinsic changes in nutrient availability, is important for optimizing the function of β cells for their environment.

Limitations of Study

The experimental systems that were used in this study have limitations to consider. In our experiments designed to isolate the role of physiological levels of glucose and amino acids on mTORC1 activation, we did not consider other nutrients and metabolites that could potentially participate in regulating mTORC1. While we demonstrated a specific role of leucine, the contribution of other individual amino acids were not investigated. In our experiments involving mice, we used an insulin promoter-driven Cre transgene (MIP-CreER; Wicksteed et al., 2010) to induce beta cell-specific gene deletion. To ensure that our conclusions are not influenced by non-specific effects, we controlled for MIP-CreER expression and tamoxifen treatment across all of the mice used in these experiments. Further, several of our experiments utilize human cadaveric islets, which display an inherent degree of functional variability between donors, due to individual variability in age, gender, and metabolic health. To mitigate this, we used only islets from healthy donors with a BMI within the normal range. Experiments were replicated with islets from multiple donors to ensure that any findings were not donor-specific. We are not aware of any genetic or metabolic syndromes in the human cadaveric islets from adults or embryos that could affect the outcomes of the experiments. Lastly, the differentiation protocol for producing the SC-beta cells used in our experiments yields some unavoidable batch-to-batch variability in beta cell function. Therefore, in each experiment we used SC-beta cells from multiple independent

differentiation flasks. SC-beta cells used in our experiments were generated only from ESC; iPSC-derived SC-beta cells were not tested.

Materials and Methods

Antibodies

The following antibodies were used: rat anti-insulin (pro-)/C-peptide (DSHB: GN-ID4), mouse anti-glucagon (Santa Cruz: sc-514592), guinea pig anti-insulin (Dako: A0564), mouse anti-Nkx6.1 (DSHB: F55A12), rabbit anti phospho-S6 (Ser240/244) (Cell Signaling: 5364), rabbit anti Mafa (Cell Signaling: 79737), goat anti Pdx1 (R&D Systems: AF2419) rabbit anti phospho-AMPKa (Cell Signaling: 2535).

Cell Culture

The hPSC line HUES8 (NIH human embryonic stem cell registry #0021) was used for all experiments. Undifferentiated HUES8 cells were maintained in supplemented mTeSR1 medium (StemCell Technologies) in 500ml spinner flasks (Corning) set at a 70rpm rotation rate in a 37°C 5% CO2 incubator. Directed differentiation into SC-β cells was conducted as described previously (Pagliuca et al., 2014). At the last stage, cell clusters were maintained for 14-20 days in CMRL 1066 Supplemented (Mediatech; 99-603-CV) + 10% FBS (HyClone, VWR; 16777) + 1% Pen/Strep. For testing the effect of amino acids dilution, clusters were grown in CMRL 1066 Supplemented (Mediatech; 99-603-CV) that was diluted to 75%, 50% and 25% with RPMI-1640 medium with no glucose (Life Technologies; 11879020) or modified nutrient-free RPMI-1640 medium (MBS652918), supplemented to 5.5mM glucose + 10% FBS (HyClone, VWR; 16777) + 1% Pen/Strep. For testing the effect of amino acids

and glucose dilution on fetal mouse islets, they were isolated from E18 embryos and grown for 72 hours in RPMI 1640 medium that was diluted to 25% with RPMI-1640 medium with no glucose (Life Technologies; 11879020) or modified nutrient-free RPMI-1640 medium (MBS652918), supplemented to 11mM glucose + 10% FBS (HyClone, VWR; 16777) + 1% Pen/Strep and changed daily.

Animals

C57BL/6 mice were used for serum metabolite profiling, islet isolation for GSIS and FACS analysis and for immunohistochemistry. For the immunohistochemistry assays, mice were fasted overnight and then received saline, glucose (0.1g/ml) or leucine (30mM) by intraperitoneal injection (20ul/g), and pancreas was harvested 30 minutes later.

Mice expressing floxed alleles of Prkaa1 and Prkaa2 were purchased from Jackson Laboratories (Nakada et al., 2010). Mice expressing a floxed allele of TSC1 were gifts from D. Kwiatkowski (Harvard Medical School). These mice were crossed with MIP-CreER mice (Wicksteed et al., 2010). Final crosses yielded mice expressing homozygous floxed Prkaa1 and Prkaa2 with MIP-CreER for β cell-specific AMPK deletion, or homozygous floxed TSC1 with MIP-CreER for β cell-specific TSC1 deletion. Three doses of 200 mg/kg Tamoxifen (Sigma, 20mg/ml in corn oil) were administered 48 hours apart by gavage into 8- to 10-week old mice to obtain β -cell specific deletion of Prkaa1 and Prkaa2 or TSC1. Glucose tolerance tests were performed 2 weeks following tamoxifen administration, and islets were collected one week later. All experiments were conducted using mouse litter batches, and where necessary experimental groups were comprised of multiple litters to allow statistical power. The

experiments were not randomized. There was no blinded allocation during experiments and outcome assessment. The ethics committee of Harvard University approved the study protocol for animal welfare.

Polar Metabolite Profiling

LC/MS-based analyses were conducted on a QExactive benchtop orbitrap mass spectrometer equipped with an Ion Max source and HESI II probe, which was coupled to a Dionex UltiMate 3000 ultra-high-performance liquid chromatography system (Thermo Fisher Scientific, San Jose, CA). External mass calibration was performed using the standard calibration mixture every 7 days. Acetonitrile was LC/MS 6HyperGrade from EMD Millipore. All other solvents were LC/MS Optima grade from Thermo Fisher Scientific. For extraction from SC-β cells, the metabolite extraction mix (stored at -20°C) was made of 80:20 (v/v) methanol:water, supplemented with a mixture of 17 isotope-labeled amino acids at 500nM each as internal extraction standards (Cambridge Isotope Laboratories, MSK-A2-1.2). For extraction from mouse plasma, the metabolite extraction mix (stored at -20°C) was made of 75:25:0.2 (v/v) acetonitrile:methanol:formic acid supplemented with a mixture of 17 isotope-labeled amino acids at 500nM each as internal extraction standards (Cambridge Isotope Laboratories, MSK-A2-1.2).

For chromatographic separation, 2.5μL of each sample was injected onto a SeQuant ZIC-pHILIC Polymeric column (2.1 x 150 mm) connected with a guard column (2.1 x 20 mm). Both analytical and guard columns are of 5 μm particle size purchased from EMD Millipore. Flow rate was set to 0.150 mL per minute, the column compartment was set to 25°C, and the autosampler sample tray to 4°C. Mobile Phase A consisted of

20 mM ammonium carbonate, 0.1% ammonium hydroxide. Mobile Phase B was 100% acetonitrile. The chromatographic gradient was as follows: (1) 0-20 min: linear gradient from 80% to 20% B; (2) 20-20.5 min: linear gradient from 20% to 80% B; (3) 20.5-28 min: hold at 80% B. The mass spectrometer was operated in full scan, polarity switching mode with the spray voltage set to 3.0 kV, the heated capillary held at 275°C, and the HESI probe held at 350°C. The sheath gas flow rate was set to 40 units, the auxiliary gas flow was set to 15 units, and the sweep gas flow was set to 1 unit. The MS data acquisition was performed in a range of 70-1000m/z, with the resolution set to 70,000, the AGC target at 106, and the maximum injection time at 20 msec.

Immunohistochemistry

Differentiated cell clusters, pancreatic tissues and kidney transplants were fixed by immersion in 4% PFA for 1 hour at room temperature (RT). Samples were washed 3 times with PBS, embedded in Histogel (Thermo), and sectioned at 10μm for histological analysis. Sections were subjected to deparaffinization using Histoclear (Thermoscientific; C78-2-G) and rehydrated. For antigen retrieval slides were emerged in 0.1M EDTA (Ambion; AM9261) and placed in a pressure cooker (Proteogenix; 2100 Retriever) for two hours. Slides were blocked with CAS-block blocking solution (Thermo fisher) for 1 hour at RT, followed by incubation in blocking solution with primary antibodies overnight at 4°C. The following primary antibodies were used: rat anti-insulin (pro-)/C-peptide (Developmental Studies Hybridoma Bank; GN-ID4, 1:300), mouse anti-glucagon (Santa Cruz; sc-514592 1:300), guinea pig anti-insulin (Dako; A0564 1:300), mouse anti-Nkx6.1 (University of Iowa, Developmental Hybridoma Bank; F55A12-supernatant) and rabbit anti phospho-S6 Ribosomal Protein (Ser240/244) (Cell

Signaling; #5364, 1:100). Cells were washed twice in PBS the next day, followed by secondary antibody incubation for 2 hours at RT (protected from light). Secondary antibodies conjugated to Alexa Fluor 405,488, or 647 were used to visualize primary antibodies. Following two washes with PBS, the histology slides were mounted in Vectashield mounting medium (Vector Laboratories), covered with coverslips and sealed with nail polish. Images were taken using a Zeiss Axio Imager 2 microscope.

Flow Cytometry

Differentiated cell clusters, human islets (Prodo labs) or mouse islets were pre-incubated in modified nutrient-free RPMI-1640 medium (MBS652918) for 1 hour. Then, clusters or islets were incubated for 30 minutes incubation in RPMI-1640 with or without glucose (11mM) and amino acids (Life Technologies; 11875-093) and other compounds in 6-well plates at 37°C. The following compounds were used: insulin (Sigma 19278, 1:1000), S961 (a gift from Novonordisk 0.01mM), exendin-4 (Sigma E7144, 0.02mM), forskolin (Santa Cruz SC3562, 0.01mM), diazoxide (Sigma D9035, 0.1mM), Torin-1 (Thermo Fisher 424710, 100nM), leucine (Sigma, 0.3 or 1mM). Then, differentiated cell clusters or islets were collected into 1.7uL Eppendorf tubes, dispersed into single-cell suspension by incubation in Accutase (StemCell Technologies) at 37°C until clusters and dissociated to single cells upon mixing by pipetting gently up and down (typically 5-10 min). Cells were spun down for 2 min at 1000rpm. Cells were resuspended in perm/fix solution and incubated for 10 min (BD 554714). Cells were then washed once in perm/wash for 15 min (BD 554714). Cells were then resuspended in perm/wash with primary antibodies and incubated at 4°C overnight. Primary antibodies diluted 1:300 unless otherwise noted: rat anti-insulin (pro-)/C-peptide (Developmental Studies

Hybridoma Bank; GN-ID4), mouse anti-glucagon (Santa Cruz; sc-514592), guinea pig anti-insulin (Dako; A0564), rabbit anti Mafa (Cell signaling; #79737), mouse anti-Nkx6.1 (University of Iowa, Developmental Hybridoma Bank; F55A12-supernatant), goat anti Pdx1 (R&D Systems; AF2419), rabbit anti phospho-AMPKα (Cell signaling; #2535), and rabbit anti phospho-S6 Ribosomal Protein (Ser240/244) (Cell Signaling; #5364). Cells were washed twice in blocking buffer and then incubated in perm/wash buffer with secondary antibodies for 2 hours (protected from light). Secondary antibodies conjugated to Alexa Fluor 405, 488 or 647 (Life Technologies) were used to visualize primary antibodies. Cells were then washed 3 times in perm/wash solution and finally resuspended in 500-700µl, filtered through a 40µm nylon mash into flow cytometry tubes (BD Falcon; 352235), and analyzed using the LSR-II flow cytometer (BD Biosciences) with at least 10,000 events recorded. Analysis of the results was performed using FlowJo software.

Nano-String Gene Expression Analysis

Sorted TSQ-expressing SC-β cells (Davis et al., 2019) were collected for RNA extraction in RLT Lysis Buffer (QIAGEN). RNA was extracted using the RNeasy Mini Kit (QIAGEN), according the manufacturer's instructions, and 100ng of RNA was used for each reaction. Nanostring set up was performed according to the protocol for the nCounter XT Gene Expression Assay. Data were analyzed in the nSolver 2.5 Software. All genes were normalized to housekeeping genes (ITCH, RPL15, RPL19, TCEB1, UBE2D3). Analysis of changes in gene expression of β cell markers was done using R.

Mouse Transplantation Studies

All animal experiments were performed in accordance with Harvard University International Animal Care and Use Committee regulations. Cell transplantations into immunodeficient SCID-Beige mice (Jackson Laboratory) were conducted as described previously with minor modifications. SC-β Clusters were resuspended in RPMI-1640 medium (Life Technologies; 11875-093), aliquoted into PCR tubes and kept on ice until loading into a catheter for cell delivery under the mouse kidney capsule. Mice were anesthetized with 0.5ml/25g 1.25% Avertin/body weight, and the left ventricle kidney site was shaved and disinfected with betadine and alcohol. A 1cm incision was made to expose the kidney, followed by insertion of the catheter needle and injection of the cell clusters. The abdominal cavity was closed with PDS absorbable sutures (POLY-DOX; 2016-06), and the skin was closed with surgical clips (Kent Scientific Corp; INS750346-2). Mice were placed on a 37°C micro-temp circulating pump and blanket during the surgery/recovery period and given a 5mg/kg carprofen dose post-surgery, re-applied 24h after the initial dose. Wound clips were removed 14 days post-surgery and mice were monitored twice a week. To retrieve grafts, kidneys containing the grafts were dissected from freshly euthanized mice 4 weeks post-transplantation. For immunohistochemistry, grafts were fixed in PBS +4% paraformaldehyde overnight, embedded in paraffin, and sectioned for histological analysis. Single-cell suspensions were washed with and resuspended in PBS, stained with TSQ at 37°C for 10min, filtered through a 40μm nylon mash into flow cytometry tubes (BD Falcon), and TSQ+ cells were sorted using MoFlo flow cytometers (Beckman Coulter) into PBS +1% BSA (Sigma) on ice. Total RNA from sorted SC-β cells was isolated by TRIzol (Invitrogen) extraction followed by RNeasy Plus Micro Kit (Qiagen), from 5 and 7 samples before

and after transplantation, respectively. Libraries were prepared and sequenced using Illumina's directional RNA sequencing protocol.

Ex Vivo Static Glucose Stimulated Insulin Secretion (GSIS)

Human Islets were placed in basal Krebs buffer (Krb) (128mM NaCl, 5mM KCl, 2.7mM CaCl2, 1.2mM MgCl2, 1mMNa2HPO4, 1.2mM KH2PO4, 5mM NaHCO3 10 HEPES, 0.1% BSA). Islets were washed twice with low-glucose (2.8mM) Krb and were then loaded into the 24 well plate inserts (Millicell Cell Culture Insert; PIXP01250) and fasted in low-glucose Krb for 1 hour to remove residual insulin in 37°C incubators. Islets were washed once in low Krb, incubated in low-glucose Krb for 1 hour, and supernatant collected. Then islets were transferred to high-glucose (16.7mM) Krb for 1 hour, and supernatant collected. This sequence was repeated one additional time and islets were washed once between high-glucose to second low-glucose incubation to remove residual glucose. Finally, islets were incubated in Krb containing 2.8mM glucose and 30mM KCl (depolarization challenge) for 1 hour and then supernatant collected. Islets were then lysed using RIPA buffer. Supernatant samples containing secreted insulin and total insulin content of the lysed islets were processed using the Human Ultrasensitive Insulin ELISA (ALPCO, 80-INSHUU-E01.1). The insulin content in the supernatant was normalized by the insulin content of the sample.

Ex Vivo Dynamic Glucose Stimulated Insulin Secretion (GSIS)

Similar numbers of Islets or SC-β clusters were divided into chambers and assayed on a fully automated Perifusion System (BioRep). Chambers were sequentially

perfused with 2.8mM, 20mM glucose or 2.8mM glucose with amino acids (physiological levels) and 2.8mM glucose with 30mM KCL in Krb buffer (128mM NaCl, 5mM KCl, 2.7mM CaCl2, 1.2mM MgCl2, 1mMNa2HPO4, 1.2mM KH2PO4, 5mM NaHCO3 10 HEPES, 0.1% BSA) at a flow rate of 100ul/min. Chambers were first perifused with low glucose (2.8mM) for 1 hour for fasting and then 15 minutes for low glucose incubation followed by low glucose with physiological levels of amino acids (Cantor et al., 2017) for 15 minutes. Samples were then perifused with high glucose (16.7mM) challenge for 30 minutes and then with low glucose and 30mM KCl for 15 minutes. Insulin concentrations in the supernatant were determined using Ultrasensitive Insulin ELISA kit (Alpco).

Preparation of Single-Cell Suspension

Islets were isolated from feta human pancreas, cultured in vitro for four days and collected, at the first or last day of incubation. The islets were allowed to settle, washed in PBS and dissociated by 5min incubation in TrypLE Express (GIBCO) at 37°C, followed by mechanical agitation through pipetting. TrypLE activity was terminated by washing with PBS+1% FCS.

Single Cell Library Preparation and Sequencing

Single-cell capture, cell lysis, reverse transcription of full-length mRNA and cDNA amplification were performed using the 10X Chromium system. Sequencing libraries were prepared using the Illumina Nextera XT DNA library preparation kit and samples were sequenced on an Illumina HiSeq. Fastq files were aligned using the 10X software. Single cell data analysis followed the guidelines and modified code of Luecken & Theis (Luecken and Theis, 2019). Counts data from the three samples was read into Scanpy and merged. Low-quality cells and empty droplets were removed by excluding barcodes

associated with fewer than 1500 counts or greater than 50,000, fewer than 700 genes detected, or with more than 20% of reads mapping to mitochondrial transcripts. Scanpy (Wolf et al., 2018) was used for filtering, principal component analysis (PCA), uniform manifold approximation and projection (UMAP), and Louvain clustering. Prior to dimensionality reduction, ComBat (Johnson et al., 2007) was used for batch correction and scran (Lun et al., 2016) was used to compute and normalize by size factors. PCA was performed on log-scaled counts for the top 4000 highly variable genes, and UMAP was computed with the top 50 principal components. Louvain clustering was performed using a resolution of 0.5, and the cluster of endocrine cells was identified by expression of the marker CHGA. Analysis was then repeated as described above using only endocrine cells, with the number of principal components reduced to 15.

Quantification and Statistical Analysis

No randomization was used in this study, and the investigators were not blinded to group allocation during experiments or outcome assessments. No statistical method was used to predetermine sample size. n marks the number of times an experiment was performed on independent mice or stem-cell differentiation batches. All data are presented as mean ± SEM. Statistical analysis was performed with unpaired Student's t test with a two-tailed distribution. $P<0.05$ was considered as statistically significant. Data were analyzed and plotted using Prism software from GraphPad.

Acknowledgments
We thank Jennifer C. Dempsey and Diana O'Day from University of Washington for their help to supply fetal human pancreas samples. We thank members of the Melton and Sabatini labs for helpful discussions. We thank Jenny Kenty for technical assistance. We thank Caroline Lewis, Bena Chan, and Tenzin Kunchok in the Whitehead Institute Metabolite Profiling Core Facility for LC-MS equipment operation and data analysis. We also thank members of the Harvard Stem Cell Institute Flow Cytometry and Histology core for technical support. A.H. was supported by a long-term fellowship from EMBO. A.L.C. is supported by a fellowship from the NIH (F31 5F31DK113665). D.A.M. is supported by grants from the Harvard Stem Cell Institute, NIH, HIRN, and the JPB foundation. D.M.S. is supported by grants from the NIH (R01 CA103866, R01CA129105, and R37 AI047389). D.M.S. is an American Cancer Society Research Professor. D.M.S. and D.A.M. are investigators of the Howard Hughes Medical Institute.

Author Contributions
A.H. and A.L.C. conceived and performed experiments, analyzed data, and wrote the manuscript. J.C.D., Q.P., and A.R. performed experiments and analyzed data. A.L.F and J.R.S. analyzed data. D.A.M. and D.M.S. supervised and wrote the manuscript.

Declaration of Interests
D.A.M. is the founder of Semma Therapeutics and equity holder of Vertex, which has licensed technology developed in D.A.M.'s lab. All other authors declare no competing interests.

References

Aguayo-Mazzucato, C., A. Koh, I. El Khattabi, W.C. Li, E. Toschi, A. Jermendy, K. Juhl, K. Mao, G.C. Weir, A. Sharm, and S. Bonner-Weir. 2011. Mafa expression enhances glucose-responsive insulin secretion in neonatal rat beta cells. *Diabetologia* 54:583–593.

Alejandro, E.U., N. Bozadjieva, M. Blandino-Rosano, M.A. Wasan, L. Elghazi, S. Vadrevu, L. Satin, and E. Bernal-Mizrachi. 2017. Overexpression of kinase-dead mTOR impairs glucose homeostasis by regulating insulin secretion and not beta-cell mass. *Diabetes* 66:2150–2162.

Arda, H.E., L. Li, J. Tsai, E.A. Torre, Y. Rosli, H. Peiris, R.C. Spitale, C. Dai, X. Gu, K. Qu, et al. 2016. Age-dependent pancreatic gene regulation reveals mechanisms governing human beta cell function. *Cell Metab*. 23:909–920.

Ardestani, A., B. Lupse, Y. Kido, G. Leibowitz, and K. Maedler. 2018. mTORC1 signaling: a double-edged sword in diabetic beta cells. *Cell Metab*. 27:314–331.

Arlotta, P. and S.P. Pas. 2019. Cell diversity in the human cerebral cortex: from the embryo to brain organoids. *Curr. Opin. Neurobiol*. 56:194–198.

Artner, I., Y. Hang, M. Mazur, T. Yamamoto, M. Guo, J. Lindner, M.A. Magnuson, and R. Stein. 2010. MafA and MafB regulate genes critical to beta-cells in a unique temporal manner. *Diabetes* 59:2530–2539.

Avrahami, D., C. Li, J. Zhang, J. Schug, R. Avrahami, S. Rao, M.B. Stadler, L. Burger, D. Schubeler, B. Glaser, and K.H. Kaestner. 2015. Aging-dependent demethylation of regulatory elements correlates with chromatin state and improved beta cell function. *Cell Metab*. 22:619–632.

Bader, E., A. Migliorini, M. Gegg, N. Moruzzi, J. Gerdes, S.S. Roscioni, M. Bakhti, E. Brandl, M. Irmler, J. Beckers, et al. 2016. Identification of proliferative and mature beta-cells in the islets of Langerhans. *Nature* 535:430–434.

Bartolome, A., and C. Guille. 2014. Role of the mammalian target of rapamycin (mTOR) complexes in pancreatic beta-cell mass regulation. *Vitam. Horm*. 95:425–469.

Beall, C., K. Piipari, H. Al-Qassab, M.A. Smith, N. Parker, D. Carling, B. Viollet, D.J. Withers, and M.L. Ashford. 2010. Loss of AMP-activated protein kinase alpha2 subunit in mouse beta-cells impairs glucose-stimulated insulin secretion and inhibits their sensitivity to hypoglycaemia. *Biochem. J*. 429:323–333.

Blandino-Rosano, M., R. Barbaresso, M. Jimenez-Palomares, N. Bozadjieva, J.P. Werneck-De-Castro, M. Hatanaka, R.G. Mirmira, N. Sonenberg, M. Liu, M.A. Ruegg, et al. 2017. Loss of mTORC1 signalling impairs beta-cell homeostasis and insulin processing. *Nat. Commun*. 8:16014.

Bliss, C.R. and G.W. Sharp. 1992. Glucose-induced insulin release in islets of young rats: time-dependent potentiation and effects of 2-bromostearate. *Am. J. Physiol*. 263:E890–E896.

Blum, B., S. Hrvatin, C. Schuetz, C. Bonal, A. Rezania, and D.A. Melton. 2012. Functional beta-cell maturation is marked by an increased glucose threshold and by expression of urocortin 3. *Nat. Biotechnol*. 30:261–264.

Cantor, J.R., M. Abu-Remaileh, N. Kanarek, E. Freinkman, X. Gao, A. Louissaint, C.A. Lewis, and D.M. Sabatini. 2017. Physiologic medium rewires cellular metabolism and reveals uric acid as an endogenous inhibitor of UMP synthase. *Cell* 169:258–272.e17.

Chau, G.C., D.U. Im, T.M. Kang, J.M. Bae, W. Kim, S. Pyo, E.Y. Moon, and S.H. Um. 2017. mTOR controls ChREBP transcriptional activity and pancreatic beta cell survival under diabetic stress. *J. Cell Biol*. 216:2091–2105.

Conrad, E., R. Stein, and C.S. Hunter. 2014. Revealing transcription factors during human pancreatic beta cell development. *Trends Endocrinol. Metab.* 25:407–414.

Davis, J.C., A. Helman, J. Rivera-Feliciano, C.M. Langston, E.N. Engquist, and D.A. Melton. 2019. Live cell monitoring and enrichment of stem cellderived beta cells using intracellular Zinc content as a population marker. *Curr. Protoc. Stem Cell Biol*. 51:e99.

Dhawan, S., S.I. Tschen, C. Zeng, T. Guo, M. Hebrok, A. Matveyenko, and A. Bhushan. 2015. DNA methylation directs functional maturation of pancreatic beta cells. *J. Clin. Invest*. 125:2851–2860.

Elghazi, L., N. Balcazar, M. Blandino-Rosano, C. Cras-Me´ neur, S. Fatrai, A.P. Gould, M.M. Chi, K.H. Moley, and E. Bernal-Mizrachi. 2010. Decreased IRS signaling impairs beta-cell cycle progression and survival in transgenic mice overexpressing S6K in beta-cells. *Diabetes* 59:2390–2399.

Fowden, A.L. 1992. The role of insulin in fetal growth. *Early Hum. Dev.* 29:177–181.

Gao, N., J. Le Lay, W. Qin, N. Doliba, J. Schug, A.J. Fox, O. Smirnova, F.M. Matschinsky, and K.H. Kaestner. 2010. Foxa1 and Foxa2 maintain the metabolic and secretory features of the mature beta-cell. *Mol. Endocrinol*. 24:1594–1604.

Gonzalez, P.N., M. Gasperowicz, J. Barbeito-Andre´s, N. Klenin, J.C. Cross, and B. Hallgrı´msson. 2016. Chronic protein restriction in mice impacts placental function and maternal body weight before fetal growth. *PLoS One* 11:e0152227.

Hamada, S., K. Hara, T. Hamada, H. Yasuda, H. Moriyama, R. Nakayama, M. Nagata, and K. Yokono. 2009. Upregulation of the mammalian target of rapamycin complex 1 pathway by Ras homolog enriched in brain in pancreatic beta-cells leads to increased beta-cell mass and prevention of hyperglycemia. *Diabetes* 58:1321–1332.

Hay, W.W., Jr. 2006. Placental-fetal glucose exchange and fetal glucose metabolism. *Trans. Am. Clin. Climatol. Assoc*. 117:321–339.

Helman, A., A. Klochendler, N. Azazmeh, Y. Gabai, E. Horwitz, S. Anzi, A. Swisa, R. Condiotti, R.Z. Granit, Y. Nevo, et al. 2016. p16(Ink4a)-induced senescence of pancreatic beta cells enhances insulin secretion.Nat. Med. 22, 412–420.

Henquin, J.C. and M. Nenquin. 2018. Immaturity of insulin secretion by pancreatic islets isolated from one human neonate. *J. Diabetes Investig*. 9:270–273.

Herring, C.M., F.W. Bazer, G.A. Johnson, and G. Wu. 2018. Impacts of maternal dietary protein intake on fetal survival, growth, and development. *Exp. Biol. Med*. (Maywood) 243:525–533.

Hrvatin, S., C.W. O'Donnell, F. Deng, J.R. Millman, F.W. Pagliuca, P. Diiorio, A. Rezania, D.K. Gifford, and D.A. Melton. 2014. Differentiated human stem cells resemble fetal, not adult, beta cells. *Proc. Natl. Acad. Sci. USA.* 111:3038–3043.

Jaafar, R., S. Tran, A.N. Shah, G. Sun, M. Valdearcos, P. Marchetti, M. Masini, A. Swisa, S. Giacometti, E. Bernal-Mizrachi, et al. 2019. mTORC1 to AMPK switching underlies beta-cell metabolic plasticity during maturation and diabetes. *J. Clin. Invest*. 130:4124–4137.

Jiang, Y., P. Park, S.M. Hong, and K. Ban. 2018. Maturation of cardiomyocytes derived from human pluripotent stem cells: current strategies and limitations. *Mol. Cells*. 41:613–621.
Johnson, W.E., C. Li, and A. Rabinovic. 2007. Adjusting batch effects in microarray expression data using empirical Bayes methods. *Biostatistics.* 8:118–127.
Kervran, A. and J Randon. 1980. Development of insulin release by fetal rat pancreas in vitro: effects of glucose, amino acids, and theophylline. *Diabetes* 29:673–678.
Koyanagi, M., S. Asahara, T. Matsuda, N. Hashimoto, Y. Shigeyama, Y. Shibutani, A. Kanno, M. Fuchita, T. Mikami, T. Hosooka, et al. 2011. Ablation of TSC2 enhances insulin secretion by increasing the number of mitochondria through activation of mTORC1. PLoS One 6:e23238.
Lemaire, K., L. Thorrez, and F. Schuit. 2016. Disallowed and allowed gene expression: two faces of mature islet beta cells. *Annu. Rev. Nutr*. 36:45–71.
Liu, J.S., and M. Hebrok. 2017. All mixed up: defining roles for beta-cell subtypes in mature islets. *Genes Dev.* 31:228–240.
Luecken, M.D., and F.J. Theis. 2019. Current best practices in single-cell RNA-seq analysis: a tutorial. *Mol. Syst. Biol*. 15:e8746.
Lun, A.T., D.J. Mccarthy, and J.C. Marioni. 2016. A step-by-step workflow for low-level analysis of single-cell RNA-seq data with bioconductor. *F1000Res*. 5:2122.
Lundy, S.D., W.Z. Zhu, M. Regnier, and M.A. Laflamme. 2013. Structural and functional maturation of cardiomyocytes derived from human pluripotent stem cells. *Stem Cells Dev.* 22:1991–2002.
Maedler, K. and A. Ardestani. 2017. mTORC in beta cells: more Than only Recognizing Comestibles. *J. Cell Biol*. 216:1883–1885.
Martinez-Sanchez, A., M.S. Nguyen-Tu, and G.A Rutter. 2015. DICER inactivation identifies pancreatic beta-cell "disallowed" genes targeted by microRNAs. *Mol. Endocrinol*. 29:1067–1079.
Matsuoka, T.A., H. Kaneto, R. Stein, T. Miyatsuka, D. Kawamori, E. Henderson, I. Kojima, M. Matsuhisa, M. Hori, and Y. Yamasaki. 2007. MafA regulates expression of genes important to islet beta-cell function. *Mol. Endocrinol*. 21:2764–2774.
Mori, H., K. Inoki, D. Opland, H. Munzberg, E.C. Villanueva, M. Faouzi, T. Ikenoue, D.J. Kwiatkowski, O.A. Macdougald, M.G. Myers, Jr., and K.L. Guan. 2009. Critical roles for the TSC-mTOR pathway in beta-cell function. *Am. J. Physiol. Endocrinol. Metab*. 297:E1013–E1022.
Morton, S.U. and D. Brodsky. 2016. Fetal physiology and the transition to extrauterine life. *Clin. Perinatol.* 43:395–407.
Nair, G.G., J.S. Liu, H.A. Russ, S. Tran, M.S. Saxton, R. Chen, C. Juang, M.L. Li, V.Q. Nguyen, S. Giacometti, et al. 2019. Recapitulating endocrine cell clustering in culture promotes maturation of human stem-cell-derived beta cells. *Nat. Cell Biol*. 21:263–274.
Nakada, D., T.L. Saunders, and S.J. Morrison. 2010. LKB1 regulates cell cycle and energy metabolism in haematopoietic stem cells. *Nature* 46:653–658.
Ni, Q., Y. Gu, Y. Xie, Q. Yin, H. Zhang, A. Nie, W. Li, Y. Wang, G. Ning, W. Wang, and Q. Wang. 2017. Raptor regulates functional maturation of murine beta cells. *Nat. Commun*. 8:15755.

Nishimura, W., S. Takahashi, and K. Yasuda. 2015. MafA is critical for maintenance of the mature beta cell phenotype in mice. *Diabetologia* 58:566–574.
Pagliuca, F.W., J.R. Millman, M. Gurtler, M. Segel, A. Van Dervort, J.H. Ryu, Q.P. Peterson, D. Greiner, and D.A. Melton. 2014. Generation of functional human pancreatic beta cells in vitro. *Cell.* 159:428–439.
Pullen, T.J. and G.A. Rutter. 2013. When less is more: the forbidden fruits of gene repression in the adult beta-cell. *Diabetes Obes. Metab.* 15:503–512.
Rachdi, L., N. Balcazar, F. Osorio-Duque, L. Elghazi, A. Weiss, A. Gould, K.J. Chang-Chen, M.J. Gambello, and E. Bernal-Mizrachi. 2008. Disruption of Tsc2 in pancreatic beta cells induces beta cell mass expansion and improved glucose tolerance in a TORC1-dependent manner. *Proc. Natl. Acad. Sci. USA* 105:9250–9255.
Rezania, A., J.E. Bruin, P. Arora, A. Rubin, I. Batushansky, A. Asadi, S. O'Dwyer, N. Quiskamp, M. Mojibian, T. Albrecht, et al. 2014. Reversal of diabetes with insulin-producing cells derived in vitro from human pluripotent stem cells. *Nat. Biotechnol*. 32:1121–1133.
Robinton, D.A. and G.Q. Daley. 2012. The promise of induced pluripotent stem cells in research and therapy. *Nature.* 481:295–305.
Rozzo, A., T. Meneghel-Rozzo, S.L. Delakorda, S.B. Yang, and M. Rupnik. 2009. Exocytosis of insulin: in vivo maturation of mouse endocrine pancreas. *Ann. N. Y. Acad. Sci.* 1152:53–62.
Russ, H.A., A.V. Parent, J.J. Ringler, T.G. Hennings, G.G. Nair, M. Shveygert, T. Guo, S. Puri, L. Haataja, V. Cirulli, et al. 2015. Controlled induction of human pancreatic progenitors produces functional beta-like cells in vitro. *EMBO J.* 34:1759–1772.
Sancak, Y., L. Bar-Peled, R. Zoncu, A.L. Markhard, S. Nada, and D.M. Sabatini. 2010. Ragulator-Rag complex targets mTORC1 to the lysosomal surface and is necessary for its activation by amino acids. *Cell*. 141:290–303.
Sancak, Y., T.R. Peterson, Y.D. Shaul, R.A. Lindquist, C.C. Thoreen, L. BarPeled, and D.M. Sabatini. 2008. The Rag GTPases bind raptor and mediate amino acid signaling to mTORC1. *Science.* 320:1496–1501.
Saxton, R.A. and D.M. Sabatini. 2017. MTOR signaling in growth, metabolism, and disease. *Cell.* 168:960–976.
Shigeyama, Y., T. Kobayashi, Y. Kido, N. Hashimoto, S. Asahara, T. Matsuda, A. Takeda, T. Inoue, Y. Shibutani, M. Koyanagi, et al. 2008. Biphasic response of pancreatic beta-cell mass to ablation of tuberous sclerosis complex 2 in mice. *Mol. Cell. Biol*. 28:2971–2979.
Sinagoga, K.L., W.J. Stone, J.V. Schiesser, J.I. Schweitzer, L. Sampson, Y. Zheng, and J.M. Wells. 2017. Distinct roles for the mTOR pathway in postnatal morphogenesis, maturation and function of pancreatic islets. *Development*. 144:2402–2414.
Slack, J.M. 1995. Developmental biology of the pancreas. *Development.* 121:1569–1580.
Sneddon, J.B., Q. Tang, P. Stock, J.A. Bluestone, S. Roy, T. Desai, and M. Hebrok. 2018. Stem cell therapies for treating diabetes: progress and remaining challenges. *Cell Stem Cell.* 22:810–823.
Stolovich-Rain, M., J. Enk, J. Vikesa, F.C. Nielsen, A. Saada, B. Glaser, and Y. Dor.

2015. Weaning triggers a maturation step of pancreatic beta cells. *Dev. Cell*. 32:535–545.
Sun, G., A.I. Tarasov, J.A. Mcginty, P.M. French, A. Mcdonald, I. Leclerc, and G.A. Rutter. 2010. LKB1 deletion with the RIP2.Cre transgene modifies pancreatic beta-cell morphology and enhances insulin secretion in vivo. *Am. J. Physiol. Endocrinol. Metab*. 298:E1261–E1273.
Swisa, A., Z. Granot, N. Tamarina, S. Sayers, N. Bardeesy, L. Philipson, D.J. Hodson, J.D. Wikstrom, G.A. Rutter, G. Leibowitz, et al. 2015. Loss of liver kinase B1 (LKB1) in beta cells enhances glucose-stimulated insulin secretion Despite profound mitochondrial defects. *J. Biol. Chem.* 290:20934–20946.
Tengholm, A. and E. Gylfe. 2017. cAMP signalling in insulin and glucagon secretion. *Diabetes Obes. Metab*. 19:42–53.
Thorrez, L., I. Laudadio, K. Van Deun, R. Quintens, N. Hendrickx, M. Granvik, K. Lemaire, A. Schraenen, L. Van Lommel, S. Lehnert, et al. 2011. Tissue-specific disallowance of housekeeping genes: the other face of cell differentiation. *Genome Res*. 21:95–105.
Van Der Meulen, T. and M.O. Huising. 2014. Maturation of stem cell-derived beta-cells guided by the expression of urocortin 3. *Rev. Diabet. Stud*. 11:115–132.
Wang, H., T. Brun, K. Kataoka, A.J. Sharma, and C.B. Wollheim. 2007. MAFA controls genes implicated in insulin biosynthesis and secretion. *Diabetologia*. 50:348–358.
Ward Platt, M. and S. Deshpande. 2005. Metabolic adaptation at birth. *Semin. Fetal Neonat. Med*. 10:341–350.
Wicksteed, B., M. Brissova, W. Yan, D.M. Opland, J.L. Plank, R.B. Reinert, L.M. Dickson, N.A. Tamarina, L.H. Philipson, A. Shostak, et al. 2010. Conditional gene targeting in mouse pancreatic ß-cells: analysis of ectopic Cre transgene expression in the brain. *Diabetes.* 59:3090–3098.
Wolf, F.A., P. Angerer, and F.J. Theis. 2018. SCANPY: large-scale single-cell gene expression data analysis. *Genome Biol*. 19:15.
Xu, Q.G., X.Q. Li, S.A. Kotecha, C. Cheng, H.S. Sun, and D.W. Zochodne. 2004. Insulin as an in vivo growth factor. *Exp. Neurol*. 188:43–51.
Yoshihara, E., Z. Wei, C.S. Lin, S. Fang, M. Ahmadian, Y. Kida, T. Tseng, Y. Dai, R.T. Yu, C. Liddle, et al. 2016. ERRg is required for the metabolic maturation of therapeutically functional glucose-responsive b cells. *Cell Metab*. 23:622–634.
Young, M. and M.A. Prenton. 1969. Maternal and fetal plasma amino acid concentrations during gestation and in retarded fetal growth. *J. Obstet. Gynaecol. Br. Commonw*. 76:333–334.
Zeng, C., F. Mulas, Y. Sui, T. Guan, N. Miller, Y. Tan, F. Liu, W. Jin, A.C. Carrano, M.O. Huising, et al. 2017. Pseudotemporal Ordering of Single Cells Reveals Metabolic Control of Postnatal beta Cell Proliferation. *Cell Metab.* 25:1160–1175.e11.
Zhang, C., T. Moriguchi, M. Kajihara, R. Esaki, A. Harada, H. Shimohata, H. Oishi, M. Hamada, N. Morito, K. Hasegawa, et al. 2005. MafA is a key regulator of glucose-stimulated insulin secretion. *Mol. Cell. Biol*. 25:4969–4976.

Chapter 4

Summary

Andrew L. Cangelosi[1,2,3]

[1] Whitehead Institute for Biomedical Research, 455 Main Street, Cambridge, MA 02142.
[2] Howard Hughes Medical Institute, Department of Biology, Massachusetts Institute of Technology, Cambridge, MA 02139.
[3] Department of Biology, Massachusetts Institute of Technology, Cambridge, MA 02139.

Summary

Even before its discovery, mTORC1 was appreciated as an important controller of physiological function. As the many regulatory inputs and cellular effectors of the pathway have been discovered, a more accurate picture has emerged of mTORC1 as an integrative decision-maker, connecting signals from the environment of the cell to numerous facets of cellular growth and metabolic function. The direct sensing of nutrients by the mTORC1 pathway therefore represents a critical node of connecting environmental factors to cellular and organismal adaption and fitness.

While recent work has brought the cellular mechanisms underlying nutrient sensing to light, the implications of nutrient sensing in the context of mammalian physiology has remained in the dark. Here, we employed genetic mouse models to identify a liver-specific role of Sestrin-mediated leucine sensing in the adaptation to physiological leucine availability. In doing so, we uncovered an unappreciated compartmentalization of leucine sensing within the architecture of the liver. Further, we found that the nutrient sensitivity of mTORC1 in pancreatic β-cells is dynamic, and must shift at birth to enable their functional maturation.

The collective work detailed here only begins to scratch the surface of the physiological implications of nutrient sensing by the mTORC1 pathway. Much remains to be understood and explored further. Several important questions for further study are detailed here.

Outstanding questions and future directions

Compartmentalization and functional role of leucine sensing in other tissues

Analogous to the zonated functionality of the liver, other tissues display spatial heterogeneity in cellular function and other properties. For instance, skeletal muscle consists of several different fiber types, often coexisting within the same muscle, which have characteristically different metabolic properties and functional capacities. In the central nervous system (CNS), feeding activates complex networks of neuronal signaling to influence whole-body metabolic function, which requires extensive communication between many functionally distinct neural populations that is not fully understood. Whether the sensing of leucine and other nutrients is spatially compartmentalized within skeletal muscle and the CNS, and how it may impact the different functional properties of distinct muscle fiber types and neuron populations would be an exciting avenue to explore.

Further, notable areas which Sestrin-mediated leucine sensing likely impinges on and would be important to study are immune function and stem cell function. Immune cells and stem cell compartments are both functionally affected by mTORC1 dysregulation (Powell et al., 2012; Zheng et al., 2007; Araki et al., 2009; Haxhinasto et al., 2008; Chen et al., 2009; Yilmaz et al., 2012), and growing evidence points towards an increasingly important role of immunity, inflammation, and tissue renewal in maintaining organismal homeostasis (Ferrucci and Fabbri, 2018; Lopez-Otin et al., 2013).

Impact of Sestrin-mediated leucine sensing in contexts of disease

The work presented here explored the role of Sestrins in dietary leucine deprived, but otherwise healthy, mice. However, the *in vivo* impact of Sestrin-mediated leucine sensing in disease states remained unanswered. During diet-induced obesity and Type 2 diabetes, circulating levels of branched chain amino acids (BCAAs), including leucine, are chronically elevated, which is thought to be a result of impaired BCAA metabolism (Newgard et al., 2009; Zhou et al., 2019). How, and in which tissues, leucine sensing by the mTORC1 pathway impacts mTORC1 activity and downstream metabolic consequences in this context would be important to understand further. Another clinically relevant setting in which the role of Sestrin-mediated leucine sensing should be assessed is in cancer. Indeed, leucine deprivation synergizes with autophagy inhibition to impede tumor growth in mice (Sheen et al., 2011). Understanding the role of the Sestrins in this vulnerability, and in which specific tumor types and therapeutic contexts targeting Sestrin's leucine sensing function may be advantageous, is currently unclear. Lastly, mTORC1 inhibition has steadily gained more and more ground as a promising potential approach for intervening in aging-associated decline, and the Sestrins as mTORC1 regulators have already begun to enter the conversation (Lu et al., 2020; Fan et al., 2020; Lee et al., 2010). However, the extent to which leucine, and its modulation of Sestrin's impact on the mTORC1 pathway, contributes to progressive functional decline during aging has not been teased apart.

Physiological role of other nutrient sensing mechanisms upstream of mTORC1

In addition to leucine sensing by the Sestrin proteins, the nutrient sensing machinery upstream of mTORC1 is also responsive to levels of arginine (via the arginine sensor CASTOR1), methionine (via sensing of methionine-derived SAM by

SAMTOR), and glucose (via the glycolytic intermediate DHAP) (Gu et al., 2017; Chantranupong et al., 2016; Orozco et al., 2020). The roles of these additional sensing mechanisms *in vivo* are not known. In particular, delineating the intratissue distribution of the different sensors, local availability of sensed metabolites, and interplay between these sensing mechanisms on mTORC1 activity and downstream tissue function is critical towards achieving a comprehensive understanding of nutrient sensing in physiology.

Nutrient sensors as potential therapeutic targets

Targeting mTORC1 activity has long been of clinical interest for a multitude of applications, including immunomodulation and as treatment against cancer and epilepsy (Martel et al., 1977; Chiarini et al., 2015; Saxena and Sampson, 2015). However, the use of rapamycin and rapalogs poses challenges, as their extended use also impairs mTORC2 signaling, leading to undesired side effects (Lamming et al., 2012; Sarbassov et al., 2006). Exploiting the current structural knowledge of the amino acid sensors and their amino acid binding properties may enable the development of amino acid mimetics or antagonists. These efforts have already begun in the development of leucine analogs targeting Sestrin2 (Sengupta et al., 2019). Such an approach may offer a strategy to target mTORC1 with greater specificity. Further, inter- and intra-tissue heterogeneity in the distribution of the nutrient sensors may introduce an additional layer of specificity towards targeting certain cell populations over others.

Nutrient sensing in stem cell-based regenerative medicine

The *in vitro* generation of human iPS cell-derived pancreatic β-cells relies heavily on exogenous growth factors to achieve insulin production (Pagliuca et al., 2014). We

found here that the functional maturation of stem cell-derived β-cells also is dependent on environmental nutrient levels and mTORC1 activity. It would be interesting to ask if media nutrient conditions similarly impact the functional maturation of stem cells in other differentiation efforts. Such applications would require a greater understanding of the particular nutrient conditions to optimize stem cell function for specific regenerative purposes. Our findings suggest that mimicking *in vivo* nutrient conditions, such as with physiological media formulations (Cantor et al., 2017), may be a useful approach in these efforts.

References

Araki, K., A.P. Turner, V.O. Shaffer, S. Gangappa, S.A. Keller, M.F. Bachmann, C.P. Larsen, and R. Ahmed. 2009. mTOR regulates memory CD8 T-cell differentiation. *Nature*. 460:108-112.

Cantor, J.R., M. Abu-Remaileh, N. Kanarek, E. Freinkman, X. Gao, A. Louissaint, C.A. Lewis, D.M. Sabatini. 2017. Physiologic Medium Rewires Cellular Metabolism and Reveals Uric Acid as an Endogenous Inhibitor of UMP Synthase. *Cell*. 169:258-272.e17.

Chantranupong, L., S.M. Scaria, R.A. Saxton, M.P. Gygi, K. Shen, G.A. Wyant, T. Wang, J.W. Harper, S.P. Gygi, and D.M. Sabatini. 2016. The CASTOR Proteins Are Arginine Sensors for the mTORC1 Pathway. *Cell*. 165:153-164.

Chen, C., Y. Liu, Y. Liu, and P. Zheng. 2009. mTOR regulation and therapeutic rejuvenation of aging hematopoietic stem cells. *Sci. Signal*. 2:ra75.

Chiarini, F., Evangelisti, C., McCubrey, J.A., and Martelli, A.M. 2015. Current treatment strategies for inhibiting mTOR in cancer. *Trends Pharmacol Sci.* 36:124-135.

Fan, X., Y. Zeng, W. Song, J. Li, S. Ai, D. Yang, X. Mao, and M. Yang. 2020. The role of Sestrins in the regulation of the aging process. *Mech Ageing Dev*. 188:111251.

Ferrucci, L. and E. Fabbri. 2018. Inflammageing: chronic inflammation in ageing, cardiovascular disease, and frailty. *Nat Rev Cardiol*. 15:505–522.

Gu, X., J.M. Orozco, R.A. Saxton, K.J. Condon, G.Y. Liu, P.A. Krawczyk, S.M. Scaria, J.W. Harper, S.P. Gygi, and D.M. Sabatini. 2017. SAMTOR is an S-adenosylmethionine sensor for the mTORC1 pathway. *Science*. 358:813-818.

Haxhinasto, S., D. Mathis, and C. Benoist. 2008. The AKT-mTOR axis regulates de novo differentiation of CD4+Foxp3+ cells. *J. Exp. Med*. 205: 565-574.

Lamming, D.W., L. Ye, P. Katajisto, M.D. Goncalves, M. Saitoh, D.M. Stevens, J.G. Davis, A.B. Salmon, A. Richardson, R.S. Ahima, D.A. Guertin, D.M. Sabatini, and J.A. Baur. 2012. Rapamycin-induced insulin resistance is mediated by mTORC2 loss and uncoupled from longevity. *Science*. 335:1638-43.

Lee, J.H., R. Bodmer, E. Bier, and M. Karin. 2010. Sestrins at the crossroad between stress and aging. *Aging*. 2:369–374.

López-Otín, C., M.A. Blasco, L. Partridge, M. Serrano, and G. Kroemer. 2013. The Hallmarks of Aging. *Cell*. 153:1194–1217.

Lu, J., U. Temp, A. Müller-Hartmann, J. Esser, S. Grönke, and L. Partridge. 2020. Sestrin is a key regulator of stem cell function and lifespan in response to dietary amino acids. *Nat Aging*. 1:60-72.

Martel, R.R., J. Klicius, and S. Galet. 1977. Inhibition of the immune response by rapamycin, a new antifungal antibiotic. Can J Physiol Pharmacol. 55:48-51.

Newgard, C.B., J. An, J.R. Bain, M.J. Muehlbauer, R.D. Stevens, L.F. Lien, A.M. Haqq, S.H. Shah, M. Arlotto, C.A. Slentz, J. Rochon, D. Gallup, O. Ilkayeva, B.R. Wenner, W.S. Yancy, H. Eisenson, G. Musante, R.S. Surwit, D.S. Millington, M.D. Butler, and L.P. Svetkey. 2009. A branched-chain amino acid-related metabolic signature that differentiates obese and lean humans and contributes to insulin resistance. *Cell Metab.* 9:311-26.

Orozco, J.M., P.A. Krawczyk, S.M. Scaria, A.L. Cangelosi, S.H. Chan, T. Kunchok, C.A.

Lewis, and D.M. Sabatini. 2020. Dihydroxyacetone phosphate signals glucose availability to mTORC1. *Nat Metab*. 2:893-901.
Pagliuca, F.W., J.R. Millman, M. Gürtler, M. Segel, A. Van Dervort, J.H. Ryu, Q.P. Peterson, D. Greiner, and D.A. Melton. 2014. Generation of functional human pancreatic β cells in vitro. *Cell*. 159:428–439.
Powell, J.D., K.N. Pollizzi, E.B. Heikamp, and M.R. Horton. 2012. Regulation of immune responses by mTOR. *Annu. Rev. Immunol*. 30:39-68.
Sarbassov, D.D., S.M. Ali, S. Sengupta, J.H. Sheen, P.P. Hsu, A.F. Bagley, A.L. Markhard, and D.M. Sabatini. 2006. Prolonged rapamycin treatment inhibits mTORC2 assembly and Akt/PKB. *Mol. Cell*. 22:159-168.
Saxena, A., and Sampson, J.R. 2015. Epilepsy in Tuberous Sclerosis: Phenotypes, Mechanisms, and Treatments. *Semin Neurol.* 35:269-276.
Sengupta, S., E. Giaime, S. Narayan, S. Hahm, J. Howell, D. O'Neill, G.P. Vlasuk, E. Saiah. 2019. Discovery of NV-5138, the first selective Brain mTORC1 activator. *Sci Rep*. 9:4107.
Sheen, J., R. Zoncu, D. Kim, and D.M. Sabatini. 2011. Defective regulation of autophagy upon leucine deprivation reveals a targetable liability of human melanoma cells in vitro and in vivo. *Cancer Cell*. 19:613–628.
Yilmaz, O.H., P. Katajisto, D.W. Lamming, Y. Gültekin, K.E. Bauer-Rowe, S. Sengupta, K. Birsoy, A. Dursun, V.O. Yilmaz, M. Selig, G.P. Nielsen, M. Mino-Kenudson, L.R. Zukerberg, A.K. Bhan, V. Deshpande, and D.M. Sabatini. 2012. mTORC1 in the Paneth cell niche couples intestinal stem-cell function to calorie intake. *Nature*. 486:490-5.
Zheng, Y., S.L. Collins, M.A. Lutz, A.N. Allen, T.P. Kole, P.E. Zarek, and J.D. Powell. 2007. A role for mammalian target of rapamycin in regulating T cell activation versus anergy. *J. Immunol*. 178:2163-2170.
Zhou, M., J. Shao, C. Wu, L. Shu, W. Dong, Y. Liu, M. Chen, R.M. Wynn, J. Wang, J. Wang, W. Gui, X. Qi, A.J. Lusis, Z. Li, W. Wang, G. Ning, X. Yang, D.T. Chuang, Y. Wang, and H. Sun. 2019. Targeting BCAA Catabolism to Treat Obesity-Associated Insulin Resistance. *Diabetes*. 68:1730-1746.